

Interactions of Hydrology and Climate in the Amazon Basin

by

Elfatih Ali Babiker Eltahir

B.Sc. in Civil Engineering with First Class Honors,
University of Khartoum (1985)

M.Sc. in Hydrology with First Class Honors,
National University of Ireland (1988)

Submitted to the Department of
Civil and Environmental Engineering
in Partial Fulfillment of the Requirements for
the Degree of

Doctor of Science

at the

Massachusetts Institute of Technology
February 1993

© 1993 Massachusetts Institute of Technology
All rights reserved

Signature of the Author _____
Department of Civil and Environmental Engineering
December 30, 1992

Certified by _____
William E. Leonhard Professor of Civil and Environmental Engineering
Rafael L. Bras
Thesis Supervisor

Accepted by _____
Professor Ole S. Madsen, Chairman
Departmental Committee on Graduate Students

ARCHIVES

MASSACHUSETTS INSTITUTE
TECHNOLOGY

FEB 17 1993

LIBRARIES

Interactions of Hydrology and Climate in the Amazon Basin

by

Elfatih Ali Babiker Eltahir

Submitted to the Department of
Civil and Environmental Engineering
in Partial Fulfillment of the Requirements for
the Degree of Doctor of Science

ABSTRACT

This study focuses on the physical interactions between the land surface and the atmosphere in the Amazon region. A precipitation recycling ratio is introduced as a quantitative measure of the potential for such interactions. A new model is developed for describing the spatial and temporal distribution of the recycling ratio. The model is applied in the Amazon basin using a sub-set of the European Center for Medium-range Weather Forecast (ECMWF) global data. It is estimated that 25% of the total precipitation in the Amazon basin is contributed by evaporation within the basin. For areas smaller than the size of the Amazon basin, it is found that the recycling ratio decreases in proportion to the square root of the linear scale.

The sensitivity of the regional climate to small-scale deforestation (~ 250 km) is studied using a modeling approach. It is evident from previous experiments on modeling of the land-atmosphere system in the Amazon region, that new accurate schemes are needed for describing interception processes in a rain-forest environment. Hence, a new scheme is developed for modeling rainfall interception over large areas. The scheme combines a physical description of the interception processes at a point, which is given by the Rutter model, and statistical description of the sub-grid scale spatial variability in rainfall and canopy storage. It is found that spatial variability in both rainfall and canopy storage play a significant role in rainfall interception processes over large areas.

The new interception scheme and other improvements in the modeling of surface hydrology are included into a meso-scale climate model which is driven by solar radiation and boundary conditions from the ECMWF data set. The model is used in simulating climate over a limited area (1600 km x 1600 km) within the Amazon basin. The sensitivity of regional climate to small-scale deforestation is studied by performing two numerical experiments: a control run, and a deforestation run in which the central area (250 km x 250 km) of the domain is deforested. The experiments are performed for the months of January and July. It is found that small-scale deforestation may result in the following local effects: less evaporation, less precipitation and warmer surface temperature. The magnitudes of the changes in evaporation and precipitation are in the order of 10%. The increase in surface temperature is in the order of 0.5 °C.

The sensitivity of regional climate to large-scale deforestation (~2500 km) is the subject of many recent studies. It is predicted that large-scale deforestation may result in: less evaporation, less precipitation and warmer surface temperature; the different models disagree on the sign of the predicted change in runoff (precipitation-evaporation). A change in annual runoff is equivalent to a change in atmospheric moisture convergence which implies a change in the tropical circulation. A theoretical framework is developed for studying the basic mechanisms contributing to the response of the tropical atmosphere to large-scale deforestation. It is suggested that large scale deforestation excites two competing responses : a diverging circulation anomaly due to the negative change in precipitation (heating) and a converging circulation anomaly due to the positive change in surface temperature. The dependence of runoff changes on these two competing anomalies implies a high sensitivity of runoff predictions by the models.

Thesis Supervisor : Rafael L. Bras

Title : William E. Leonhard Professor of Civil and
Environmental Engineering

ACKNOWLEDGMENTS

I would like to thank my advisor Professor Rafael L. Bras for his support, encouragement, and friendship. I found in his research group the ideal environment which encourages learning, hard work, and independent thinking.

I would like to acknowledge the useful comments and suggestions from the members of my Doctoral committee : Professor Peter S. Eagleson, Professor Reginald E. Newell, Professor Ignacio Rodriguez-Iturbe, and Professor Dara Entekhabi.

I would like to thank Gary Bates of the National Center for Atmospheric Research (NCAR), for his help with the MM4 climate model.

I would like to thank every one in the Parsons Laboratory for the friendly environment which I enjoyed during my period of study at MIT. I also enjoyed the moments of learning and the useful discussions with my fellow graduate students and friends, particularly, Shafiqul Islam, Harihar Rajaram, David Tarboton, Vivek Kapoor, Luis Garrote, and Ede Ijjasz-Vasquez.

The first two years of my study at MIT were partially supported by scholarships from the Government of Sudan and from Chevron Oil Company. The research reported in this thesis is supported by the National Aeronautics and Space Administration (NASA) (agreement NAG 5-1615) and through a NASA Graduate Student Fellowship (agreement NGT 30086).

The support and love of every one in my family is greatly appreciated; they remain the source of motivation in all of my work.

This Thesis is dedicated to
my parents
Nafisa Hassan Musa
and
Ali Babiker Eltahir

LIST OF CONTENTS

ABSTRACT	2
ACKNOWLEDGMENT	4
LIST OF CONTENTS	6
LIST OF FIGURES	10
LIST OF TABLES	14
LIST OF NOTATIONS	15
CHAPTER 1 : Introduction	17
1.1 Scope	17
1.2 Outline	20
CHAPTER 2 : Literature Review	22
2.1 Introduction	22
2.2 Hydrologic Processes and Regional Climate	22
2.3 Precipitation Recycling and Rainfall Dynamics	28
2.4 Hydrologic Studies in the Amazon basin	30
2.4.1 Amazon Region Micrometeorological Experiment	32
CHAPTER 3 : Precipitation Recycling in the Amazon Basin	35
3.1 Introduction	35
3.2 Precipitation Recycling Model	38
3.3 Comparison of the Recycling Models	43
3.4 Estimation Procedure	44
3.5 Precipitation Recycling in the Amazon Basin	46
3.6 Scaling of Precipitation Recycling in the Amazon Basin	58
3.7 Why recycling in the Amazon is overestimated by Previous Studies ?	60
3.8 Discussion and Conclusions	62

CHAPTER 4 : A Description of Rainfall Interception	68
Over Large Areas	
4.1 Introduction	68
4.2 Rutter Model of Interception	73
4.3 A Description of Rainfall Interception Over Large Areas	76
4.4 Simulations of Rainfall Interception in a Rain-forest Environment	82
4.5 Conclusions	86
CHAPTER 5 : Description of the Climate Model	89
5.1 Introduction	89
5.2 The MM4 Model for Meteorological Studies	89
5.3 The MM4 model for Climate Studies	90
5.4 The Biosphere-Atmosphere Transfer Scheme	91
5.5 Modifications of the Land-surface Hydrology Scheme	92
CHAPTER 6 : Sensitivity of Regional Climate to	96
Small-scale Deforestation	
6.1 Introduction	96
6.2 Design of Experiments	97
6.3 Boundary and Initial Conditions	101
6.4 Results for January	101
6.4.1 January Climate : Pre-Deforestation	102
6.4.2 January Climate : Post-Deforestation	117
6.5 Results for July	118
6.5.1 July Climate : Pre-Deforestation	118
6.5.2 July Climate : Post-Deforestation	126
6.6 Discussion and Conclusions	133
CHAPTER 7 : Sensitivity of Regional Climate to	136

Large-scale Deforestation	
7.1 Introduction	136
7.2 Effects of Deforestation on Climate	141
7.3 A Simple Model of the Tropical Atmosphere	143
7.4 Response of Tropical Atmosphere to Deforestation of Amazon Rain-forest	147
7.5 Sensitivity of Amazonian Runoff to Large-scale Deforestation	156
7.6 Concluding Discussion	159
CHAPTER 8 : Conclusions	162
8.1 Introduction	162
8.2 Summary of the Results	162
8.2.1 Precipitation Recycling in the Amazon Basin	162
8.2.2 Modelling of Rainfall Interception Over large Areas	163
8.2.3 Sensitivity of Regional Climate to Small-scale Deforestation	164
8.2.4 Sensitivity of Regional Climate to Large-scale Deforestation	165
8.3 General Conclusions	166
8.4 Future Research	171
REFERENCES	173
APPENDICES	
3.1 Relative Magnitude of the Change in Water Vapor Storage	179
4.1 Interception in BATS	181
4.2 Shuttleworth Interception Scheme	182

4.3 Continuity Equation for the New Interception Scheme	184
7.1 Analytical Solution of the Linear Model	186
BIOGRAPHICAL NOTE	188

LIST OF FIGURES

Figure		
1.1	The Amazon basin. (from Molion (1975)).	18
1.2	Schematic of the study outline.	21
3.1	Schematic of the atmospheric control volume.	40
3.2	Comparison between atmospheric fluxes of water vapor and rate of change in water vapor storage at a grid point in the Amazon basin, from ECMWF data set.	42
3.3	Flow chart of the estimation procedure.	45
3.4	Comparison of the evaporation estimates for Manaus, from the ECMWF data set and from the ARME experiment.	48
3.5	Spatial distribution of annual recycling in the Amazon basin.	51
3.6	Spatial distribution of precipitation recycling for the different months. (a) March (b) June (c) August (d) December	52
3.7	Distribution of water vapor flux over the Amazon basin, in cubic kilometer. (a) June (b) December	54
3.8	Evaporation in the Amazon basin, in mm/month, (a) June (b) August	56
3.9	Seasonal variability of precipitation recycling ratio in the Amazon basin.	57
3.10	Scaling of the precipitation recycling ratio.	59
3.11	Hydrologic cycle of a closed atmospheric system.	61
3.12	Water vapor flux at the boundaries of the Amazon basin.	63
3.13	Hydrologic cycles, (a) the Amazon basin, (b) the Mississippi basin.	64
4.1	Comparison of interception loss from the simulations of Dickinson and Henderson-Sellers (1988) with the observations of Shuttleworth (1988a).	70
4.2	Drainage function of the new interception scheme.	78

Figure		
4.3	Comparison of the drainage function of the Rutter model and the drainage function of the new interception scheme.	79
4.4	Interception loss function of the new interception scheme.	81
4.5	Comparison of interception loss simulated by the Rutter model, BATS interception, Shuttleworth interception scheme and the new interception scheme.	85
6.1	Location of the numerical experiment.	98
6.2	Location of the deforested region.	99
6.3	Sea level pressure in mb, for January, ECMWF data and differences between the simulated fields and the observed fields.	103
6.4 (a)	Temperature in ° K at 850 mb, ECMWF data and differences between the simulated fields and the observed fields.	104
6.4 (b)	same as 6.4(a) except at 500 mb.	105
6.4 (c)	same as 6.4(a) except at 200 mb.	106
6.5 (a)	Mixing ratio at 850 mb, for January, ECMWF data and differences between the simulated fields and the observed fields.	107
6.5 (b)	same as 6.5(a) except at 500 mb.	108
6.5 (c)	same as 6.5(a) except at 200 mb.	109
6.6	Ground temperature in ° C, for January, (a) pre-deforestation field (b) (post-deforestation field- pre-deforestation field).	111
6.7	Air temperature in ° C, for January, (a) pre-deforestation field (b) (post-deforestation field- pre-deforestation field).	112
6.8	Net surface energy in W/m ² , for January, (a) pre-deforestation field (b) (post-deforestation field- pre-deforestation field).	113

Figure		
6.9	Evaporation in mm, for January, (a) pre-deforestation field (b) (post- deforestation field- pre-deforestation field).	114
6.10	Precipitation in mm, for January, (a) pre-deforestation field (b) (post- deforestation field- pre-deforestation field).	115
6.11	Sea level pressure in mb for July , ECMWF data and differences between the simulated fields and the observed fields.	119
6.12 (a)	Temperature in ° K at 850 mb for July, ECMWF data and differences between the simulated fields and the observed fields.	120
6.12 (b)	same as 6.12(a) except at 500 mb.	121
6.12 (c)	same as 6.12(a) except at 200 mb.	122
6.13 (a)	Mixing ratio at 850 mb for July, ECMWF data and differences between the simulated fields and the observed fields.	123
6.13 (b)	same as 6.13(a) except at 500 mb.	124
6.13 (c)	same as 6.13(a) except at 200 mb.	125
6.14	Ground temperature in ° C for July, (a) pre-deforestation field (b) (post- deforestation field- pre-deforestation field).	128
6.15	Air temperature in ° C, for July, (a) pre-deforestation field (b) (post- deforestation field- pre-deforestation field).	129
6.16	Net surface energy in W/m ² , for July, (a) pre-deforestation field (b) (post- deforestation field- pre-deforestation field).	130
6.17	Evaporation in mm, for July. (a) pre-deforestation field (b) (post- deforestation field- pre-deforestation field).	131
6.18	Precipitation in mm, for July, (a) pre-deforestation field (b) (post- deforestation field- pre-deforestation field).	132

Figure		
7.1	Predictions of the regional climatic change due to deforestation of the Amazon rainforest, (a) temperature change ,(b) evaporation change, (c) precipitation change and (d) change in the wind vector at 700 mb.	139
7.2	The forcing function of Equation 7.8 .	151
7.3	The boundary layer circulation resulting from forcing the model with (a) precipitation forcing, (b) temperature forcing and (c) both precipitation and temperature. The forcings are estimated from the results of Nobre et al. (1991).	152
7.4	The boundary layer circulation resulting from forcing the model with (a) precipitation forcing, (b) temperature forcing and (c) both precipitation and temperature. The forcings are estimated from the results of Dickinson and Henderson-Sellers (1988).	153
7.5	Sensitivity of Amazonian runoff to large-scale deforestation.	158
8.1	Effects of large-scale deforestation on climate.	169

LIST OF TABLES

4.1	Description of the model forcings.	83
6.1	Parameters of land cover and soil for rain-forest and short grass environments.	100
6.2	Pre-Deforestation climate in January.	110
6.3	Sensitivity of regional climate to small-scale deforestation in the Amazon Basin.	116
6.4	Pre-Deforestation climate in July.	127
7.1	Predictions of the spatially-averaged regional changes in key atmospheric variables due to deforestation of the Amazon rainforest.	138
7.2	Estimates of the forcings due to the predicted changes in surface temperature, precipitation and deforestation in the Amazon.	148
7.3	Predictions of the spatially averaged regional changes in key atmospheric variables and the corresponding forcings from the experiments of Lean and Warrilow (1989)	155

LIST OF NOTATIONS

α	infiltration capacity of the surface layer when completely dry
b	parameter of the Rutter Model
a, b	constants in the linear model of the tropical atmosphere
β	derivative of the Coriolis parameter with respect to distance
C	canopy storage
C_m	maximum storage capacity of canopy
c	wave speed
D_r	canopy drainage
D_m	maximum canopy drainage
E	evaporation
e	evapotranspiration
e_c	evaporation from wet canopy
e_s	saturation vapor pressure
e_t	transpiration by plant
e'	interception loss
ϵ	coefficient of Rayleigh friction
F	observed flux of water vapor
FG	forcing of the linear model
f	Coriolis parameter
f^*	infiltration capacity of the surface layer
Φ'	mass-weighted integral of perturbation in geopotential height in the boundary layer
g	gravitational acceleration
I	inflow of atmospheric moisture
i	climatological rainfall intensity
K, b	constants in the Rutter model
L	linear scale
N	number of molecules of water vapor
P	precipitation
p	fraction of rain falling directly to the ground
P_j	pressure level

P'	perturbation to precipitation field
O	outflow of atmospheric moisture
ρ	precipitation recycling ratio
RH	relative humidity
r	surface runoff
U	wind speed
S	parameter of the Rutter model
s	soil saturation of the surface layer
T	temperature
T_s'	perturbation to surface temperature field
u',v'	perturbations in horizontal components of mass flux in the boundary layer
w'	perturbation to the vertical velocity field above the boundary layer
q_p	fraction of area with rainfall greater than zero
q_c	fraction of area with canopy storage greater than zero

CHAPTER 1

Introduction

1.1 Scope

The recent interest in studying hydrologic processes over large areas is motivated by the need to include descriptions of these processes in models of the land-atmosphere-ocean system. These models are the appropriate tools for studying global environmental problems such as possible climatic changes due to observed increase in greenhouse gases, and the possible impact of deforestation on climate. The results of the early experiments using these models suggest that hydrologic processes at the land-atmosphere boundary play a significant role in the dynamics of the system. The realization that land-surface hydrology is not a passive component of the land-atmosphere system opened the way for new approaches in the study of hydrologic processes over large areas. New interesting questions are being asked about the role of the hydrologic cycle, and the possible effects on climate which may result from natural or anthropogenic changes in the hydrologic cycle.

The subject of this study is the hydroclimatology of the Amazon basin. The focus is on the complete hydrologic cycle including both the land phase and the atmospheric phase. Considered is the continental scale of the Amazon basin which covers about six millions squared kilometers, see Figure 1.1. The objective of the study is to improve our understanding of the role of hydrology in the land-atmosphere system of that region. The data used is part of the global data set provided by the European Center for Medium Range Weather

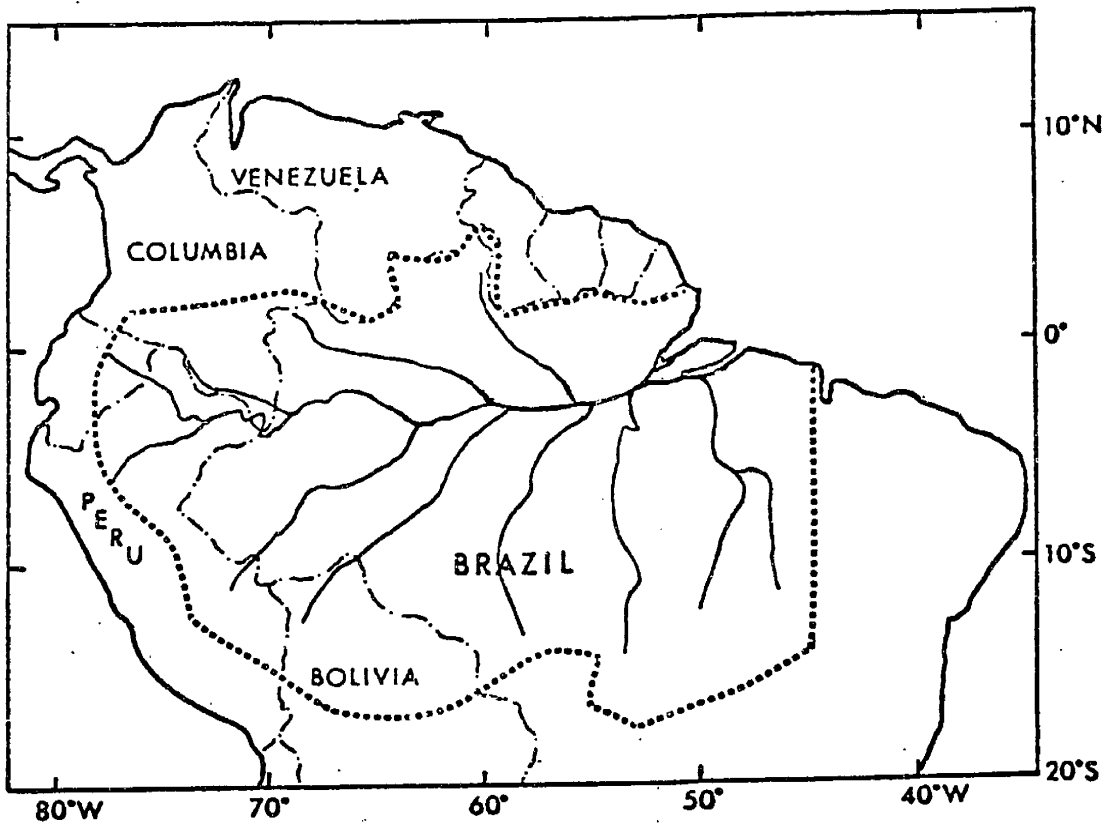


Figure 1.1 The Amazon basin. (from Molion (1975))

Forecast (ECMWF). The hydrologic cycle is treated as an active component of a complex geophysical system which includes the atmosphere and the land-surface. The basic questions raised are about the estimation of the different components of the hydrologic cycle and about the response of the land-atmosphere system to possible changes in the hydrologic cycle.

The study consists of three parts: the first part provides new estimates of spatial and temporal distribution of a precipitation recycling ratio. The recycling process is studied over different scales ranging from the scale of the Amazon basin (~2500 kilometers) to the resolution of the data (~250 kilometers). The second part of the study outlines the development of a new scheme for describing rainfall interception over large areas. The new interception scheme is included as part of the climate model which is used in the third part. The last part of this study focuses on the sensitivity of regional climate to changes in land-surface properties. The changes considered are those due to small-scale and large-scale deforestation in the Amazon basin.

The first and third parts of this thesis consist of diagnostic and prognostic studies on the hydroclimatology of the Amazon basin. While the first part describes a diagnostic measure of the potential for interactions between land-surface hydrology and regional climate in the Amazon basin, the third part is a prognostic study of those interactions. The first part is about the role of regional hydrologic processes in the current climate equilibrium, and the third part deals with the sensitivity of regional climate to possible changes in these hydrologic processes which are caused by deforestation.

1.2 Outline

The outline of this work is summarized schematically in Figure 1.2. The thesis is organized in eight chapters. Chapter 2 is a literature review of the relevant research. Chapter 3 describes the study on precipitation recycling in the Amazon basin. Chapter 4 outlines the development of a new rainfall interception scheme. Chapter 5 describes the model which is used for studying the effects of small-scale deforestation on climate. The sensitivity of regional climate to small-scale deforestation is described in Chapter 6. The possible effects of large-scale deforestation on the regional climate of the Amazon basin are discussed in Chapter 7. The conclusions of this study are presented in Chapter 8.

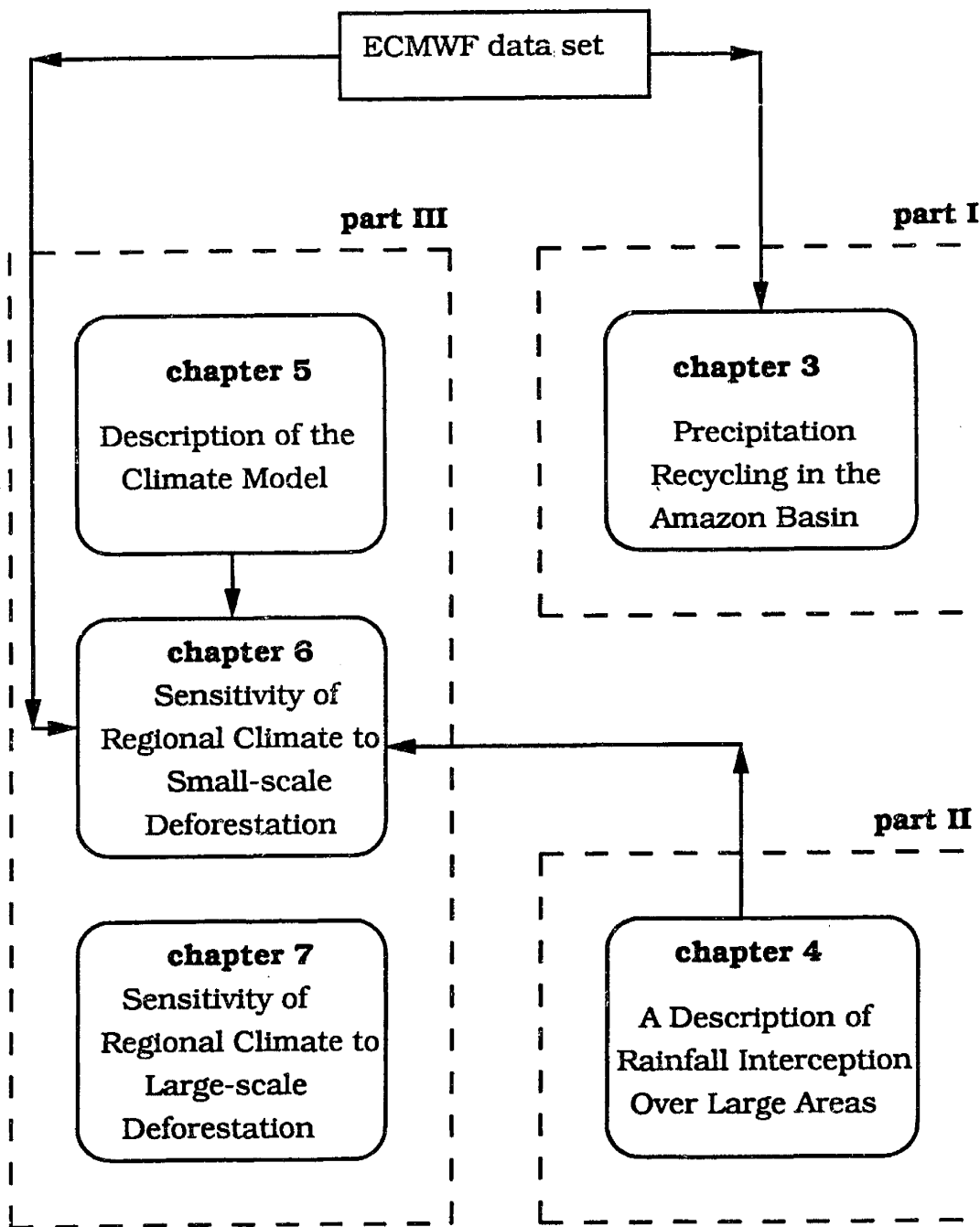


Figure 1.2 Schematic of the study outline

CHAPTER 2

Literature Review

2.1 Introduction

This Chapter presents a general review of previous research dealing with the interactions and feedbacks between hydrology and climate. The following chapters will also include some detailed discussion of the relevant research. The general review is presented in three sections: the role of hydrologic processes in regional climate, precipitation recycling and dynamics of rainfall, and hydrologic studies in the Amazon basin.

2.2 Hydrologic Processes and Regional Climate

Holzman (1937) cites the words of S. Aughey who wrote in 1880 about the physical geography of Nebraska, " year by year as cultivation of the soil is extended, more of the rain that falls is absorbed and retained to be given off by evaporation or to produce springs. This of course must give increasing moisture and rainfall ". This is one of the earliest speculations, in the literature, about the role of evaporation from land surfaces and the possible impacts of changes in land use on regional rainfall and climate. It suggests that local moisture recycling has a significant contribution to atmospheric moisture and rainfall. This theory was widely accepted until the early decades of the present century. No rigorous proof was provided and indeed the data available was not enough for such a purpose. The data was limited to hydrologic data and surface meteorological data from few scattered stations.

In early years of the present century more hydrologic data became available and various estimates of regional precipitation, evaporation and runoff were obtained. It was estimated that around 30% of total precipitation over continental areas returns to the oceans by surface runoff and the remaining 70% evaporates back to the atmosphere. These new findings lead many researchers to conclude that 70% of total precipitation over the continents is contributed by evaporation from land areas. These conclusions are based on a simple and inaccurate picture of the hydrologic cycle where atmospheric moisture inflow is equal to runoff and hence recycled precipitation is equivalent to evaporation. But surface runoff is, in general, equivalent to the convergence of atmospheric moisture.

Many other studies contributed to the theory that evaporation from land surfaces has a significant effect on regional rainfall and climate. Jensen (1935) analyzed annual rainfall series from midwestern United States to study drought in that region. The observation that deficiency in rainfall was significantly larger in eastern and central Nebraska than in the western parts lead him to speculate that this trend is associated with the advent of irrigation in western Nebraska. It was further suggested that dams should be built to impound runoff and hence increase evaporation and rainfall. Ives (1936) described observed desert floods in Sonoyta valley in Mexico and classified floods into primary and secondary according to the origin of the moisture in rainfall. Primary floods are caused by rainfall whose moisture comes from outside the valley while secondary floods are caused by rainfall whose moisture comes from

within the valley. This classification was based on purely subjective visual description of the conditions in the valley !.

An excellent review of the research in this topic is presented by Holzman (1937), he criticized the long held view that continental evaporation contributes significantly to atmospheric moisture or rainfall and pointed to the lack of rigorous proof supporting this theory. He used upper air meteorological data to estimate atmospheric water depths and upper air wind. Most of the previous research was limited to analysis of surface meteorological data. The paper argues that the contribution of evaporation to atmospheric moisture and rainfall is not significant due to the great mobility of atmospheric air masses. It emphasized the important role of rainfall producing mechanisms and suggested that no direct relation exists between atmospheric moisture over any region and rainfall. The paper concludes that most of the supply of moisture for precipitation over the United States is derived from maritime air masses that obtain their moisture mainly from evaporation over the oceans, only a very small part is attributable to continental evaporation. The principal amount of moisture returned to the atmosphere by continental evaporation is absorbed by dry continental air masses that, in general, do not produce rainfall over continents.

Horton (1943) estimated the contribution of the different moisture sources to precipitation in eastern United States. He studied the variability of chlorine content in runoff and deduced that the contribution of oceanic water in rainfall varies from 100 % at the Atlantic coast to about 5 % at 300 miles west of New York city !. This finding lead to the conclusion that "little or no vapor of truly oceanic

origin may ever reach small tributary areas at the headwaters of large rivers ". It seems that the tracer used in this study was influenced by some factors other than the moisture source.

Although hydrology is defined as the study of the complete hydrologic cycle, which includes atmospheric and land phases, most of the water balance studies are carried for the land phase only. Benton et al. (1950) studied the role of the atmosphere in the hydrologic cycle. They focused on the water balance of the Mississippi basin, considering both the atmospheric and the land phases of the hydrologic cycle. They followed an approach similar to that of Holzman (1937) in relating the hydrologic cycle to the air mass cycle. Air masses are classified into maritime and continental. Maritime air masses originate from the gulf of Mexico or the Pacific ocean, continental air masses originate from Canada, Arctic or the southwest. In classifying the air masses they analyzed precipitation and upper air meteorological data at Huntington station for one year. The results of the water balance suggest that 90% of precipitation comes from maritime air masses and 10% from continental air masses. Precipitation over the basin is equivalent to about 20% of moisture advection into the basin. Benton et al. (1950) concluded that "modification of the evapotranspiration regime even over a wide spread area can have comparatively little direct effect on the average quantity of precipitation recorded or that on neighboring region". It is interesting to note that although 80% of precipitation evaporates back to the atmosphere, precipitation recycling contribution is very small.

In a rather humorous paper McDonald (1962) criticized the suggestions that local precipitation may be increased by increasing local evaporation. He emphasized two basic misconceptions regarding the role of rainfall producing mechanisms and the scales involved in the hydrologic cycle pointing that on average water molecules travel for hundreds of miles before precipitating.

Most of the above referenced studies focused on the United States, Budyko (1974) studied the precipitation recycling process in USSR, he used the ratio of total precipitation to precipitation of advected origin, β , as a measure for the significance of recycling process. This measure assumes complete mixing of the advected and the evaporated moisture. β is estimated for the European part of the USSR as 1.12, which implies a contribution of local evaporation of about 10 %.

How significant are the effects of irrigation projects on regional climate is a controversial subject. A classical example is the Columbia Basin Project, Washington, which is one of the most studied cases. The size of the project is 200,000 hectares, it was developed in the period 1950 - 1965 and the water supplied for irrigation is about 3 cubic kilometers. Fowler and Helvey (1974) found little or no change in July temperature which is attributable to the development of the project, although they detected a significant positive trend in evaporation data collected in the basin. Stidd (1975) analyzed summer (July and August) rainfall measured at about a hundred stations located within 240 kilometers from the center of the project. The stations within the Columbia basin were classified as target stations and these are located, roughly, within 200 kilometers from the

center, the rest of the stations are the control stations. The measure used in the analysis is the ratio of mean summer rainfall for the period (1959 - 1973) to the normal. The normal is estimated by the mean for the period (1931 - 1950). It is found that this measure computed from the target stations is significantly larger than that for the control stations. A reasonable explanation is that the moisture added by irrigation enhanced evaporation and resulted in increased precipitation. Fowler and Helvey (1975) questioned the length of the record used in estimating normal rainfall and pointed to the possible effects of the bias in those estimates.

Charney (1973) describes a mechanism which emphasizes the effects of surface albedo in the dynamics of deserts and droughts. A reduction in rainfall may result in loss of vegetation cover, increased reflection of solar radiation and hence local cooling, which modifies the atmospheric circulation favoring even further reduction in rainfall. In a humid climate the loss of vegetation results in a significant decrease of evaporation and hence local heating, for this reason the Charney mechanism is more applicable to semi-arid regions where evaporation rates are relatively small e.g. the Sahel.

An important question related to precipitation recycling is the distribution in space of precipitation resulting from any evaporation event. Koster et al. (1986) developed a tracer model built within a General Circulation Model(G.C.M) which allows to " tag " moisture evaporated at any location and determine where and how much of it precipitates.

2.3 Precipitation Recycling and Rainfall Dynamics

The rate of evaporation at any location depends to some extent on the availability of water from previous rainfall events. In a region where evaporation contributes significantly to atmospheric water vapor and hence to rainfall, it is plausible that rainfall dynamics should reflect this feedback mechanism. The significance of this mechanism and its spatial and temporal scales depend on the control exerted on evaporation by the land system and also on the rainfall producing mechanism.

There were early speculations about the possible feedback in regional precipitation due to recycling. McNish (1936) discussed the statistical nature of some meteorological time series and offered the following mechanism as a physical cause of correlation in rainfall over the central part of a continent, " a year during which the rainfall has been very great will result in the accumulation of considerable groundwater which by its subsequent evaporation through the soil will supply humidity to the air giving rise to further rainfall and tending to perpetuate the wet cycle until the development of some other condition causes a change in this trend ". He did not support this theory by analyzing observed data or even specifying a region of the world where such a mechanism may be evident.

The Bahr Elghazal basin in Sudan is an interesting hydrologic system, all the rainfall in that basin is lost in evaporation. The high evaporation rates in the basin, which is equivalent to one meter per year, suggests a significant role in the regional climate. Chan and Eagleson (1980) speculated that draining of Bahr Elghazal swamps may have impacts on the regional climate. Eltahir (1989) suggested a feedback mechanism applicable to regions with large swampy areas or

shallow lakes. A wet year increases the storage volume of the swamp and hence extends its surface area and results in increased evaporation in that year and the following years. The increase in evaporation may result in increased rainfall over the swamp and in the surrounding regions. A wet year favors wet following years and vice versa. The water balance dynamics of the Bahr Elghazal swamps and the observed dependence in annual rainfall series in the surrounding regions are consistent with this mechanism.

Rodriguez-Iturbe et al. (1990a) presented a model which describes the inter-annual soil moisture dynamics at the regional scale. The model assumes that recycled precipitation is partly a function of evaporation; advection of atmospheric water vapor is assumed constant. Evaporation is nonlinearly related to the degree of saturation of the active soil depth; infiltration is treated in a similar way. The analytic solution of the stochastic soil moisture differential equation results in a bimodal distribution for the spatially averaged soil saturation. The report argues that this bimodal distribution may explain some of the features observed in rainfall time series in the Sahel region of Africa, namely the prolonged wet and dry periods. In a companion report Rodriguez-Iturbe et al. (1990b) analyzed the behavior of the inter-seasonal soil moisture dynamics. The nonlinear water balance equation exhibits a chaotic behavior which implies limited predictability of the soil moisture state. These findings emphasize that the nonlinearity introduced into the simple soil moisture balance equation in representing the recycling process may result in a very interesting behavior, which is totally different than

the results obtained by ignoring the dependence of rainfall on soil moisture.

2.4 Hydrologic Studies in the Amazon Basin

The Amazon river basin is one of the most studied regions, it has the largest annual discharge of about 5500 cubic kilometers. The area of the basin is about 6.3×10^6 squared kilometers. It has a unique topographical setting with a mild slope from west to east, open from the east to the easterly flow from the Atlantic ocean and bounded in the other three directions by highlands and mountains.

In 1970 the Brazilian government announced a plan for integration of the basin by moving people from other parts of the country into the Amazon region. This plan may result in deforestation of about 45% of the rainforest. Molion (1975) carried a "climatonomic" study of the Amazon basin considering the effects of deforestation. Climatology is a methodology to study energy and water balance of land and the atmosphere, it uses some of the concepts of linear systems theory. The Amazon basin is divided into six subregions each 5° longitude wide. The atmospheric fluxes of moisture across these subregions were estimated from the maps of Newell et al. (1972). Those maps are based on data from three stations extending for only two years. Precipitation and surface meteorological data from forty stations were analyzed for the period (1931-1960). The net vapor exchange over the basin was estimated at about 50% of total precipitation. The study of Molion (1975) provides a rough estimate of the water balance of the atmosphere and land surface in the Amazon basin.

Precipitation recycling plays a significant role in the Amazon basin, Lettau et al. (1979) estimated that about "88% of the water precipitating in the western subregion falls at least a second time from the air", this estimate was made by computing the ratio of precipitation observed in the subregion to an estimate of precipitation of oceanic origin, the ratio found is 1.88. Based on this estimate we compute that the ratio of the precipitation of local origin to the total precipitation observed in that subregion is given by $(1 - (1/1.88) = 0.47)$. Hence, the conclusion of Lettau et al (1979) is incorrect; it should be restated with 47% replacing 88%.

An attractive procedure for identifying the sources of precipitation water is the isotopic analysis of the natural composition of water. Fractionation takes place when water undergoes condensation or evaporation, naturally heavy isotopes favor the liquid phase. Due to condensation the atmospheric water vapor is gradually depleted in heavy isotopes as it moves across the Amazon basin from the east to the west. Salati et al. (1979) analyzed data of the O^{18} concentration from different stations in the basin and found that the inland gradient is smaller than those observed in other regions, e.g. in Europe. They attributed this difference to the significant contribution of local evaporation to atmospheric water vapor. A major difficulty in isotope hydrology is the non-uniqueness of the data interpretation, e.g. temperature effects and sub-cloud conditions may contribute to the variability in isotopic composition.

It is speculated that deforestation of the Amazon rainforest may have impacts on the Earth climate. Newell (1971) indicated that "the study by atmospheric modeling of the Brazilian and other proposed

tropical changes is a little above CO₂ in my list of priorities and a little below stratospheric aerosol problem". Dickinson (1981) suggested that global climate changes due to even complete tropical deforestation are not likely to be larger than natural climate fluctuations but that regional climate changes are likely to be considerably larger. Dickinson and Henderson-Sellers (1988) used a General Circulation Model (G.C.M.) for studying the possible effects on climate due to deforestation of the whole Amazon basin. They predicted a decrease in evaporation and rainfall and increase in runoff and surface temperature, these effects extend roughly over the whole basin with no further global effects. In similar studies Lean and Warrilow (1989), Shukla et al. (1990) and Nobre et al. (1991) predicted a decrease in evaporation and rainfall and an increase in surface temperature, but they also found a decrease in runoff. Shukla et al. (1990) and Nobre et al. (1991) are reporting on the same experiment. Salati and Vose (1984) discussed the impact of deforestation on the hydrologic cycle and on the whole ecosystem.

An interesting hydrologic study is the Amazon Region Micrometeorological Experiment (ARME), due to the importance of this study it is described with some detail.

2.4.1 Amazon Region Micrometeorological Experiment (ARME)

ARME is an Anglo-Brazilian collaboration which took place in the period September 1983 - September 1985 over undisturbed tropical rainforest at a site which is located at 25 kilometers distance northeast from the city of Manaus in the central Amazon basin. The objective of the experiment was to collect hydrological data about the

rainforest biomass which can be used in calibrating climate models. Despite the on-going human interventions, the Amazon basin is relatively a uniform natural formation and hence intensive data collection at a single well chosen site may be very useful in calibrating land surface hydrology in climate models.

Throughout the experiment routine measurements of temperature, humidity, wind speed and rainfall were taken from a tower extending above the 35 meters high canopy. Soil tension and throughfall were also routinely monitored. During the experiment three intensive campaigns were carried out to measure evaporation, sensible heat flux and momentum flux using the HYDRA instrument which integrates eddy correlation measurements to calculate these fluxes. During these campaigns radiation components were also measured above the canopy and at the ground. This data has been analyzed and fitted to a Penman-Monteith-Rutter model to describe interception and evapotranspiration. This model is a combination of the Peman-Monteith evapotranspiration model and the interception model of Rutter et al. (1971). The parameters of the model have been calibrated using the data collected in the intensive campaign periods and the routine measurements were used in estimation of evapotranspiration and interception losses for the period of the experiment, Shuttleworth (1988a).

Although monthly evapotranspiration estimated by the Penman-Monteith-Rutter model are very close to estimates of monthly potential evaporation, daily estimates are significantly different. Evapotranspiration is about 25% less than potential evaporation in dry days and about 50% greater than potential evaporation in wet

days. This is explained by the increased resistance of the transpiration process in the dry days and the fact that roughness of the canopy enhances evaporation of intercepted rain in the wet days. These findings underline the importance of accurate modeling of interception in this region.

Some of the results of this experiment are summarized in the followings:

- (1) About 50% of rainfall evaporates to the atmosphere.
- (2) 25 % of evaporation is from intercepted rain.
- (3) Solar radiation reaching the surface is in the order of 1% of that at the top of the canopy.
- (4) Active soil depth is about 1 meter.
- (5) Energy available for evaporation from the bare soil is in the order of 4 watts per square meter, which is small compared to evaporation from the canopy.

CHAPTER 3

Precipitation Recycling in the Amazon Basin

3.1 Introduction

Precipitation recycling is the contribution of evaporation within a region to precipitation in that same region. The studied region can be part of the ocean, the land or it may contain both ocean and land surfaces. The estimates of precipitation recycling for a continental land mass provide a measure of the potential for interactions between land surface hydrology and regional climate. A high estimate of precipitation recycling is not sufficient to conclude a strong role for land surface hydrology in the regional climate. It rather suggests a strong potential for that role; by strong role we mean that significant changes in surface hydrology necessarily result in significant impacts on the regional climate. On the other hand a low estimate of precipitation recycling implies that the only possible role of land surface hydrology is through the effects of vegetation on the surface albedo. Hence studying precipitation recycling of land areas provides useful information on the possible interactions of hydrology and climate.

The current rates of deforestation in the Amazon have prompted wide concern about the possible impacts of deforestation on climate. Previous studies, e.g. Dickinson and Henderson-Sellers (1988) , Lean and Warrilow (1989) and Shukla et al. (1990), have focused on the impacts on regional climate due to deforestation of the Amazon rain-forest. The precipitation recycling model which will be described in this Chapter is developed primarily for studying recycling in the

Amazon; but the model formulation is general and hence applicable to other regions.

Early studies of precipitation recycling focused on the continental land mass of North America. While McNish (1936) and Horton (1943) and other researchers suggest that the contribution of evaporation from land regions to precipitation in the same regions is significant, the studies of Holzman (1937), Benton et al. (1950), and McDonald (1962) criticize these suggestions and emphasize the large mobility of atmospheric air masses and the important role of rainfall producing mechanisms. Most of the above studies involved limited data analysis and little theoretical description of the recycling process.

Budyko (1974) developed a model for estimating recycling in large regions. Budyko's model describes the process along a single streamline and provides a lumped estimate of recycling. Budyko (1974) used the model to estimate recycling in the European part of USSR and estimated that the contribution of recycled precipitation is about 10%. In a recent study, Brubaker et al. (1991) modified Budyko's model to account for the fact that the spatial orientation of the region under study may not lie parallel to a streamline. The modified model is used in studying recycling in different regions of the world including the Amazon basin. It is estimated that recycling in the Amazon basin varies in the range of 15% to 30% in the different months.

Many previous studies have provided estimates for precipitation recycling in the Amazon basin. Molion (1975) estimates that recycled precipitation accounts for about 56% of the total precipitation. This estimate is the ratio of total evaporation to total precipitation in the

basin. The accuracy of this estimate will be discussed in section 3.7. Lettau et al. (1979) presented a model of recycling based on their climatology theory. The model describes the recycling process along a single streamline. Lettau et al. (1979) estimate that the contribution of recycled precipitation varies from about 16% at the eastern subregion to 47% at the western subregion of the Amazon basin.

Salati et al. (1979) analyzed data of the O^{18} concentration from different stations in the Amazon basin and found that the inland gradient is smaller than those observed in Europe. They attributed this difference to the significant contribution of local evaporation to atmospheric water vapor. The isotopic data collected in the Amazon basin is inhomogeneous which may indicate significant spatial and seasonal variability in the recycling process. A comparison between the isotopic composition of the advected vapor flux and the isotopic composition of the river discharge indicates a significant flux of water vapor out of the basin. Although isotopic analysis provides useful information about the recycling process, it is difficult to make quantitative estimates of recycling based solely on isotopic data. That is why the study of Salati et al. (1979) does not provide a quantitative estimate of recycling in the Amazon. Models of precipitation recycling which utilize water vapor flux and evaporation data, e.g. the models of Budyko (1974) and Lettau et al. (1979), provide these quantitative estimates.

In this Chapter we present a model of precipitation recycling which describes both the spatial and the seasonal variability of the recycling process. The model involves only two assumptions, it assumes that atmospheric water vapor is well mixed and that the rate

of change of storage of water vapor is negligible compared to water vapor fluxes at the time scale for which the model is applicable. We discuss observational evidence which indicate that both assumptions are reasonable idealizations of the real world.

This Chapter is organized in eight sections. Section 3.2 outlines the development of the new recycling model. Section 3.3 compares the new recycling model with similar recycling models from previous studies. The details of the estimation procedure are presented in Section 3.4. The application of the model to the Amazon basin is described in Section 3.5. It includes estimates of the seasonal and spatial distributions of precipitation recycling. Section 3.6 discusses the scaling of the precipitation recycling ratio in the Amazon basin. Section 3.7 explains why previous studies overestimated precipitation recycling in the Amazon basin. Section 3.8 includes discussion and conclusions of this study.

3.2 Precipitation Recycling Model

In developing this model we consider two species of water vapor molecules: those which evaporate outside the region and molecules which evaporate within the region. The definition of the word "region" includes all the area under study, e.g., the Amazon basin. It is not restricted to the area of a single grid point. For a finite control volume of the atmosphere located at any point within the region, conservation of mass requires the following :

$$\frac{\partial N_w}{\partial t} = I_w + E - O_w - P_w \quad (3.1)a$$

$$\frac{\partial N_o}{\partial t} = I_o - O_o - P_o \quad (3.1)b$$

where w denotes molecules which evaporate within the region and o denotes molecules which evaporate outside the region. The variables which appear in the above equations are defined as follows: I and O are inflow and outflow, P is precipitation, and E is evaporation (see Figure 3.1). N , I , O , P and E are variables in space and time. Each of I and O is a summation of the components of flux in the two horizontal directions.

It is observed that water vapor is well mixed in the Planetary Boundary Layer (PBL) of the Earth's atmosphere. The depth of the PBL is in the order of one kilometer and contains most of the water vapor in the atmosphere. Observations of the vertical distribution of water vapor and other conserved tracers show a practically uniform distribution through the PBL up to the level where the air from the PBL mixes with the upper air. (for observations in mid-latitudes see Crum and Stull (1987), for observations from the Amazon region see Harris et al.(1988) and companion papers describing the Amazon Boundary Layer Experiment (ABLE)). Mixing of water vapor in the PBL is primarily achieved by dry thermal convection. This process is very efficient in mixing of water vapor and other pollutants. Lamb (1982) compiled the results of many field experiments studying air pollutants which are released at the surface, the data indicate that mixing in the PBL occurs at very short time scales. It takes about 15 minutes for water vapor molecules evaporating at the surface to mix

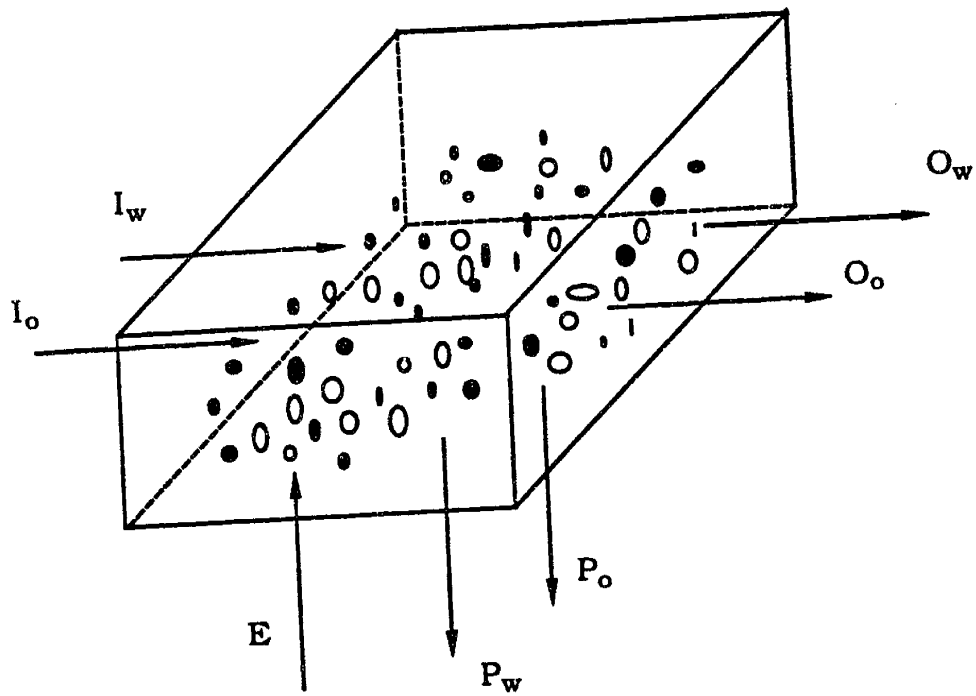


Figure 3.1 Schematic of the atmospheric control volume.

in the vertical for up to a depth of one kilometer. Above the boundary layer it is frequently observed that the air forming clouds mixes with the surrounding environment, Paluch (1979). Based on these observations, we make the assumption that water vapor molecules from the two species defined above are well mixed which implies that

$$\rho = \frac{P_w}{(P_w + P_o)} = \frac{O_w}{(O_w + O_o)} = \frac{N_w}{(N_w + N_o)} \quad (3.2)$$

ρ is defined as the precipitation recycling ratio. At any location within the region, ρ estimates the ratio of recycled precipitation to the total precipitation falling at that location. Recycled precipitation consists of molecules of water vapor which were in the atmosphere as a result of an evaporation event at that location or somewhere else in the region under study.

Figure 3.2 shows a comparison between the monthly outflow of water vapor, evaporation and the change in storage of water vapor at a single location in the Amazon basin. It is evident that at the monthly time scale, the rate of change of storage of water vapor is very small compared to atmospheric water vapor fluxes. This observation combined with the well mixing assumption suggest that change of storage of any of the two species, N_w or N_o , is small compared to its flux (see Appendix 3.1). We then make the assumption that the derivatives in Equation 3.1 are equivalent to zero, rearranging Equation 3.1 we get

$$I_w + E = O_w + P_w \quad (3.3)a$$

$$I_o = O_o + P_o \quad (3.3)b$$

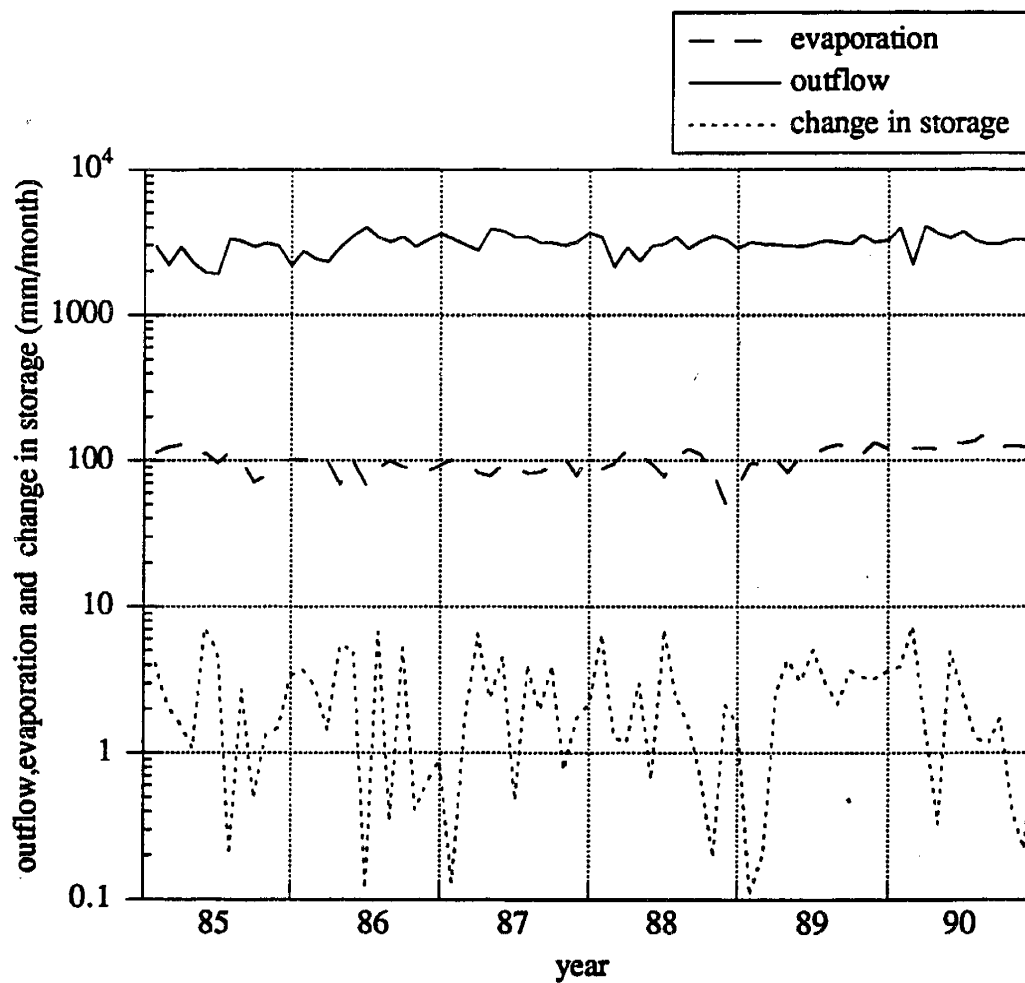


Figure 3.2 Comparison between atmospheric fluxes of water vapor and rate of change in water vapor storage at a grid point in the Amazon basin, from ECMWF data set.

substituting for O_w , P_w , O_o and P_o from Equation 3.2 into Equations 3.3, we get

$$I_w + E = \rho(O_w + O_o) + \rho(P_w + P_o) \quad (3.4a)$$

$$I_o = (1 - \rho)(O_w + O_o) + (1 - \rho)(P_w + P_o) \quad (3.4b)$$

By dividing Equation 3.4a by Equation 3.4b and rearranging, we get

$$\rho = \frac{(I_w + E)}{(I_w + E + I_o)} \quad (3.5)$$

Equation 3.5 is the formula for estimating recycling in this model.

The spatial resolution of the data should be small enough to resolve significant spatial variability in evaporation and fluxes. The temporal resolution should be large enough for the above assumption of negligible change in storage to hold; it should also be large compared to the travel time across the region studied.

3.3 Comparison of Recycling Models

In the following we compare the new recycling model with the models of Budyko (1974) and Lettau et al. (1979). The new model describes the spatial variability of the process in two dimensions while Budyko's model provides a lumped estimate of recycling. The Lettau's model describes the variability of the process in one dimension along a single streamline. Further the new model does not make assumptions about the spatial distribution of evaporation and precipitation while Budyko's model assumes a uniform distribution for evaporation and precipitation. The Lettau's model involves a linearity assumption in relating precipitation to evaporation and

precipitable water. Hence the recycling model introduced in this chapter achieves more in terms of the spatial distribution of the recycling process but makes fewer or milder assumptions.

3.4 Estimation Procedure

The estimation procedure suggested with the new recycling model consists of the following steps which are illustrated by Figure 3.3.

1. The flux and evaporation data are interpolated in a rectangular grid which covers the total area of the region. ρ is estimated at points which lie at half the distance between the grid points.
2. The estimation procedure is a trial and error technique where ρ is first guessed at all points in the data grid. Equation 3.2 is then used in partitioning the flux at every point and in both directions into O_w and O_o . These estimates of fluxes are then used in Equation 3.5 to arrive at improved estimates of the distribution of ρ and the procedure is then repeated. Notice that O_w and O_o for one grid point are I_w and I_o for an adjacent point. This procedure is found to converge very quickly and to be insensitive to the initial guess of ρ .
3. The recycling ratio for the total area of the basin, ρ_t and for any month k is obtained by

$$\rho_t(k) = \sum_{ij} p(i,j,k) \rho(i,j,k) \quad (3.6)$$

where $p(i,j,k)$ is precipitation at the grid box (i,j) and month k normalized by the total precipitation in the basin for that month.

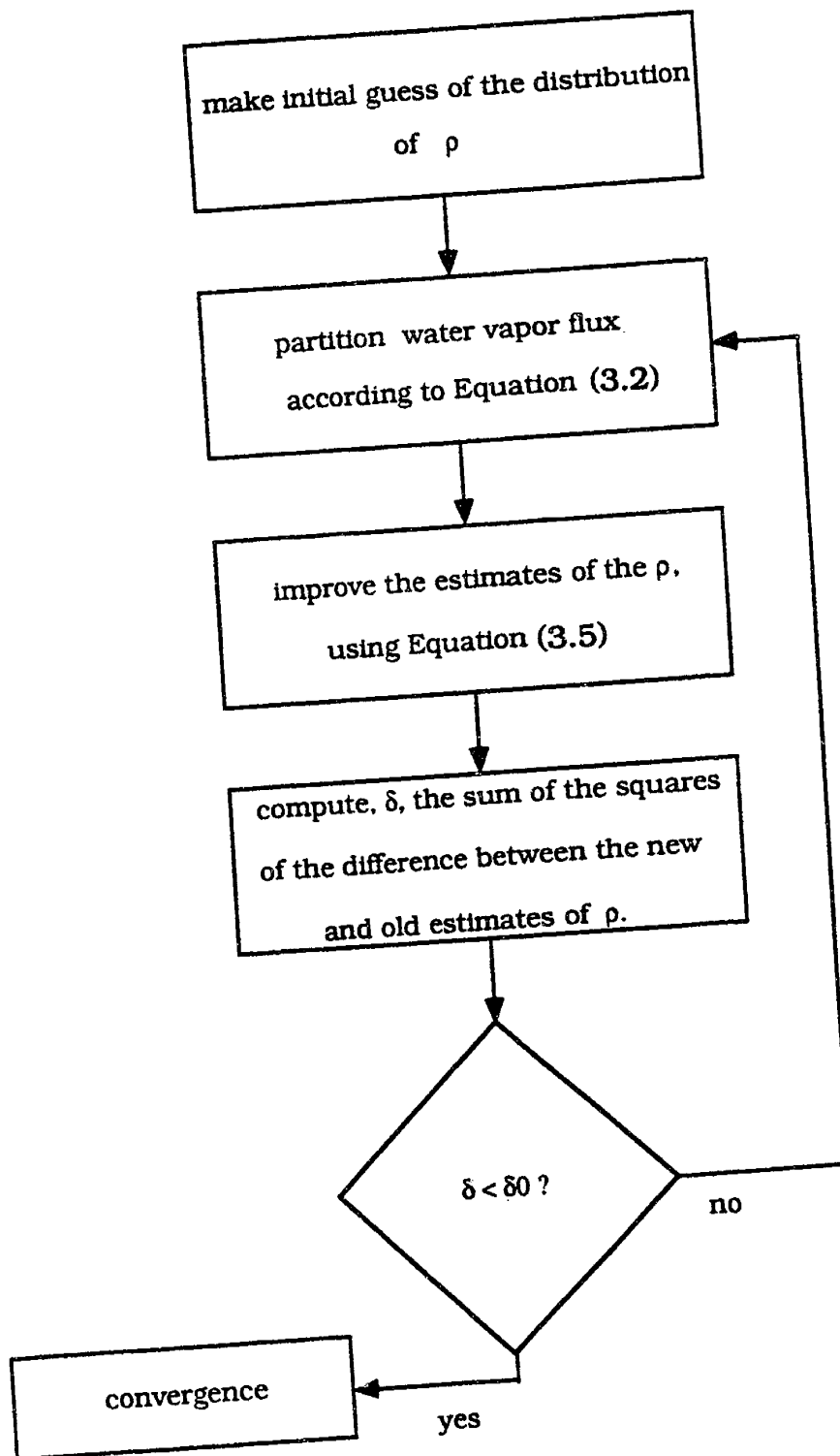


Figure 3.3 Flow chart of the estimation procedure.

4. Similarly, the annual estimate of ρ at any grid point (i,j) is computed by

$$\rho_y(i,j) = \sum_k p(i,j,k) \rho(i,j,k) \quad (3.7)$$

where $p(i,j,k)$ is defined this time as the precipitation at the grid box (i,j) and month k normalized by the yearly precipitation at (i,j).

3.5 Precipitation Recycling in the Amazon Basin

The model described in the previous sections is used to estimate recycling in the Amazon basin. The data used in this study is a subset of the European Center for Medium Range Weather Forecast (ECMWF) global data. It consists of temperature, relative humidity, and wind at fourteen pressure levels (1000, 850, 700, 500, 400, 300, 250, 200, 150, 100, 70, 50, 30, and 10 mb). It also includes evaporation data. The evaporation data are accumulated amounts over six hours and available every six hours. The rest of the data is provided twice daily. The data covers the period 1985-1990 inclusive. It has a spatial resolution of 2.5° latitude by 2.5° longitude. Trenberth and Olson (1988) point that the ECMWF analyses are believed to be the best operational global analyses available for general use.

The data assimilation system at the ECMWF combines data from surface meteorological stations, upper air observations and satellite data. The radiosondes network in the region consists of about ten stations which are located within a 2000 kilometers distance from the center of the Amazon basin. These stations provide

daily measurements. There are about twenty five surface stations in the region providing twice daily measurements. It is clear that the frequency and spatial coverage of conventional observations in the Amazon basin are limited. Illari (1989) studies the quality of the ECMWF humidity analysis and shows that, in the tropics, the data obtained from radiosondes, satellites and from the model's first-guess are similar in terms of quality and informational content. This is particularly important since it shows that the coverage of the tropics by satellite data supplements significantly the sparse radiosondes data.

The ECMWF data set includes estimates of surface evaporation. These estimates are calculated by a surface hydrology scheme using surface parameters and atmospheric variables. Surface hydrology is modeled using a simple 'bucket' hydrology representation and evaporation is computed using a similarity formulation. In order to validate the evaporation data we compare the ECMWF data with the observations of Shuttleworth (1988a). Figure 3.4 shows the average monthly evaporation computed from the ECMWF data for six years at the grid-cell which covers Manaus in the Amazon. It also shows the estimates of monthly evaporation at a single site near Manaus averaged from two years of the Amazon Region Micro-meteorological Experiment (ARME). The two data sets are in reasonable agreement; the difference between the estimates of yearly evaporation is in the order of 5%.

The atmospheric water vapor flux is computed from the data on wind, temperature, and humidity. By making a hydrostatic assumption and utilizing the relation between water vapor mixing

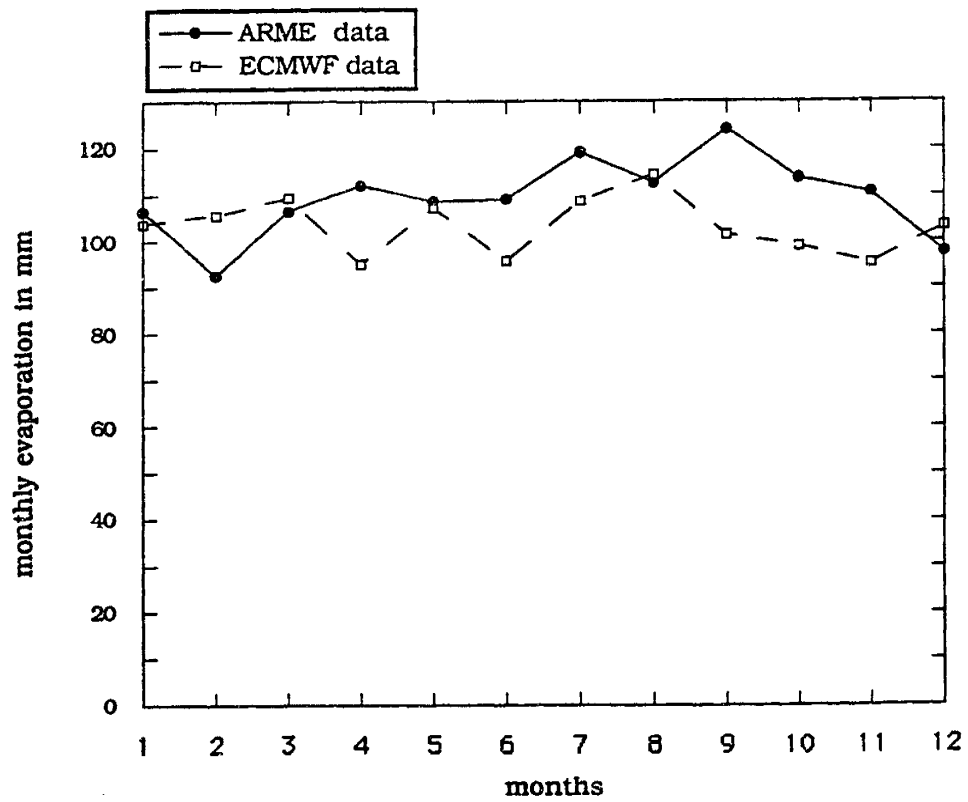


Figure 3.4 Comparison of the evaporation estimates for Manaus, from the ECMWF data set and from the ARME experiment.

ratio and vapor pressure, we derive the following formula for computing flux

$$F_i = \frac{\epsilon L_i}{g} \sum_j RH_j \cdot e_s(T_j) \cdot U_{ij} \cdot d \ln P_j \quad (3.8)$$

where $i = 1, 2$ corresponds to the zonal and meridional directions respectively. j indicates the pressure level. The variables and parameters in Equation 3.8 are defined as follows: ϵ is the ratio of the molecular weight of water vapor to that of dry air, g is gravitational acceleration, L is the linear scale perpendicular to the flux direction, RH is relative humidity, e_s is saturation vapor pressure, T is temperature, U is wind and P is pressure. The above formula is used in computing the flux at each grid point. The monthly fluxes and evaporation are estimated by integrating the corresponding data for each month.

The ECMWF data set does not include precipitation. Hence, precipitation is estimated from the water balance of the atmospheric column above each grid point. Since the change in storage of water vapor is small compared to the fluxes, as illustrated by Figure 3.3, the continuity equation for each grid box is reduced to

$$E - P - \nabla \cdot F = 0 \quad (3.9)$$

The estimates of precipitation by this method are less accurate than the estimates of flux and evaporation. The noise in those estimates is reduced by averaging the data for each month of the year from the six years data. The estimates of monthly precipitation are only used as the weighing factors in Equations 3.6 and 3.7.

The estimation procedure outlined in Section 3.4 is applied using the evaporation, flux and precipitation data. Figure 3.5 is the annual recycling map for the Amazon basin. It shows that recycling increases westward and southward. The maximum rate of recycling occurs at the southwestern corner of the basin. At that corner more than 50% of the precipitation is contributed by evaporation within the Amazon basin. In order to compute a lumped estimate of the annual precipitation recycling ratio in the Amazon basin, the annual recycling map is averaged by a weighing procedure similar to that of Equation 3.6. The only difference being the use of annual precipitation instead of monthly precipitation. We estimate that 25% of all the rain which falls in the Amazon basin is contributed by evaporation within the basin.

The recycling maps for some months of the year are shown in Figure 3.6. The spatial distribution of recycling in the Amazon basin has significantly different patterns in the different seasons. During most of the year the east-west gradient dominates the recycling map consistent with the predominantly easterly winds in the basin. But during the southern hemisphere summer, especially in December, the south-north gradient is larger, consistent with the southward migration of the Inter-Tropical Convergence Zone (ITCZ) and the resulting northerly flux over most of the Amazon basin. It is revealing to compare the recycling maps for the months of June and December with the corresponding flux maps in Figure 3.7. The recycling model is capable of describing the changes in the recycling patterns which result from the seasonal variability of the water vapor flux patterns.

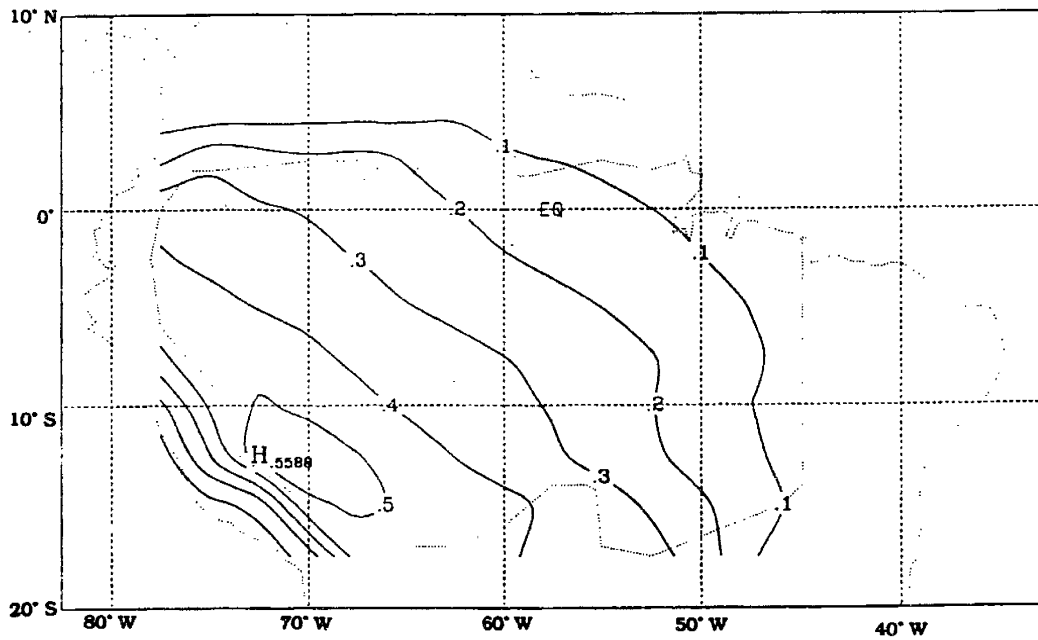


Figure 3.5 Spatial distribution of annual recycling in the Amazon basin.

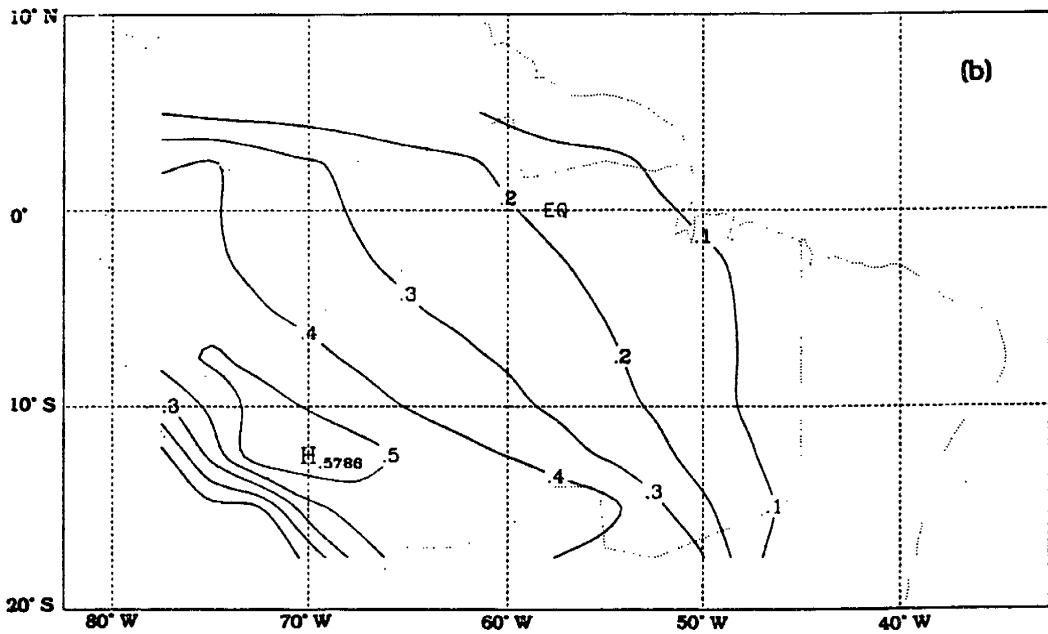
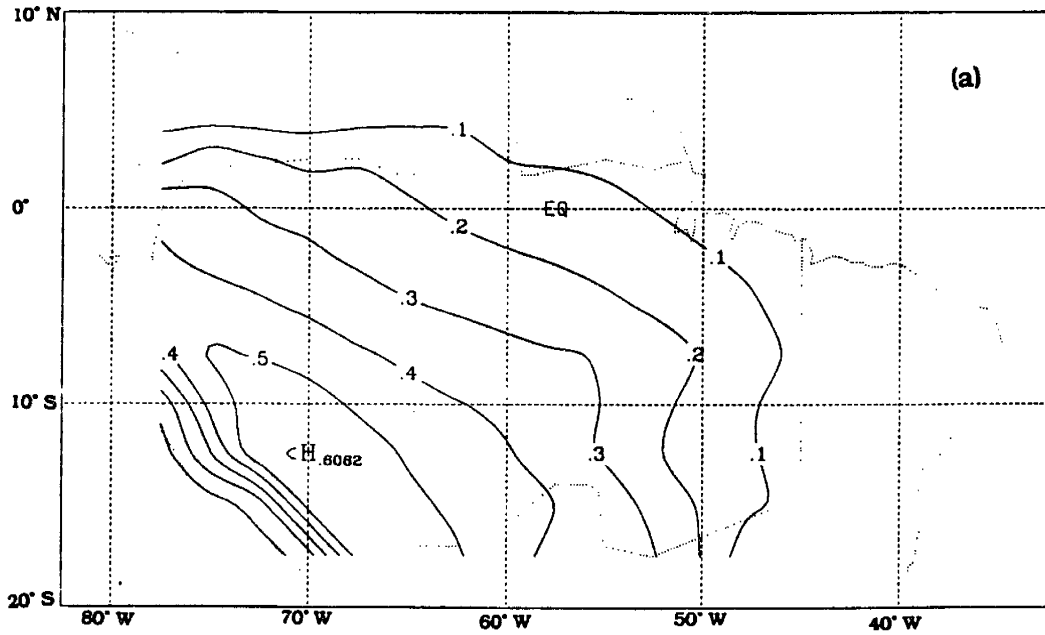
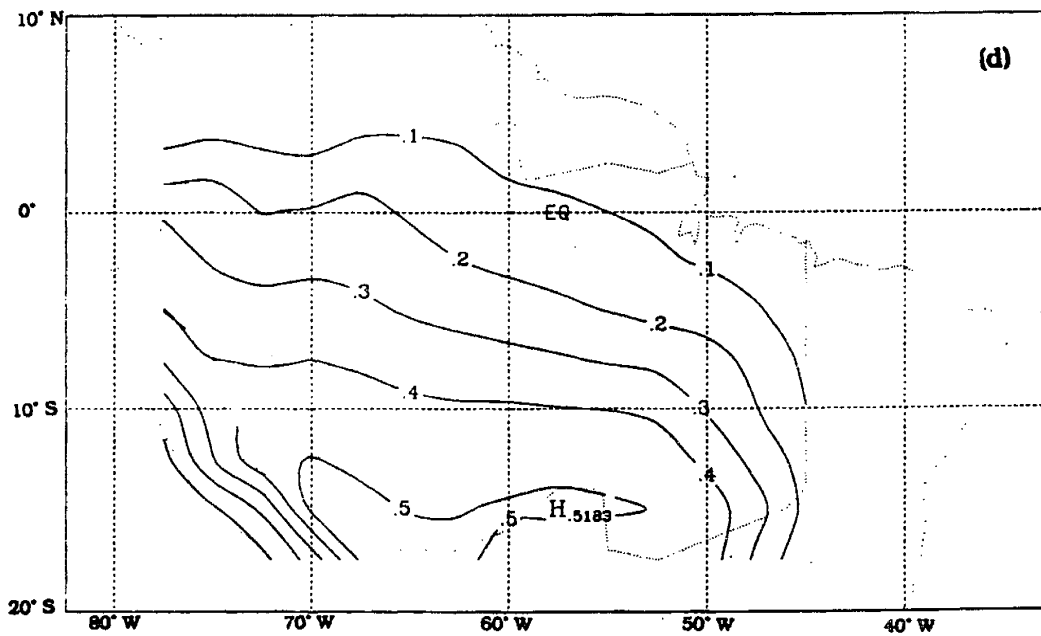
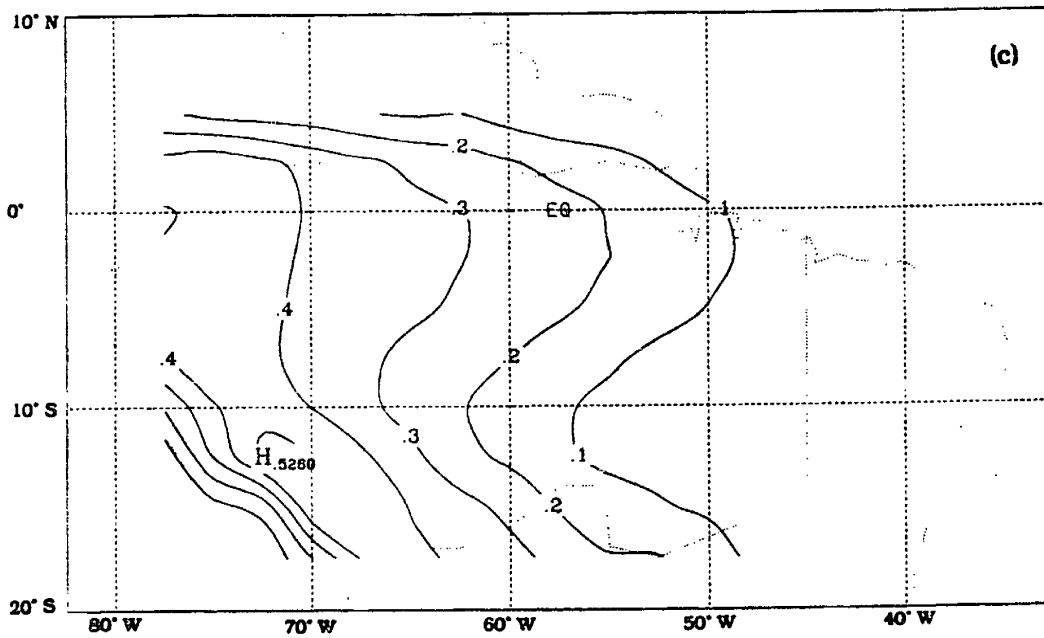


Figure 3.6 Spatial distribution of precipitation recycling for the different months. (a) March (b) June (c) August (d) December



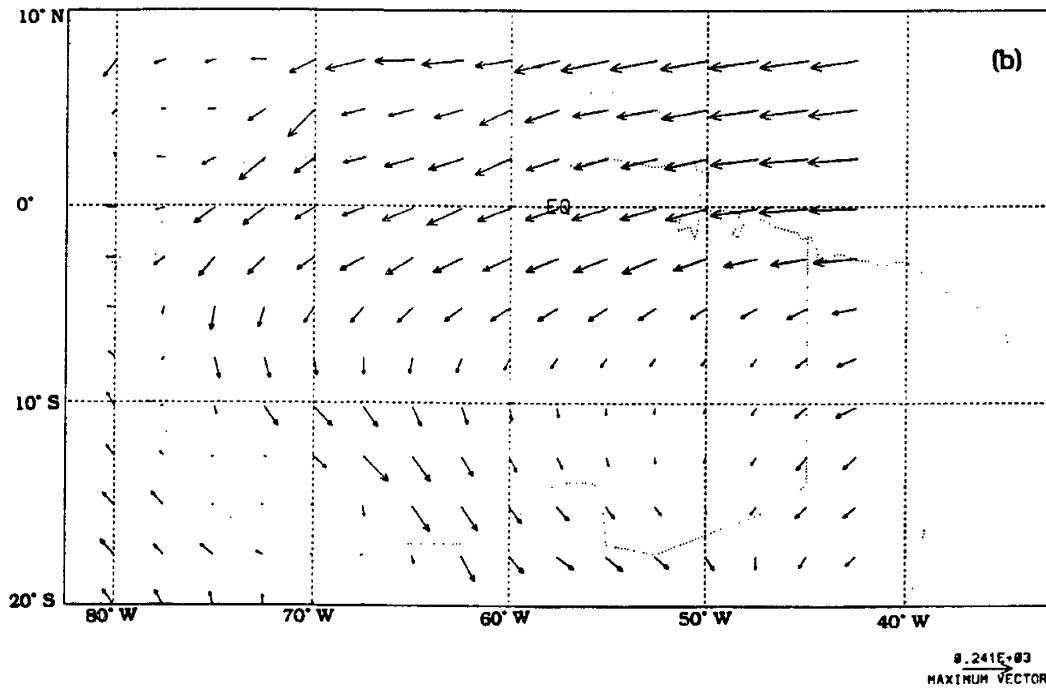
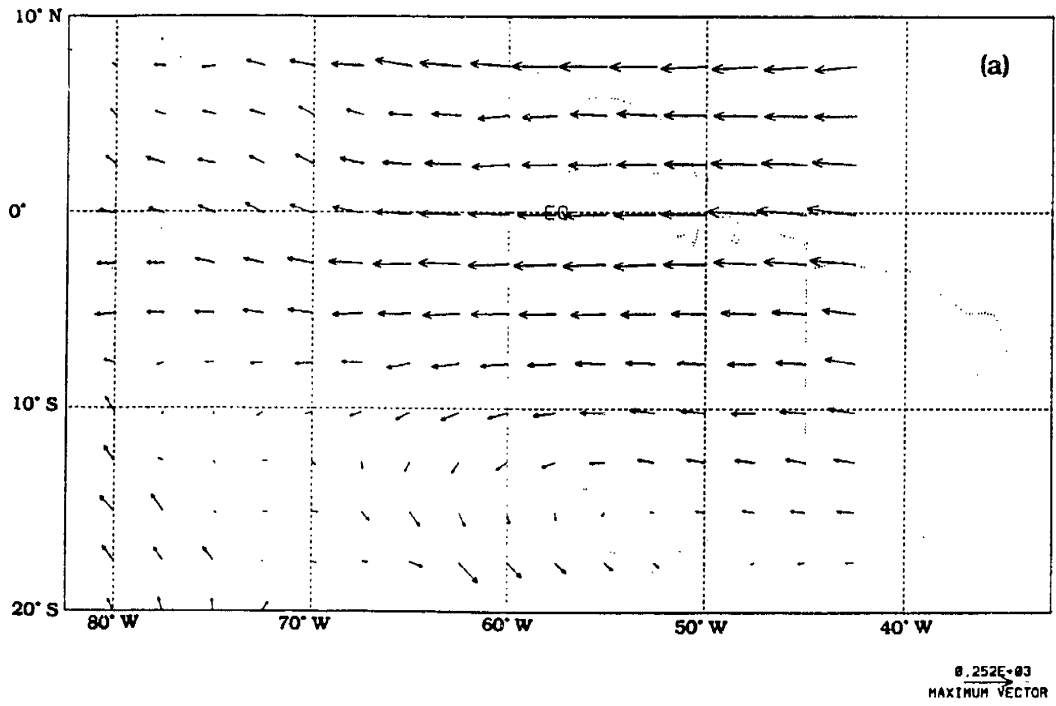


Figure 3.7 Distribution of water vapor flux over the Amazon basin, in cubic kilometer. (a) June (b) December

Another important feature is the ability of the recycling model to reflect the effects of the spatial variability of evaporation in the recycling pattern. This is illustrated by comparing the recycling maps for the months of June and August. Evaporation in August is significantly smaller than evaporation in June, particularly at the southeastern sub-region, see Figure 3.8. The August recycling map reflects this feature in the significant reduction of the recycling ratio over a large area.

The seasonal variability of ρ_t is estimated by applying Equation 3.6 to the recycling map of each month. Figure 3.9 (a) shows ρ_t for the different months. The seasonal variability in the recycling estimates is small compared to the average and to the accuracy of the estimates themselves.

Since the estimates of precipitation, from Equation 3.9, are less accurate compared to the evaporation and flux data, the data used in this study is compared to the precipitation estimates of Figure 3.10 and Nobre (1990). The two data sets agree in winter but some differences exist in summer rainfall (January). The sensitivity of the recycling results to the accuracy of the precipitation information is assessed by computing ρ_t assuming a uniform spatial distribution of precipitation. The results are shown in Figure 3.9 (b). The comparison of Figure 3.9 (a) and Figure 3.9 (b) suggests that the estimates of recycling are only slightly sensitive to the rainfall distribution. The differences between the estimates of recycling ratios in the two figures are small and within the error bars of the estimates ($\sim \pm 0.05$).

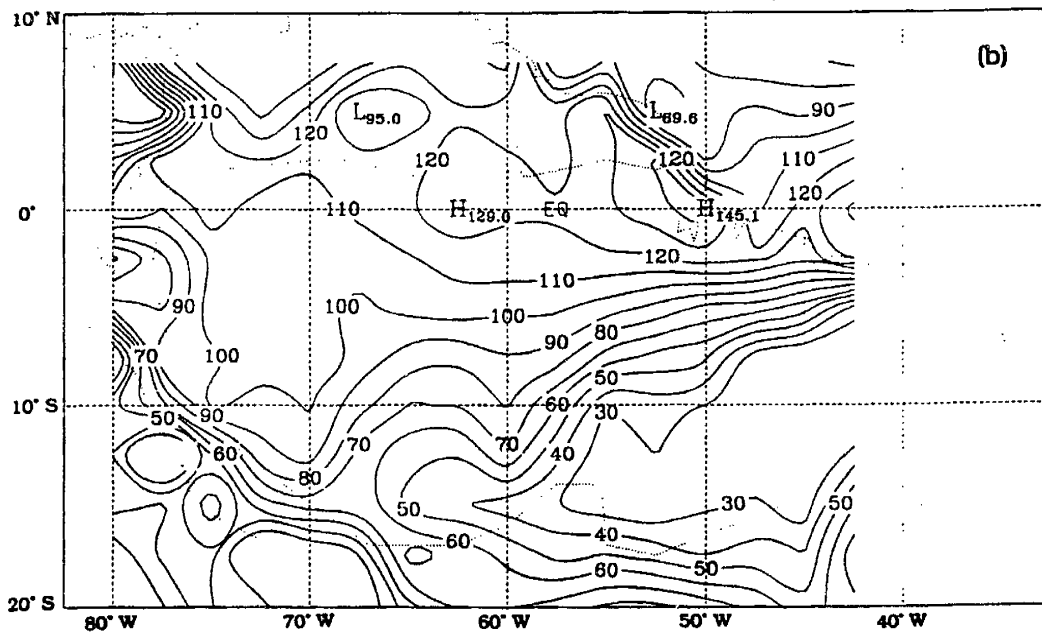
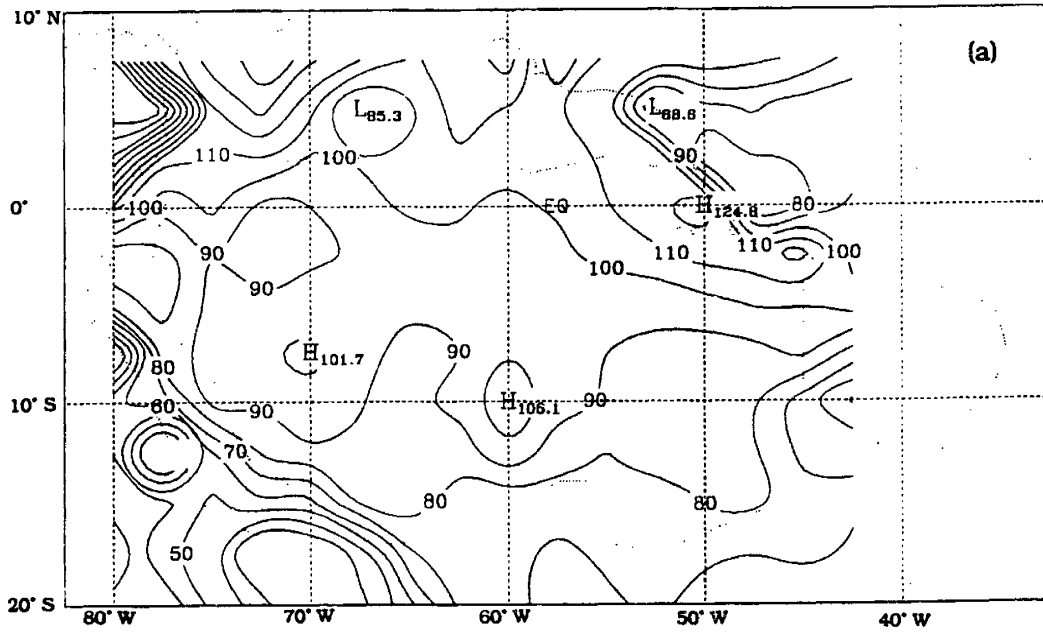


Figure 3.8 Evaporation in the Amazon basin, in mm/month.(a) June (b) August

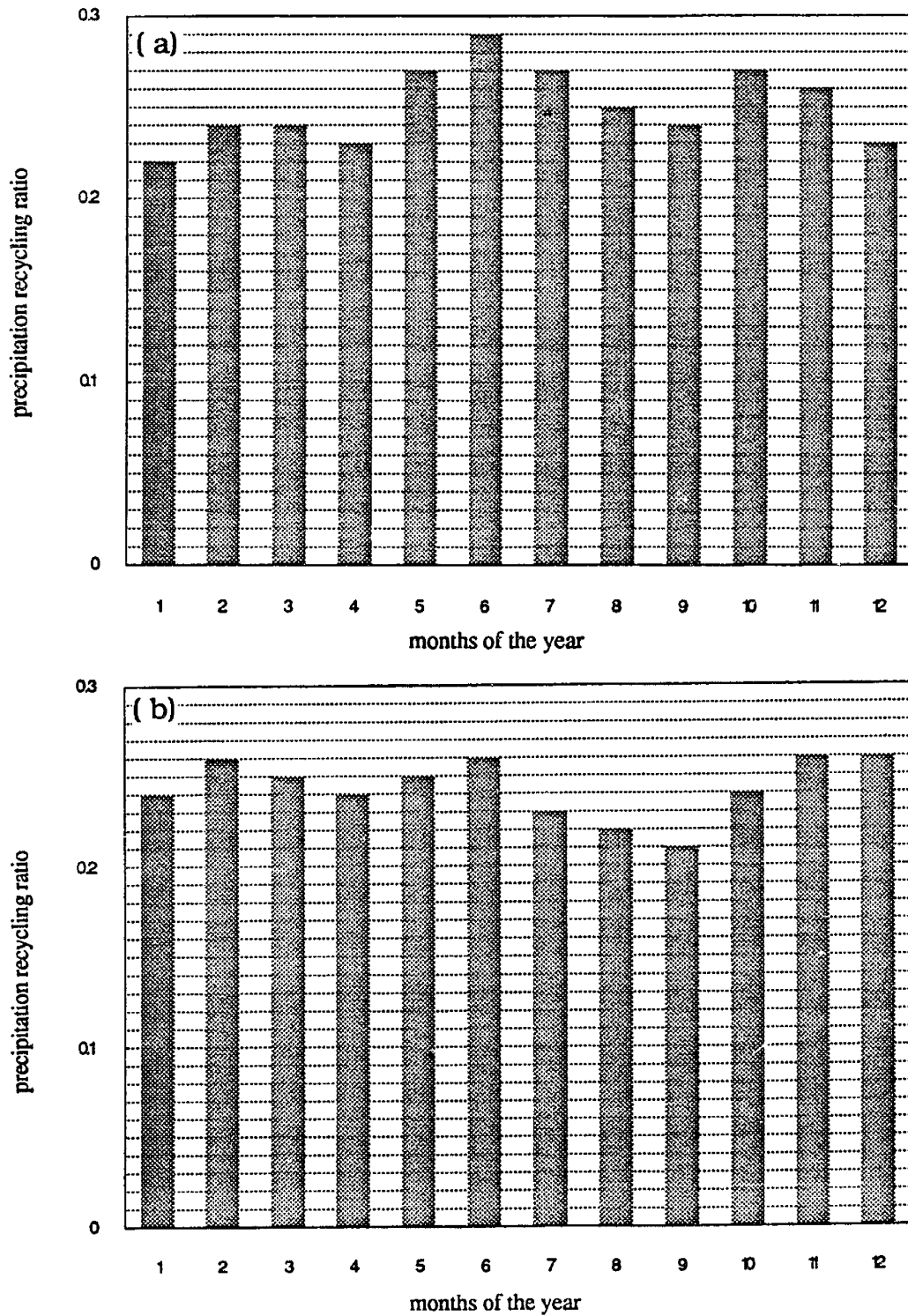


Figure 3.9 Seasonal variability of precipitation recycling ratio in the Amazon basin.

3.6 Scaling of Precipitation Recycling in the Amazon Basin

It is estimated that 25% of annual precipitation in the *total area* of Amazon basin is contributed by evaporation within the *total area* of the basin. The contribution of local evaporation to precipitation in any region would increase as the scale of that region increases. Hence estimation of the scaling behavior of the recycling ratio provides a more complete description of the recycling process. In this section the recycling model presented in section 3.3 is used in the estimation of the precipitation recycling ratio in the Amazon basin over a range of scales extending from the scale of the Amazon basin (~2500 kilometers) to the resolution of the ECMWF data (~250 kilometers).

The analysis is repeated for square areas having a range of scales and located within the Amazon basin. For each scale (e.g. 250 kilometers), the basin is divided into small square cells of equal sizes and with the length of each side equivalent to that scale. For each of these cells the recycling model is applied to estimate the recycling ratio for that cell. It is defined as the ratio of precipitation which is contributed by evaporation within the cell to total precipitation in that cell. Each cell is treated as a single well mixed box, hence for any of the cells the inflow of local moisture is equal to zero and the inflow of imported atmospheric moisture is equivalent to total atmospheric moisture inflow, refer to Equation 3.5. The recycling ratios are then averaged from all the cells with the same scale. The procedure is repeated for different scales and Figure 3.10 shows the scaling behavior of the precipitation recycling ratio. It shows a plot of the average recycling ratio for the different scales considered. The scaling exponent is about 0.5.

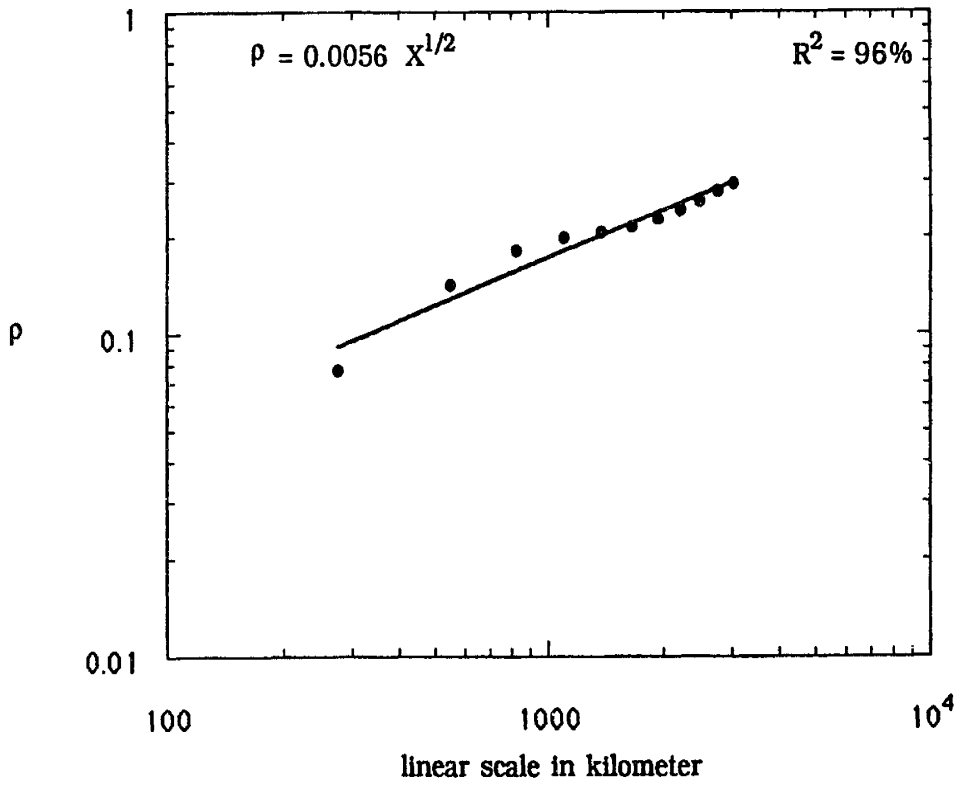


Figure 3.10 Scaling of the precipitation recycling ratio.

3.7 Why Recycling in the Amazon is Overestimated by Previous Studies?

The studies of Molion (1975) and Marques et al. (1977) estimate that about 50% of precipitation in the Amazon basin is contributed by evaporation within the basin. These estimates are significantly larger than our estimates of recycling. The topography in the Amazon basin is such that the plain land is surrounded by mountains and high lands from the north, west and south. It is only open to the east where most of the atmospheric moisture enters the region from the Atlantic Ocean. This unique topographical setting may suggest that the atmosphere above the basin is a closed system. If that is true then the hydrologic cycle in the basin can be described by Figure 3.11. In fact both of studies mentioned above implicitly assume a hydrologic cycle similar to that in Figure 3.11.

The atmospheric moisture flux into the region in Figure 3.11 is finite while the flux out of the region is zero, hence all the evaporation within the region precipitates. For the hydrologic cycle of Figure 3.11 the ratio of recycled precipitation to total precipitation is equivalent to the ratio of total evaporation to total precipitation. Oltman (1967) estimates that the ratio of evaporation to precipitation in the Amazon basin is about 56% and based on this estimate Molion (1975) suggests that precipitation recycling in the Amazon accounts for about 56% of total precipitation. In a different study Marques et al. (1977) consider the region between Belem and Manaus and estimate that the recycling ratio in this region is 48%; this ratio is also equivalent to the ratio of evaporation to precipitation in that region. Hence the accuracy of these estimates of recycling depends on the

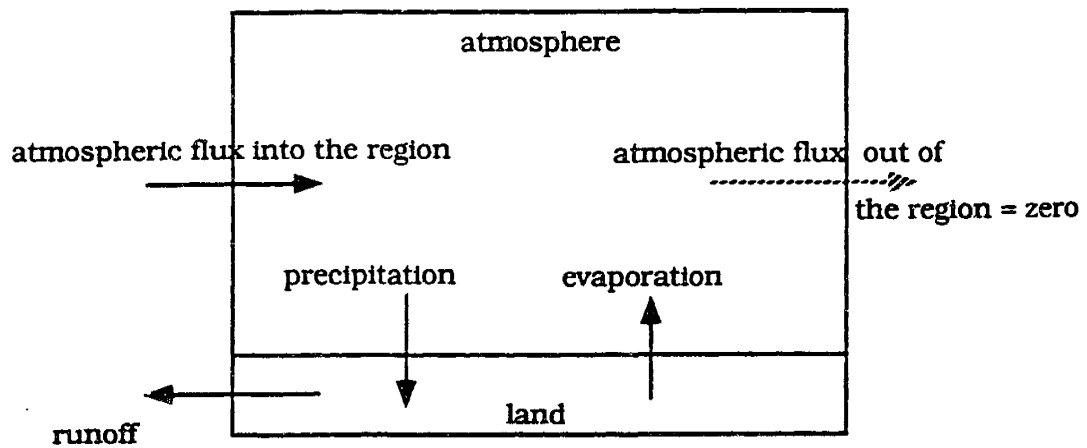


Figure 3.11 The hydrologic cycle of a closed atmospheric system.

assumption that the outflow from the Amazon basin is negligible i.e. the Amazon basin represents a closed system open only to inflow from the Atlantic ocean.

The hypothesis that the atmosphere above the Amazon basin is a closed system is disproved by two observations. First, the isotopic data of Salati et al. (1979) suggests significant migration of atmospheric moisture out of the basin. The second evidence is given by the data in Figure 3.12. It shows atmospheric moisture flux over the Amazon basin estimated from the ECMWF data set. The flux out of the basin accounts for about 68% of the flux into the basin, which indicates that the atmosphere above the Amazon is far from being a closed system and indeed Figure 3.11 is an inaccurate description of the hydrologic cycle in the Amazon basin. Hence, the estimates of the recycling ratio mentioned above represent an overestimate.

3.8 Discussion and Conclusions

The estimated recycling ratio in the Amazon basin of 25% indicates a significant potential for interactions between surface hydrology and climate. Based on the new estimate of recycling the hydrologic cycle in the Amazon basin is described in Figure 3.13; the inflow and outflow of water vapor are computed from the ECMWF data for the six years. The same figure compares the hydrologic cycles of the Amazon basin and the Mississippi basin from Benton et al. (1950). Recycling ratio in the Amazon basin is significantly higher than recycling ratio in the Mississippi basin(0.25 compared to 0.1). Another interesting difference between the two basins is that the ratio of precipitation to atmospheric inflow of water vapor is significantly

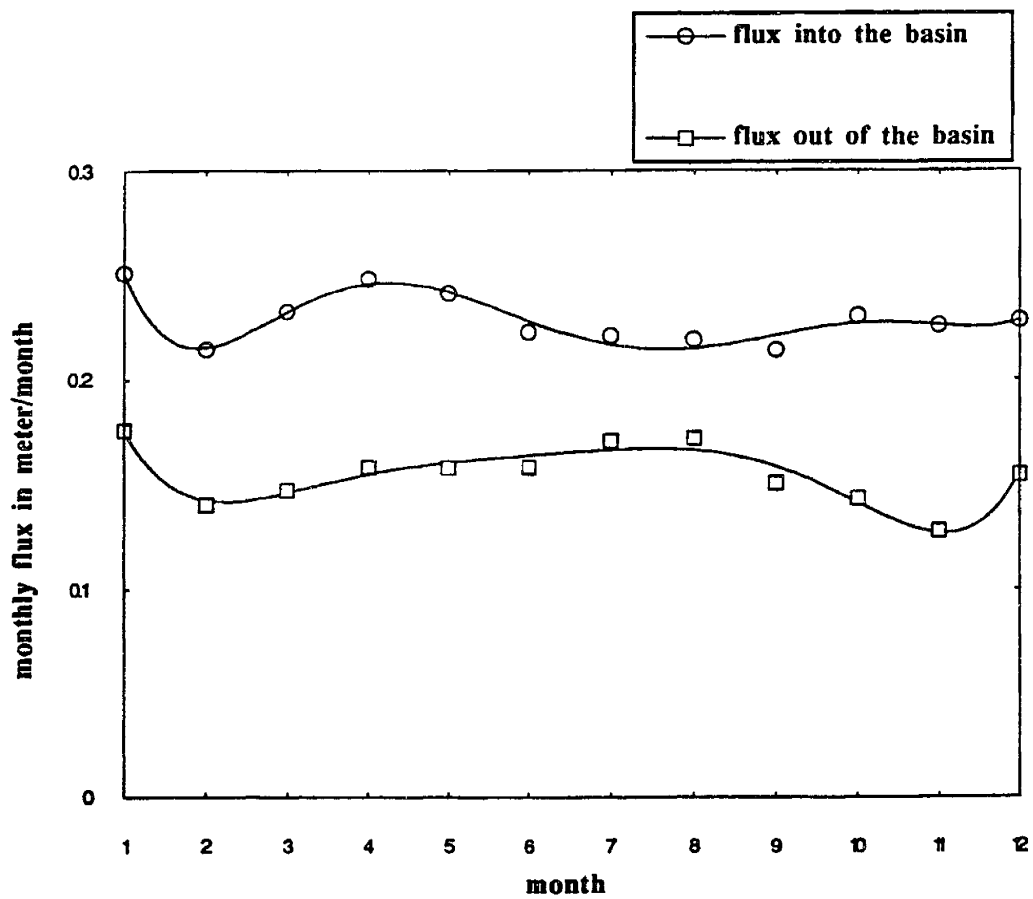


Figure 3.12 Water vapor flux at the boundaries of the Amazon basin.

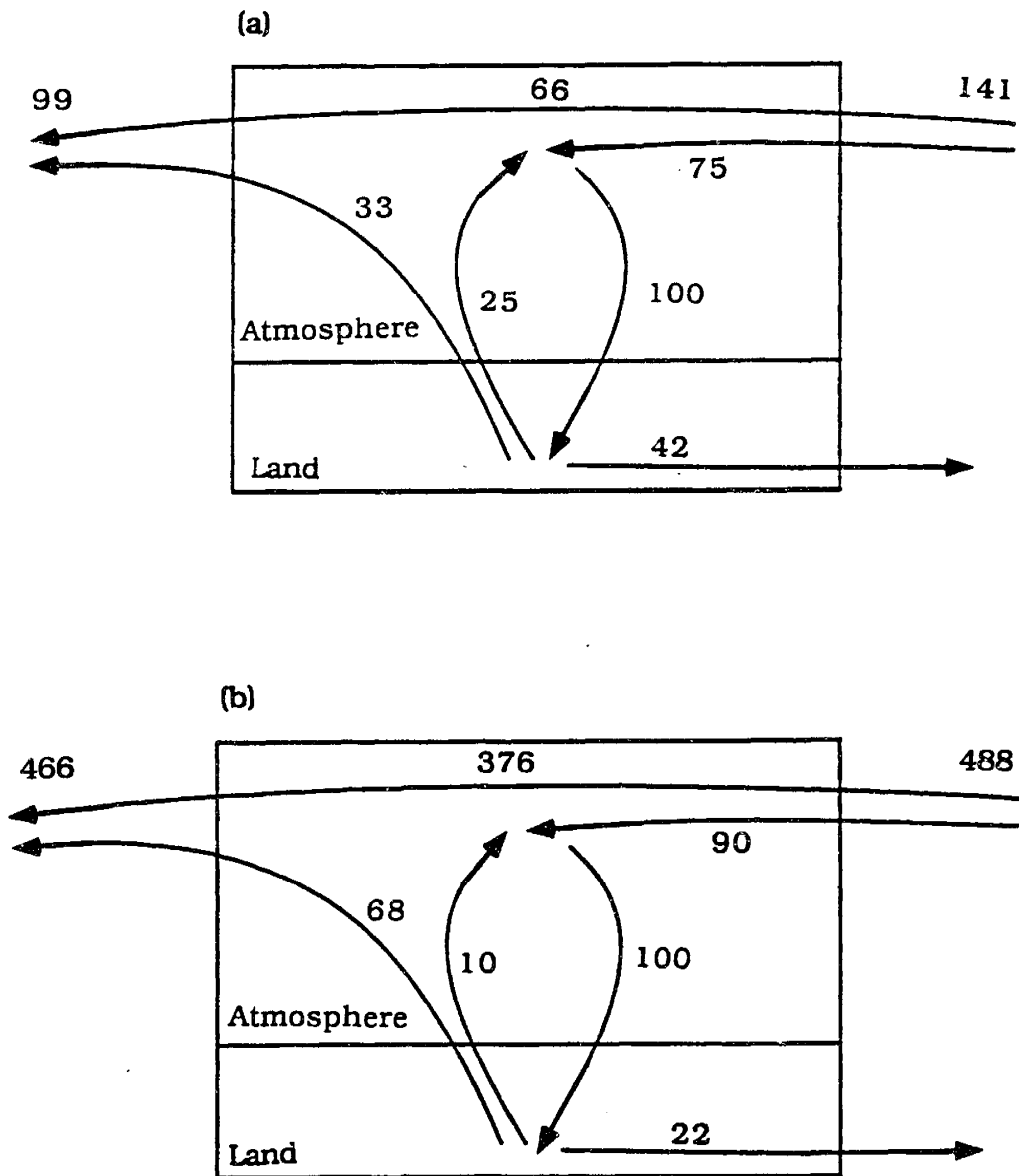


Figure 3.13 Hydrologic cycles, (a) the Amazon basin, annual precipitation=1.95 meter = 100 units (b) the Mississippi basin, annual precipitation=0.75 meter = 100 units (estimates for the Mississippi basin are from Benton et al. (1950)).

higher in the Amazon basin (0.71 compared to 0.21). These two comparisons reflect not only the difference in atmospheric dynamics and rainfall producing mechanisms between the tropics and mid-latitudes, but also the differences of the topographic settings and the vegetational cover of the two basins.

Precipitation recycling in this study refers to the contribution of evaporation from the *total area of the Amazon basin* to precipitation at any point in the same basin. This definition is different from the contribution of evaporation within a 2.5°x2.5° grid-cell to precipitation in that same cell. The recycling estimate for any region depends on the spatial scale considered, the estimate of ρ would decrease with the size of the area considered. The scale of this study is the total area of the Amazon basin and the resolution is 2.5°x 2.5°. The estimate of recycling of 25% is not sensitive to the resolution used in this study for describing the spatial distribution of precipitation recycling. This sensitivity can easily be studied by considering the extreme case of treating the total area of the basin as one grid-cell. Using Equation 3.5 and the data from Figure 3.13(a) ($I_w=0$, $I_o=141$, $E=58$) ρ is computed as $\rho = (0 + 58) / (0 + 58 + 141) = 0.29$. This estimate of ρ is not significantly different from the conclusions of this study using 2.5°x 2.5° as a resolution.

For complete description of the recycling process, it is necessary to estimate the dependence of the recycling ratio on scale. We estimate that the precipitation recycling ratio for the total area of the Amazon basin is 25%; for smaller areas this ratio decreases as the square root of linear scale. This relation is valid in the range of scales between 2500 kilometers and 250 kilometers.

Precipitation in any region is directly proportional to the latent heat transported vertically from the boundary layer to the upper troposphere. The diabatic heating associated with condensation of water vapor is an important energy transport mechanism; it is strongly coupled to the dynamics of the tropical atmosphere, Gill (1980). The precipitation recycling ratio is a measure of how much of that energy is contributed by evaporation within the Amazon basin. Hence the results of this study indicate that 25% of the latent heat released over the Amazon basin is a result of recycling the net surface radiation which is consumed in evaporation by the rain-forest. The other 75% of the latent heat released over the basin results from advecting energy from the Atlantic ocean. The advected latent energy is part of the net surface radiation that is consumed by evaporation from the ocean. This interpretation of the recycling results is important since it provides information about the degree of coupling between the atmospheres over the two adjacent regions.

The recycling maps presented in this Chapter reflect significant spatial and seasonal variability in recycling of water vapor in the Amazon basin. This variability is also reflected in the isotopic data of Salati et al. (1979). Under these conditions the sensitivity of regional climate to changes in surface hydrology, e.g. deforestation, may very well depend on the location of the perturbation to surface hydrology.

The conclusion that the atmosphere above the Amazon basin is not a closed system suggests that outflow of atmospheric moisture from the basin may contribute important input to the hydrologic cycle in the surrounding regions. This is particularly important since it implies that changes in the Amazon basin evaporation, e.g. through

deforestation, can *potentially* affect the moisture supply and rainfall in the surrounding regions.

The estimates of precipitation recycling ratio provide *diagnostic* measures of the coupling between hydrology and climate. It would be inappropriate to make specific *prognostic* statements regarding the effects of deforestation or any other disturbance of surface parameters based solely on the estimates of precipitation recycling and before studying the equilibrium of the disturbed climate system.

CHAPTER 4

A Description of Rainfall Interception Over Large Areas

4.1 Introduction

This Chapter outlines the development of a new rainfall interception scheme. In Chapter 5 the new interception scheme is included into a climate model which will be used for studying the sensitivity of regional climate in the Amazon basin to small-scale deforestation.

Vegetation affects land-surface hydrology in many different ways. It intercepts rainfall before reaching the ground surface and controls the subsequent rates of canopy evaporation and canopy drainage. The significance of these interception processes increases with the density of the vegetation layer. In forest environments interception plays a significant role in the partition of rainfall into evaporation and runoff. The coverage of the land surface by a vegetation layer increases surface roughness and enhances eddy transport of heat and water vapor near the surface. Because of this physical effect evaporation of intercepted rain occurs at rates which are higher than potential evaporation. Evaporation of intercepted rain, which is usually referred to as interception loss, accounts for a significant part of total rainfall. It ranges from a few percent to about twenty five percent depending on the nature of rainfall and the size of the canopy storage capacity. The main objective of interception modeling is to describe accurately the partition of total rainfall into canopy drainage and interception loss.

The recent interest in describing surface hydrologic processes at large spatial scales is motivated by the need for including land-surface hydrology in climate models. The typical spatial resolution of a climate model is in the order of hundreds of kilometers. Hence it is necessary to develop descriptions of surface hydrologic processes over such large areas. The early versions of land-surface hydrology parameterizations did not include representation of interception processes. But more recent schemes such as the Biosphere-Atmosphere Transfer Scheme (BATS), Dickinson et al. (1986), include descriptions of interception. The BATS treatment of interception is described in Appendix 4.1.

Dickinson and Henderson-Sellers (1988) used BATS as part of a climate model in studying the possible impacts on global climate due to deforestation of the Amazon basin. Figure 4.1 shows the simulated interception loss over the whole Amazon basin compared to interception loss measured at a single site in the basin. Although the two quantities are not perfectly comparable it seems that the simulations overestimated interception loss by about 150%. Total evaporation was also overestimated in these simulations. A partial explanation for those results is given by Dickinson (1989), overestimation of interception loss is partly due to overestimation of surface net radiation. Another possible explanation is the use of large canopy storage capacity. But Shuttleworth and Dickinson (1989) argue that overestimation of net radiation by about 70% or the use of large canopy storage capacity can not wholly explain the large overestimation of interception loss. They suggest that a much more serious source of error is the neglect of spatial variability in rainfall.

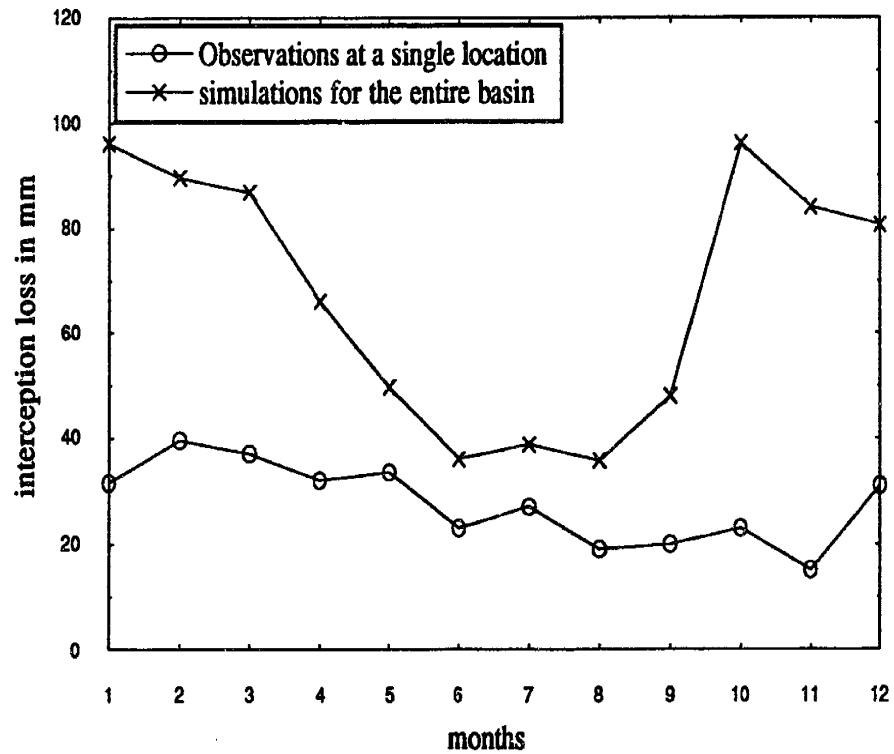


Figure 4.1 Comparison of interception loss from the simulations of Dickinson and Henderson-Sellers (1988) with the observations of Shuttleworth (1988)a.

Shuttleworth (1988b) developed a scheme for parameterizing interception which treats rainfall as a spatially variable process but assumes that canopy storage is constant in space. The scheme is described in Appendix 4.2.

In a recent paper Dolman and Gregory (1992) addressed the problem of parameterization of rainfall interception in climate models. They studied two interception schemes which include some of the effects of spatial variability in rainfall. Although these schemes assume that rainfall is distributed over a small fraction of the grid-cell area, the depth of water on the canopy is assumed constant over the entire area of the grid-cell. The two interception schemes are similar to the scheme of Shuttleworth (1988b).

Lean and Warrilow (1989) used the U.K. meteorological office climate model in their simulations of the Amazon climate. The simulated interception loss at the model grid point which corresponds to the site of the data in Figure 4.1 is larger than the observed interception loss by 184% . Total evaporation is overestimated by 15%. Lean and Warrilow (1989) argue that 'overestimation of canopy evaporation is probably present in other land surface schemes and this may be due to the extension of single point description of the rainfall interception process to the grid scale area in a region where convective rainfall events dominate' . We agree with these conclusions.

Overestimation of interception loss in climate models is a serious problem. Shuttleworth (1988a) estimated that interception loss at a single site in the Amazon basin is 25% of the total

evaporation and that evaporation accounts for about 90% of the net radiation at the surface. Under these conditions overestimation of interception loss may result in a significant error in the partition of net radiation into latent and sensible heat fluxes .

Although interception models may provide accurate description of the process at a point, as demonstrated by Rutter et al. (1975), using these descriptions in climate models result in large errors. It seems that sub-grid scale spatial variability in rainfall and canopy storage play a significant role which tend to reduce the spatially averaged interception loss. The basic question in representation of interception processes in climate models is : How to describe interception over large areas considering both the basic physics of the process at a single location and the spatial variability within the large-area? This Chapter will try to address that question.

Our approach is a combination of the physical description of interception at a point and statistical treatment of the sub-grid scale spatial variability of rainfall and canopy storage. The Rutter model is used in describing interception at a point. The physical parameters which control interception at a single location are assumed constant in space. Analytical expressions are derived to relate the spatial average of canopy drainage and interception loss to the spatial average of canopy storage. These expressions are based on reasonable assumptions about the spatial distributions of rainfall and canopy storage. These set of relations are proposed as a new interception scheme designed to describe the process over large areas

and hence provide the suitable parameterizations of interception processes in climate models.

In the following the Rutter model of interception is described in some detail. The derivation of the new interception scheme is then presented. An off-line version of BATS is used in comparing the new scheme with previous schemes. The Chapter concludes by discussing the results of these comparisons and the limitations of the new interception scheme .

4.2 Rutter Model of Interception

This model was introduced by Rutter et al. (1971) to provide a predictive tool of rainfall interception. Canopy storage is created by rainfall and depleted by canopy drainage and evaporation (canopy storage is a variable of the interception processes; it is different from canopy storage capacity which is a parameter of the canopy). The Rutter model specifies the functional dependence of canopy drainage and canopy evaporation on canopy storage. Canopy drainage is described by

$$D_r = K \cdot e^{\left(\frac{C}{B}\right)} \quad (4.1)$$

where D_r is canopy drainage, C is canopy storage, K and b are constants characteristics of the canopy. It is important to note the exponential dependence of canopy drainage on canopy storage. This strong dependence results in rapid depletion of excessive local storage. Equation 4.1 is based on empirical observations, see Rutter et al. (1971).

Evaporation from the canopy has two components: interception loss and transpiration. It is described by

$$e = \frac{C}{S} \cdot e_c + \left(1 - \frac{C}{S}\right) \cdot e_t, \quad 0 \leq C \leq S,$$

$$e = e_c, \quad C \geq S \quad (4.2)$$

where e_t is transpiration by the plant, e_c is evaporation from wet canopy and S is a constant characteristic of the canopy. S is the amount of water retained by the canopy after being completely wet and then drained for a "sufficiently" long period.

Canopy storage is added by rainfall and depleted by drainage and evaporation. The rate of change of canopy storage is given by,

$$\frac{\partial C}{\partial t} = (1-p) \cdot P - \frac{C}{S} \cdot e_c - D_r \quad (4.3)$$

where p is fraction of rain falling directly to the ground and P is rainfall.

The parameters of the model are S , p , K and b . Calibration of the model requires estimation of these four parameters. S and p are estimated from data of throughfall and total rainfall. S is the intercept of the rainfall-throughfall curve corresponding to storms with negligible interception loss. p is the slope of rainfall-throughfall curve corresponding to storms with total depth smaller than S . The estimate of p is used in computing canopy drainage from data on rainfall and throughfall. The estimates of p and S can then be substituted in Equation 4.3 to compute canopy storage from rainfall data. K and b are estimated from a regression between the canopy drainage and canopy storage.

Rutter et al. (1975) extended the model to account for stemflow and used the model in describing interception in several catchments in England. The model was successful in predicting observed interception loss with reasonable accuracy. In a recent study by Shuttleworth (1988a) the Rutter model was successfully used in describing interception in the Amazon basin which indicate that the model is robust and capable of describing interception in the rainforest environment. The results of these two studies suggest that the Rutter model provide an adequate tool for describing interception processes at a point.

The exponential dependence of canopy drainage on canopy storage results in large drainage for large canopy storage. Hence when applying the model in describing interception processes using real data, e.g., Rutter et al. (1975), it is observed that canopy storage does not exceed a maximum of about 2 or 3 mm. The Rutter model is modified here to include a maximum limit for canopy storage, C_m , the maximum storage which the canopy can hold at any instant of time. This limit constrains primarily Equation 4.3 such that C does not exceed C_m . Equation 4.1 is also modified to

$$D_r = K \cdot e^{\left(\frac{C}{b}\right)}, C < C_m,$$

$$D_r = K \cdot e^{\left(\frac{C_m}{b}\right)}, C \geq C_m \quad (4.4)$$

The integrations which will be carried in the next section require that the mathematical form of the drainage function converges for all possible values of canopy storage. This is the reason for making this modification. To explain the physical meaning of C_m we resort to the analogy between the canopy layer and the soil layer. If S is the

parameter of the canopy which corresponds to the field capacity of the soil layer, then C_m is the equivalent to the product of soil porosity and the total soil depth. In the next section the Rutter model is used in describing interception at every point within the large area.

4.3 A Description of Rainfall Interception over Large Areas

A new interception scheme is developed in this section. It combines the Rutter model and statistical description of the spatial variability in rainfall and canopy storage. It is assumed that rainfall is distributed in space according to

$$f_p = (1 - q_p) \cdot \delta(P - 0) + \frac{q_p^2}{E(P)} \cdot e^{-\left(\frac{q_p \cdot P}{E(P)}\right)} \quad (4.5)$$

where P is rainfall at any point in space, q_p is fraction of the area with $P > 0$, $E(\)$ denotes the expected value of and δ denotes the Dirac delta function. The observations of Eagleson et al. (1987) support the assumption of exponential distribution for rainfall.

Canopy storage controls the local amounts of canopy drainage and evaporation. It is assumed that canopy storage is distributed in space according to an exponential distribution. In absence of any observations of the spatial distribution of canopy storage the choice of the exponential is a matter of convenience. The assumption is justifiable when rainfall variability is a major causal factor for variability in canopy storage. Another possible justification comes from the fact that quick drainage from the saturated canopy reduces

any large canopy storage and hence results in large areas with small canopy storage which is consistent with form of the exponential distribution. It is assumed that canopy storage is distributed in space according to

$$f_C = (1 - q_c) \cdot \delta(C - 0) + \frac{q_c^2}{E(C)} \cdot e^{-\left(\frac{q_c \cdot C}{E(C)}\right)} \quad (4.6)$$

where C is canopy storage at any point in space, $E(C)$ is the spatially averaged canopy storage and q_c is the fraction of the area with $C > 0$.

The spatially averaged canopy drainage is obtained by taking the expected value of both sides in Equation 4.1. $E(D_r)$ is given by

$$E(D_r) = \int_{C=0}^{\infty} D_r(C) f_C dC$$

$$= \left[1 - q_c + \frac{q_c^2 \cdot b}{(b \cdot q_c - E(C))} \right] \cdot K + \left[q_c + \frac{q_c^2 \cdot b}{(b \cdot q_c - E(C))} \right] \cdot K \cdot e^{-\left[\frac{(b \cdot q_c - E(C)) \cdot C_m}{b \cdot E(C)} \right]} \quad (4.7)$$

The above expression relates the spatial average of canopy drainage to the parameters of the Rutter model (K , b and C_m) and the parameters of the distribution of C ($E(C)$ and q_c). Figure 4.2 shows $E(D_r)$ as function of $E(C)$ for different values of q_c . $E(D_r)$ decreases with q_c for small values of $E(C)$ and increases with q_c for large values of $E(C)$. Figure 4.3 compares the drainage function of the Rutter model and that of the scheme developed in this section; it compares Equation 4.1 and Equation 4.7. The new scheme shows enhanced canopy drainage for small values of $E(C)$ and reduced drainage for large values of $E(C)$. Average canopy storage amounts are usually in the order of 1 mm or less which falls in the enhancement range for typical values of the Rutter model parameters.

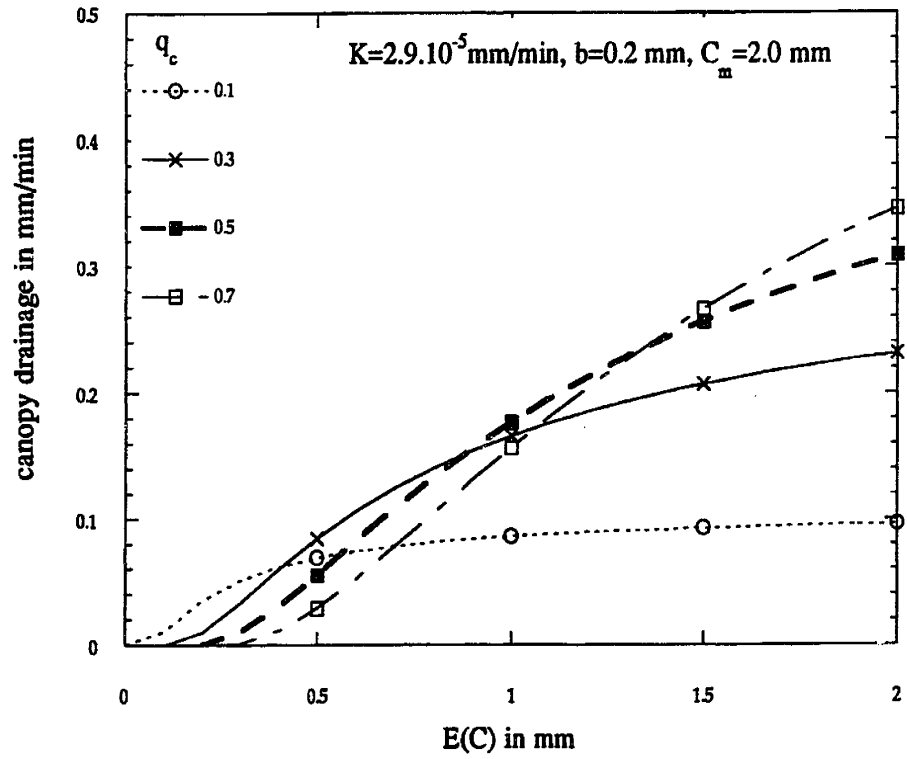


Figure 4.2 Drainage function of the new interception scheme.

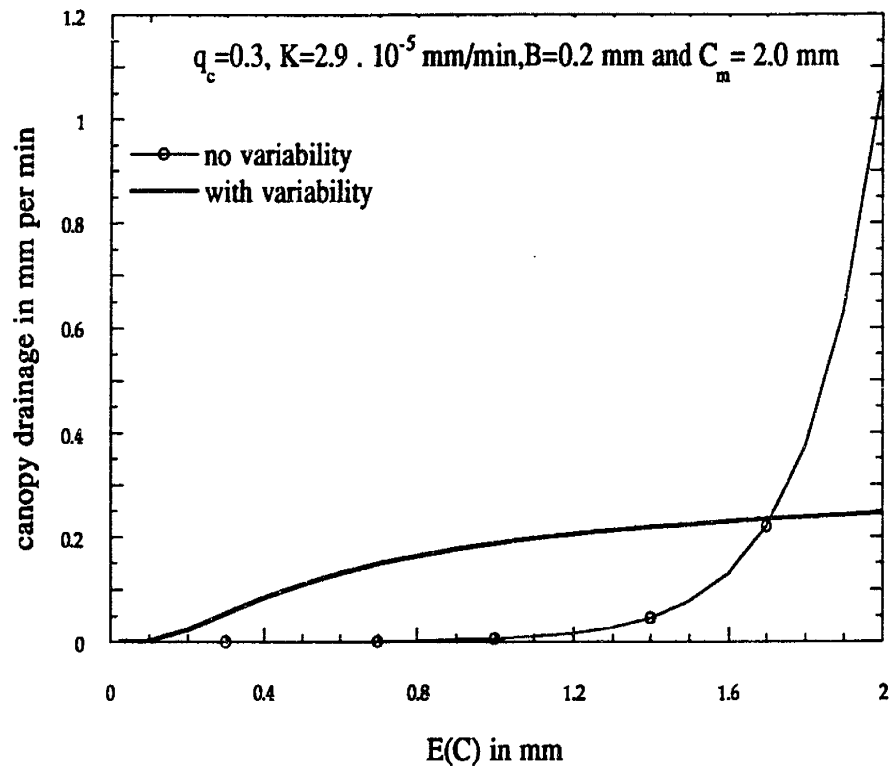


Figure 4.3 Comparison of the drainage function of the Rutter model and the drainage function of the new interception scheme.

The spatially averaged evaporation is obtained by taking the expected value of both sides in Equation 4.2. $E(e)$ is given by

$$E(e) = \int_{C=0}^{\infty} e(C) \cdot f_C \, dC = e_t + (e_c - e_t) \cdot \frac{E(C)}{S} \cdot \left(1 - e^{-\left(\frac{S \cdot q_c}{E(C)}\right)}\right)$$

and

$$E(e') = e_c \cdot \frac{E(C)}{S} \cdot \left(1 - e^{-\left(\frac{S \cdot q_c}{E(C)}\right)}\right) \quad (4.8)$$

where e' is interception loss. Figure 4.4 shows $E(e')$ normalized by e_c as function of $E(C)$ for different values of q_c . Normalized interception loss increases with $E(C)$ and approaches an asymptotic limit equivalent to q_c consistent with the mathematical form of Equation 4.8. Physically, as the average canopy storage increases a fraction of the total area, q_c , will have water available for evaporation.

Throughfall has three components: the fraction of rain falling directly to the ground through gaps in the canopy, drainage from the canopy and rainfall in excess of drainage at locations with maximum canopy storage. The spatial average of throughfall is given by

$$E(T) = p \cdot E(P) + E(D_r)$$

$$\begin{aligned} & + \int_{C=C_m}^{\infty} \int_{P=\frac{D_m}{(1-p)}}^{\infty} [(1-p) \cdot P - D_m - e'(C)] \cdot f_C \cdot f_P \cdot dP \cdot dC \\ & = p \cdot E(P) + E(D_r) \\ & + [q_c \cdot (1-p) \cdot E(P) - q_c \cdot q_p \cdot e_c] \cdot e^{-\left[\frac{q_c \cdot C_m}{E(C)} + \frac{q_p \cdot D_m}{(1-p) \cdot E(P)}\right]} \end{aligned} \quad (4.9)$$

where D_m is $D_r(C_m)$.

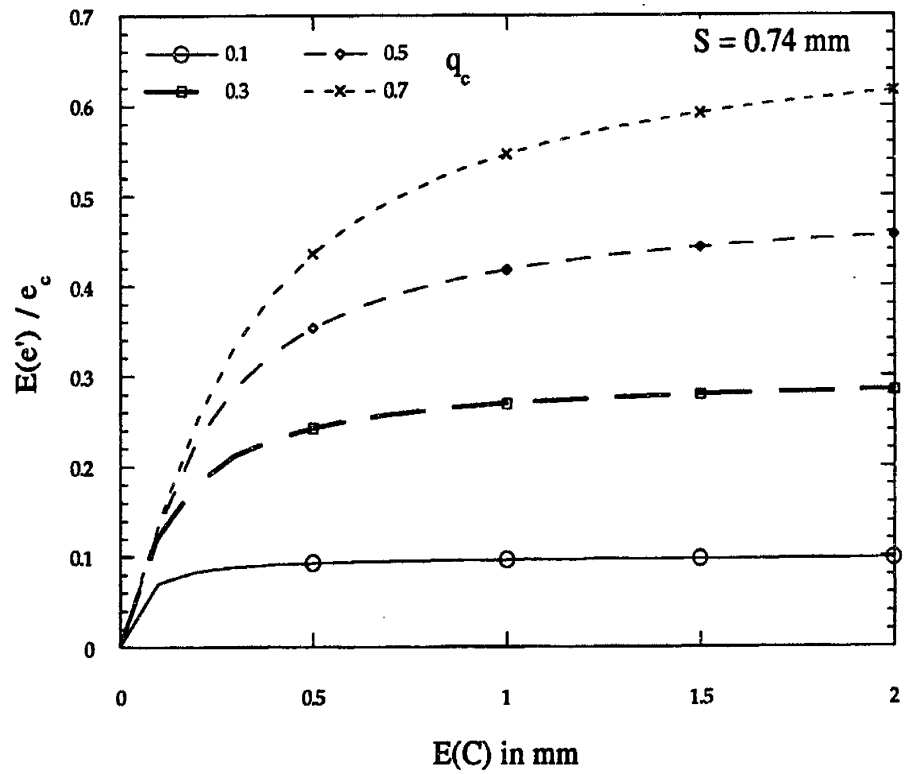


Figure 4.4 Interception loss function of the new interception scheme.

The rate of change of the spatially averaged canopy storage is obtained by taking the expected value of both sides in Equation 4.3 . The derivation of the continuity equation for the new scheme is described in Appendix 4.3.

The above equations are the mathematical expression of the new interception scheme. In the next section this scheme will be tested and compared to other descriptions of interception.

4.4 Simulations of Rainfall Interception in a Rain-forest Environment

An off-line version of the BATS is used in testing the new interception scheme. It is driven by the following forcings: solar radiation, above canopy temperature, above canopy humidity and a time series of surface rainfall. The forcings are designed to simulate a typical rainforest environment. The forcings are described in Table 4.1.

The rainfall series is generated using the stochastic model of Rodriguez-Iturbe and Eagleson (1987). The model simulates the rainfall rate process in space and time for each storm. The storm arrival process is described by a non-homogeneous Poisson process which favors occurrence of storms in the afternoons. This is consistent with the recent observations of Lloyd(1990) in the Amazon basin. The parameters of the model are selected to simulate convective storms which are characteristic of the rainforest environment. The rainfall simulated by the model is averaged in space over an area of ten thousands squared kilometers. The total duration of the

maximum solar radiation at the surface	890 W/m ²
average above canopy temperature	300° K
daily range of above canopy temperature	6° K
relative humidity above the canopy	80%.
mean of the rainfall series	0.22 m/month

Table 4.1 : Description of the model forcings

simulation is two months. The parameters of vegetation and soil are specified according to those of rainforest conditions from Tables 2 and 3 of Dickinson, et al. (1986). The Rutter model parameters are specified according to those calibrated for an Amazonian rainforest and described in Shuttleworth (1988a).

The scheme is compared to the following alternative descriptions : the Rutter model, the BATS treatment of interception which is described in Appendix 4.1 and the Shuttleworth scheme which is described in Appendix 4.2. Figure 4.5 shows normalized interception loss, which is interception loss divided by the total rain, as function of the wind speed over the canopy. Wind speed is a surrogate for potential evaporation since the two quantities are linearly related. Each point in Figure 4.5 represents a two months simulation. The results of the Rutter model, Shuttleworth scheme or the BATS interception are marginally different from each other but the new interception scheme produces significantly less interception loss. For conditions similar to those in the tropics, i.e. wind speeds in the order of 1 m/s, the new interception scheme results in interception loss which differs by a factor of 2 from that of the BATS interception.

The significant reduction in interception loss is explained by Figure 4.3. It compares the drainage functions of the Rutter model and the new interception scheme, Equations 4.1 and 4.7 respectively. Including the spatial variability in canopy storage results in enhanced drainage for small average canopy storage. Enhancement of canopy drainage comes from the buckets of large canopy storage which result from randomly distributing the canopy storage within the grid cell

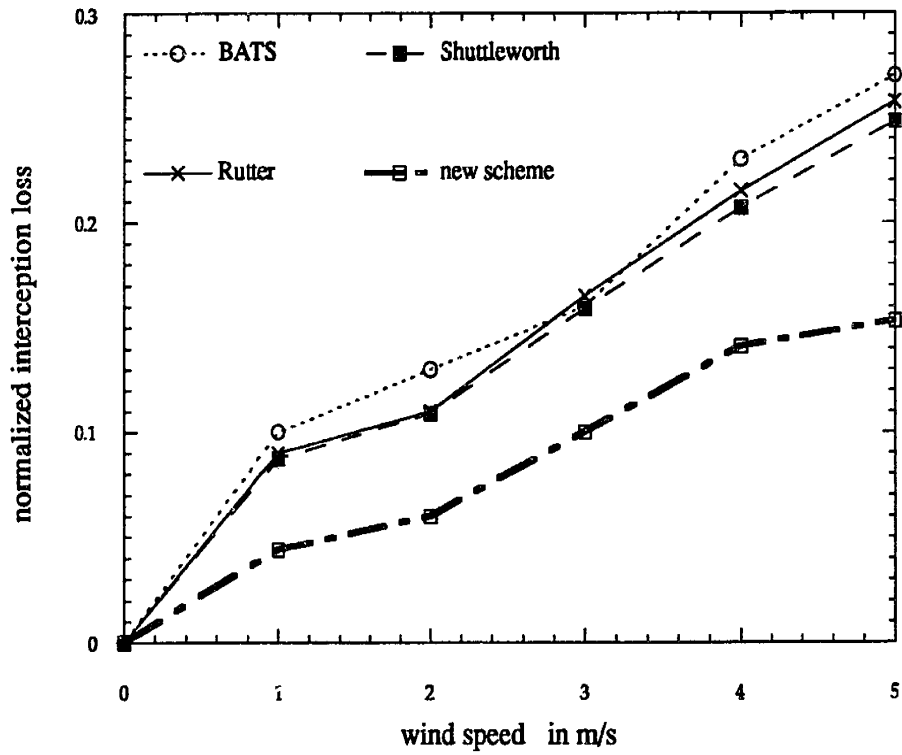


Figure 4.5 Comparison of interception loss simulated by the Rutter model, BATS interception, Shuttleworth interception scheme and the new interception scheme. ($q_C = q_P = 0.3$)

and recalling the exponential dependence between local drainage and local canopy storage. The enhancement of average canopy drainage reduces the amount of intercepted water available for evaporation and that significantly reduces interception loss. Another reason for the reduction in interception loss is the assumption that canopy evaporation occurs over a fraction q_c of the grid point area.

The objective of the comparison between the different interception schemes is to explore the effects of including spatial variability in modeling of interception loss. The new scheme is compared to : schemes which assume that rainfall and canopy storage are constant in space, and a scheme which assumes that rainfall is variable in space but canopy storage is constant. These comparisons reveal the *relative* effects of including rainfall variability and canopy storage variability. The results of the simulations using the off-line model are sensitive to the specified set of forcing and parameters and more importantly to the values of q_p and q_c . The purpose in using the off-line model is the *relative comparison* between the different schemes. Accurate simulation of interception loss by some of the schemes in Figure 4.5 should not be taken as a proof of their capability in modeling interception over large areas. This capability can only be tested by using 3-D climate models.

4.5 Conclusions

The approach of combining physical models of hydrologic processes at a point and statistical description of the subgrid scale spatial variability is a powerful technique in deriving

parameterizations of these processes for climate models. It provides useful insight into the nature of these processes over large areas.

A new interception scheme is introduced for describing interception over large areas. It combines a physical description of interception at a point, which is the Rutter model of interception, and statistical description of the spatial variability of canopy storage and rainfall. The interception loss predicted by the new scheme is significantly smaller than those predicted by other schemes which assume that canopy storage and rainfall are constant in space. This result may explain why climate models overestimate interception loss; it suggests that the neglect of spatial variability is a significant source of error in describing interception over large areas.

The interception loss simulated by the Shuttleworth scheme is slightly smaller than the losses simulated by the BATS interception or the Rutter model. Recalling that the Shuttleworth scheme treats rainfall as a spatially variable forcing, the comparison in Figure 4.5 suggests that for adequate description of interception over large areas it is necessary to include *both* the effects of spatial variability of canopy storage and rainfall.

Observations of the spatial distribution of canopy storage are not available at the scales considered in this study. Hence the assumption about the statistical distribution of canopy storage is not supported by observations. Nevertheless it is more reasonable to acknowledge the spatial variability in canopy storage than to assume canopy storage is constant in space. We emphasize that although the form of the distribution of canopy storage is assumed constant in time

(exponential), the exact distribution varies in time. This is achieved by updating the mean of the distribution at each time step.

In the above derivations it is assumed that the distribution of canopy storage is independent from the distribution of rainfall. Since rainfall variability is the main causing factor of the variability in canopy storage, the two distributions may be related. The parameters of the Rutter model are assumed constant in space at the sub-grid scale. The possible effects due to spatial variability in these parameters is an open question for future research. The success of the new scheme in describing interception processes over large areas depends very much on the quality of the two assumptions about the distribution of canopy storage and the variability of the model parameters.

CHAPTER 5

Description of the Climate Model

5.1 Introduction

Chapter 6 deals with the sensitivity of regional climate in the Amazon basin to small-scale deforestation using a modeling approach. This chapter describes the climate model which is used in the sensitivity experiments.

The original version of the model is known as the Pennsylvania State University/National Center for Atmospheric Research (PSU/NCAR) model. It is also referred to as the Meso-scale Model version 4 (MM4). It was originally developed for meso-scale meteorological studies. The climate model which is used in this study is an augmented version of MM4; it has been modified to suit climate studies. The land-surface hydrology scheme which is used as part of the augmented model is the Biosphere-Atmosphere Transfer Scheme (BATS). In this study BATS is modified to improve on the hydrology of the scheme.

In the following, the original MM4 model is described in section 5.2, the version of MM4 which is suitable for climate studies is described in section 5.3. BATS is described in section 5.4 and the new modifications to the land-surface hydrology scheme are described in section 5.5.

5.2 The MM4 model for Meteorological Studies

MM4 is a compressible and hydrostatic model which solves the primitive equations in a terrain varying vertical coordinate. The model

is driven by boundary conditions and solar radiation. It includes the bulk boundary layer parameterization of Deardorff (1972) and the cumulus parametrization of Anthes (1977), which is of the Kuo type. MM4 includes a simple long-wave radiative cooling scheme. The basic structure of the MM4 model is described by Anthes et al. (1987). The MM4 model has been used successfully in a large number of meteorological studies.

5.3 The MM4 model for Climate Studies

For climate studies it is necessary to include into the model accurate descriptions of radiative transfer in the atmosphere and near the surface. The augmented version of MM4 model has the same structure as the original MM4 except that it includes a sophisticated surface physics and soil hydrology package, an explicit boundary layer formulation and a more detailed treatment of radiative transfer.

The surface physics and soil hydrology package is the Biosphere-Atmosphere Transfer Scheme (BATS), Dickinson et al. (1986). It will be described in some detail in the next section. The radiation parameterization is the same scheme as the one used in NCAR General Circulation Model (GCM); it performs separate calculations of atmospheric heating rates and surface fluxes for solar and infrared radiation for clear and cloudy skies. The solar clear sky scheme follows the parameterization of Lacis and Hansen (1974). The solar cloudy sky scheme accounts for reflection at the top of the clouds, multiple reflections between the clouds, and between the ground and clouds. Infrared radiative transfer scheme includes the contribution of atmospheric gases and clouds.

Two recent studies, Anthes et al. (1989) and Giorgi and Bates (1989), focus on the climatological skill of the MM4 model. They test the skill of the model in simulating observed climatology when driven by the corresponding observed boundary and initial conditions. The model performed reasonably good in these experiments.

The MM4 model has been used recently in many studies to simulate details of regional climates, Giorgi(1990). The model is driven with output from a General Circulation Model (G.C.M.), the high resolution of the MM4 is utilized in resolving some physical effects which are not resolved by the G.C.M. , e.g., effects of topography. This one-way nesting procedure can be very useful in making predictions about changes in the regional climate. These predictions are not usually possible to make using G.C.M.s due to their coarse resolution. Implicit in this nesting procedure is the assumption that the improvements in description of the physical processes inside the model domain will not have any effect on the surrounding model atmosphere.

5.4 The Biosphere-Atmosphere Transfer Scheme (BATS)

BATS describes a land-surface which consists of a vegetation layer, a surface soil layer and a deep soil layer (root zone). A seasonally dependent fraction of the grid-cell area is covered by vegetation; the remaining fraction is assumed covered by bare soil. Soil temperature is predicted using a prognostic equation which describes the force-restore method of Deardorff (1972). The temperatures of the canopy and that of the air within the canopy are determined using diagnostic equations which describe conservation of

energy and conservation of water mass at the land-surface. This energy balance equation includes radiative, latent and sensible heat fluxes.

The land-surface hydrology scheme consists of prognostic water balance equations which predict the water content of the surface layer and of the root zone. The components of this water balance are rainfall, throughfall, infiltration, evapotranspiration, surface runoff, ground water runoff, infiltration below root zone and diffusive exchange of water between the two layers. The soil water movement formulation is parameterized to fit the results of the simulations by Dickinson (1984) using a high resolution soil model. It is assumed that the coefficient of surface runoff is equivalent to the fourth power of saturation in the surface soil layer (saturation is the ratio of the water depth in the soil layer to the maximum capacity of the layer). The treatment of interception in BATS is described in Appendix 4.1.

The fluxes of latent heat, sensible heat and momentum are calculated using the similarity theory approach. The drag coefficients are calculated based on surface roughness and atmospheric stability of the surface layer. For neutral and stable conditions turbulent vertical transport is modeled using an eddy diffusion formulation. For unstable conditions transport is modeled by a dry convective adjustment scheme. BATS is described in detail by Dickinson et al. (1986).

5.5 Modifications of the Land-surface Hydrology Scheme

BATS includes a detailed description of the vertical structure of surface layer, in contrast the scheme assumes constant surface

properties and uniform forcing in the horizontal. Subgrid scale spatial variability in rainfall, canopy storage and soil moisture play a significant role in some important processes taking place in a rain-forest environment. The partition of rainfall into throughfall and interception loss, and the subsequent partition of throughfall into infiltration and surface runoff are examples of these processes which are sensitive to the effects of subgrid scale spatial variability. This sensitivity is basically due to the non-linearity involved in the interception and runoff processes. The BATS treatment of interception and runoff are modified in this study to account for the effects of the subgrid scale spatial variability. These modifications are important because they balance the emphasis on *vertical* details by accounting for some of the important effects resulting from spatial variability in the *horizontal*.

A new interception scheme which accounts for the effects of spatial variability in rainfall and canopy storage is included into the BATS. The details of this scheme are described in Chapter 4.

A runoff scheme similar to that of Entekhabi and Eagleson (1989) is developed for modeling surface runoff. A slightly different form of the infiltration function is used; it is given by

$$f^* = \alpha (1 - s) \quad (5.1)$$

where f^* is infiltration capacity of the soil, α is infiltration capacity of the soil when completely dry, and s is saturation level of the surface layer (taken as the top 10 centimeters of the soil). This infiltration function is a simplified form of the infiltration function used by Entekhabi and Eagleson (1989).

The spatial variability in rainfall and soil moisture are modeled using a statistical approach. It is assumed that rainfall is exponentially distributed in space according to Equation 4.5. Soil saturation of the top layer is assumed distributed in space according to

$$f_s = \frac{1}{E(s)} e^{-\frac{s}{E(s)}} \quad (5.2)$$

$E(s)$ is the spatial average of soil saturation.

Runoff occurs at a point where rainfall intensity exceeds the infiltration capacity of the soil (Hortonian runoff) or where rainfall occurs on a saturated soil (Dunne runoff). The areally averaged runoff is then given by

$$r = \int_{s=0}^1 \int_{P=f^*}^{\infty} (P - f^*) f_p dP f_s ds + \int_{s=1}^{\infty} \int_{P=0}^{\infty} P f_p dP f_s ds = r_H + r_D \quad (5.3)$$

where r_H is Hortonian runoff and r_D is Dunne runoff. Evaluating the above integrals results in

$$r = \frac{E(P)}{d E(s)} e^{-\frac{q_p \alpha}{E(P)}} (e^d - 1) + E(P) e^{-\frac{1}{E(s)}} \quad (5.4)$$

where d is given by

$$d = \frac{q_p \alpha}{E(P)} - \frac{1}{E(s)}$$

Eltahir and Bras (1992) provide a new formula for computing the fractional coverage of rainfall, q_p . The new procedure is based on

the observation that the average rainfall over the total area of the grid-cell (including wet and dry regions), $E(P)$, divided by q_p is a constant for a certain region and season of the year. This constant is equivalent to the climatological rainfall rate, i . The new procedure for computing the fractional coverage of rainfall is consistent with the observations of convective storms.

The new formula for computing the fractional coverage of rainfall implies that the runoff coefficient R_f is given by

$$R_f = \frac{r}{E(P)} = \frac{e^{-\left(\frac{\alpha}{i}\right)} (e^d - 1)}{E(s) d} + e^{-\frac{1}{E(s)}} \quad (5.5)$$

where d is given by

$$d = \frac{\alpha}{i} - \frac{1}{E(s)}$$

By comparing Equations 5.4 and 5.5 we note that the substitution for q_p using the formula of Eltahir and Bras (1992) $q_p = E(P) / i$, changes the form of the dependence of R_f on rainfall. Equation 5.4 shows that R_f is dependent on q_p and $E(P)$ among other variables. On the other hand, the formula developed for R_f in Equation 5.5 suggests that R_f is a function of i ; which is equivalent to average rainfall intensity over large raining areas.

In *small-scale* hydrologic applications it is often assumed that the runoff coefficient is a function of the rainfall intensity over the small area. Equation 5.5 is consistent with this practice in suggesting that over *large-scales* the runoff coefficient is also a function of a measure of the rainfall intensity over the large area. This measure is the spatial average of rainfall intensity which is estimated by the climatological rainfall rate, i .

CHAPTER 6

Sensitivity of Regional Climate to Small-Scale Deforestation

6.1 Introduction

Since the impact of deforestation on climate depends on the scale of the deforested area, the sensitivity of regional climate to deforestation can be studied at different scales. The previous studies on the Amazon deforestation problem, e.g. Dickinson and Henderson-Sellers (1988), Lean and Warrilow (1989) and Nobre et al. (1991), focus on the sensitivity of climate to deforestation of large areas in the order of 10^6 squared kilometers, which is the scale of the Amazon basin. It is interesting to study the deforestation problem at this large-scale, but the observations of the current rates of deforestation and those of the size of the cleared areas in the Amazon region suggest that deforestation is occurring at smaller scales. It is estimated that the rate of deforestation in the Amazon is in the order of 2×10^4 squared kilometer per year, Nobre et al. (1991). It is also important to note that the scaling analysis of the recycling ratio in Chapter 3 indicates significant dependence on the scale considered. Hence the potential for interactions between hydrology and climate depends on the scale considered.

This Chapter deals with the sensitivity of regional climate in the Amazon basin to small-scale deforestation. Small-scale refers to areas with a linear scale of about 250 kilometers each side.

The climate model which is described in Chapter 5 is used in performing the sensitivity experiments. The design of the experiments is presented in section 6.2. The boundary and initial conditions are

described in section 6.3. The results of the experiments are presented in sections 6.4 and 6.5 followed by a concluding discussion in section 6.6.

6.2 Design of the Experiments

The sub-region of the Amazon rain-forest considered in these experiments is centered at 6.5° S and 67.5° W, Figure 6.1. The scale of this region is 1600 kilometers each side. The sensitivity experiments are performed for the months of January and July to represent typical summer and winter conditions respectively. For each of the two months the sensitivity experiments consist of two runs using the meso-scale climate model : a control run to simulate the pre-deforestation state of the land-atmosphere system, and a perturbed run to simulate the post-deforestation state of the same system.

Deforestation is modeled by replacing the rainforest with short grass in a region which is also centered at 6.5° S and 67.5° W but with a smaller scale of 250 kilometers each side. The location of the deforested region is shown in Figure 6.2. Deforestation is achieved in the model by changing the values of the parameters describing land cover and soil from those corresponding to rain-forest to the values corresponding to short grass. These values are specified by Tables 2 and 3 of Dickinson et al. (1986) and some of them are shown in Table 6.1.

The spatial resolution which is used in this study is 50 kilometers in the horizontal. Fourteen pressure levels are distributed between the surface and the tropopause in the vertical. The temporal resolution is 90 seconds.

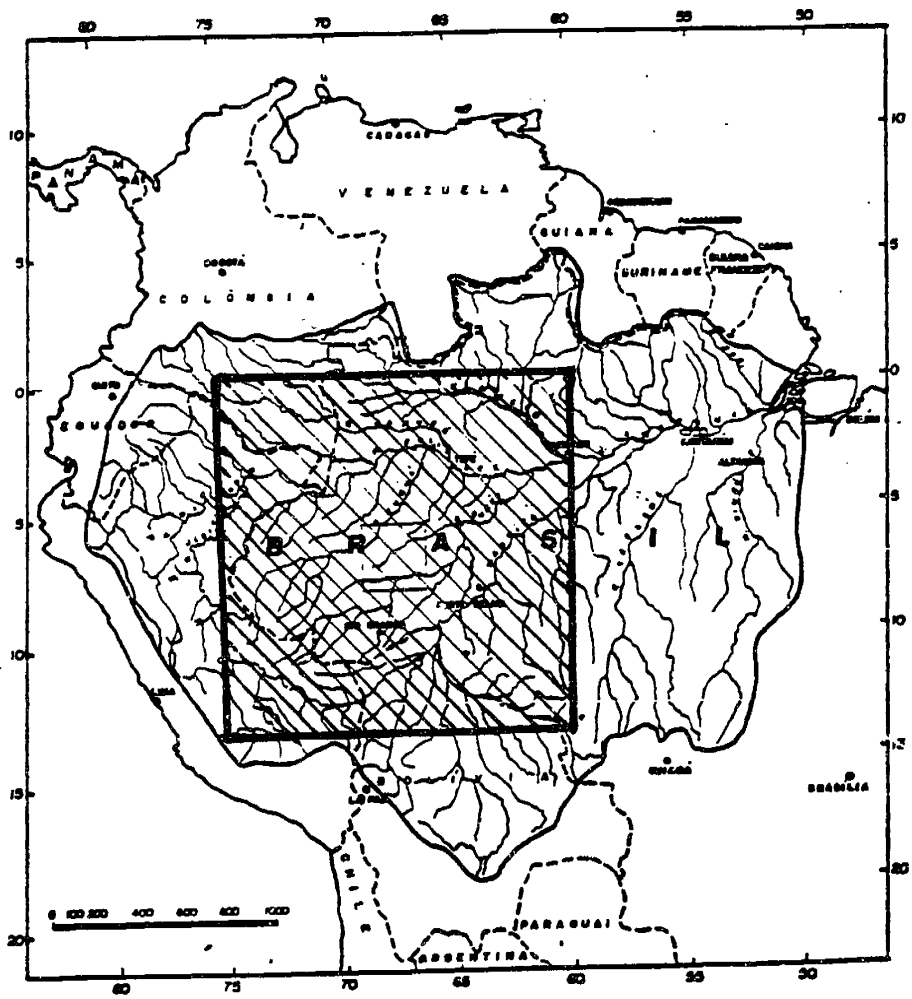


Figure 6.1 Location of the numerical experiment(square box with hatching).

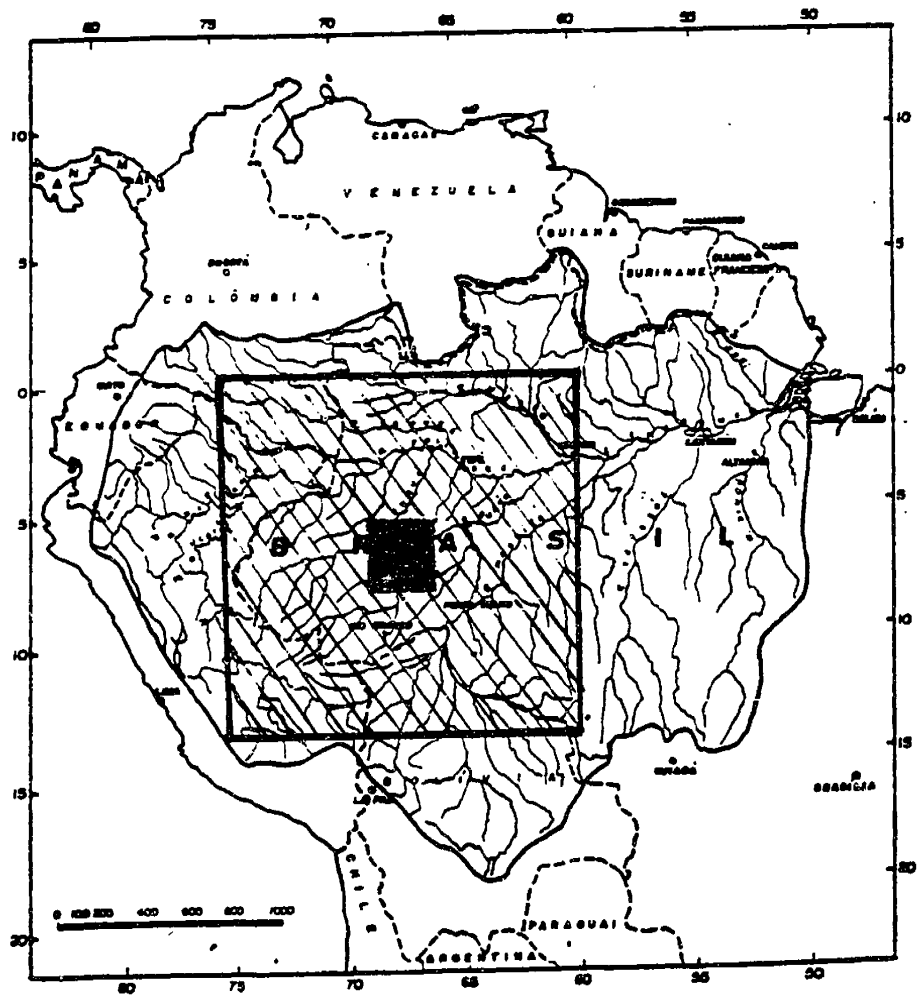


Figure 6.2 Location of the deforested region(dark square box).

Parameter	Rain-forest	Short Grass
fractional vegetational cover	0.9	0.8
roughness length(meter)	2.0	0.02
vegetation albedo for wavelengths $\geq 0.7 \mu m$	0.2	0.3
vegetation albedo for wavelengths $< 0.7 \mu m$	0.04	0.10
maximum leaf area index	6	2
porosity	0.54	0.48
saturated hydraulic conductivity (mm/s)	3.2×10^{-3}	6.3×10^{-3}
parameters of surface hydrology :		
α (mm/hour)	8.0	8.0
i (mm/hour)	4.9	4.9
K (mm/min)	2.9×10^{-5}	2.9×10^{-5}
b (mm)	0.2	0.2
C_m (mm)	2.0	2.0
S (mm)	0.75	0.15

Table 6.1 : Parameters of land cover and soil for rain-forest and short grass environments.

6.3 Boundary and Initial Conditions

The climate model is driven by solar radiation and boundary conditions from the ECMWF global data set, which is described in Chapter 3 (see section 3.5). Temperature and pressure are specified at the boundaries according to the ECMWF data. Wind and specific humidity are specified at the inflow boundaries from the ECMWF analysis but the same two variables are predicted by the model solution at the outflow boundaries. Inflow boundaries are those where the component of the wind vector (which is estimated from the ECMWF data) perpendicular to the boundary points into the domain of the simulation. Outflow boundaries are those where the component of the wind vector perpendicular to the boundary points away from the domain of the simulation. The upper boundary condition is a no flow boundary.

The boundary conditions are specified in the manner described above in order to obtain a smooth solution with insignificant boundary effects. Specification of wind and specific humidity from the ECMWF data at all the boundaries may result in simulations with strong boundary effects; in these simulations some of the variables, e.g. rainfall, have large gradients near the boundaries.

For each month initial conditions are specified using the corresponding conditions from the ECMWF data. The initial soil moisture conditions are specified according to the standard values recommended by the original MM4 modeling system, Anthes et al. (1987). These values describe typical conditions for each season and land cover type. We used the values corresponding to January and July.

The January and July climates are simulated by driving the model with the ECMWF data for January and July of the years 1985, 1986 and 1989. Since the years 1987 and 1988 include El Niño events, they are not included in these simulations. The control and perturbed climate states are estimated from the averages for January and July of the three years.

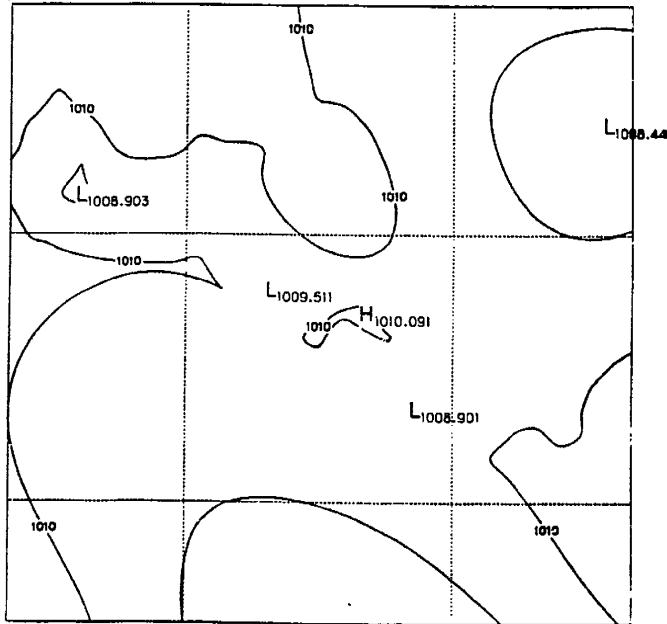
6.4 Results for January

The results of the sensitivity experiments for January are presented in this section. The results of the control runs and the perturbed runs are presented separately. They describe the pre-deforestation and post-deforestation states of the land-atmosphere system as simulated by the climate model.

6.4.1 January Climate: Pre-Deforestation

The skill of the model in simulating the climate of the Amazon region is tested by comparing the fields for key atmospheric variables simulated by the model and the corresponding fields estimated from ECMWF data. Figures 6.3, 6.4, and 6.5 show fields of the following variables : sea level pressure, temperature and humidity(at 850 mb, 500 mb and 200 mb) . The same figures compare the fields simulated by the model with those from ECMWF data set. The comparison indicates that the model is capable of reproducing the average climate of the region. The amounts of water vapor in the upper troposphere are very small, hence although the error in simulating these amounts is small in absolute value, the relative error (in comparison to the water vapor amount) is significant.

SLP AT P=1000.000. MEAN FROM 85010100 TO 85013100. Obs



SLP AT P=1000.000. MEAN FROM 85010100 TO 85013100. Model

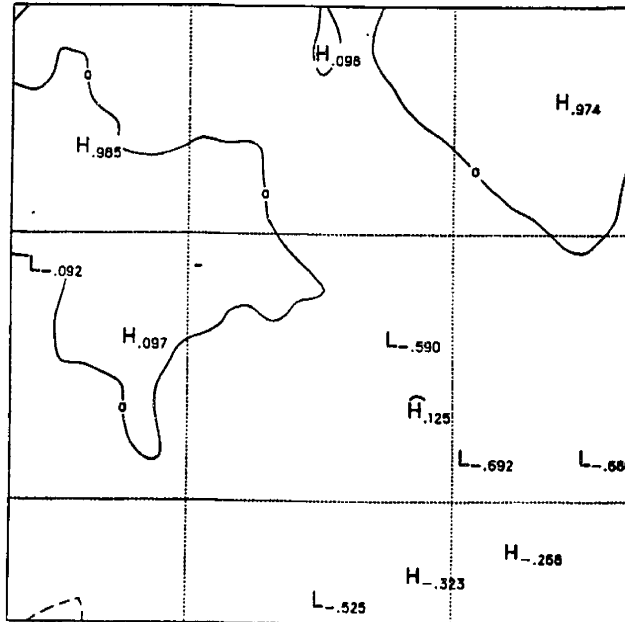
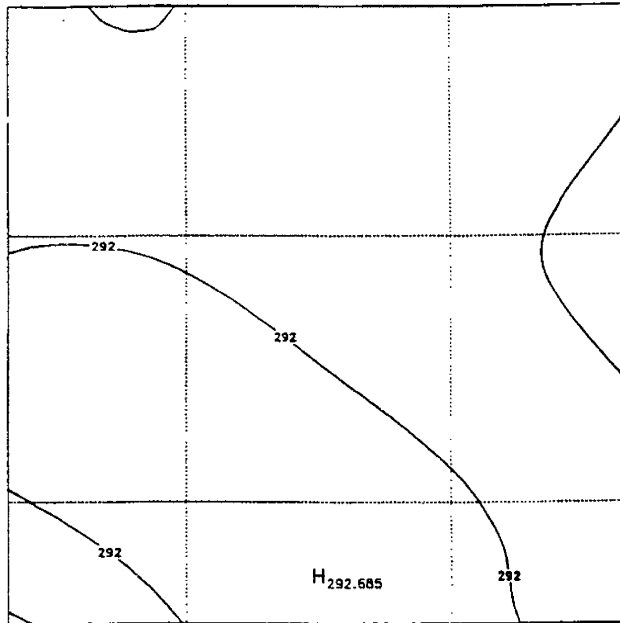


Figure 6.3 Sea level pressure in mb, for January, "obs" refers to ECMWF data and "model" refers to differences between the simulated fields and the observed fields.

T AT P= 850.000. MEAN FROM 85010100 TO 85013100. Obs



T AT P= 850.000. MEAN FROM 85010100 TO 85013100. Model

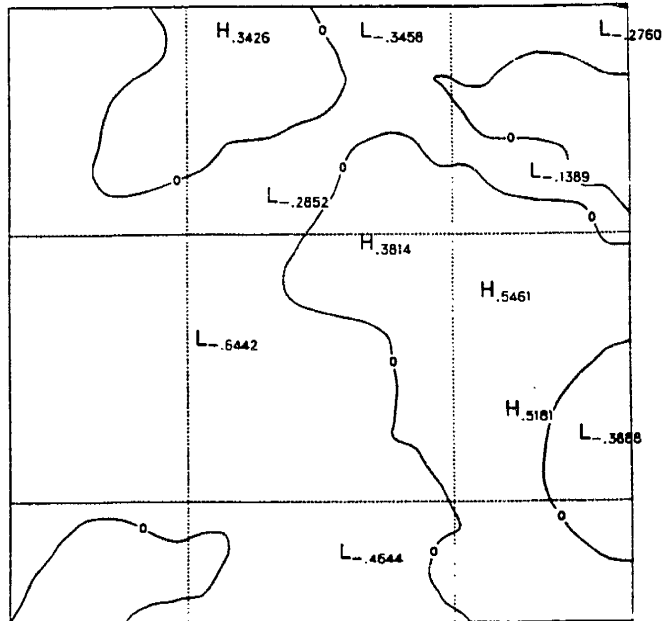
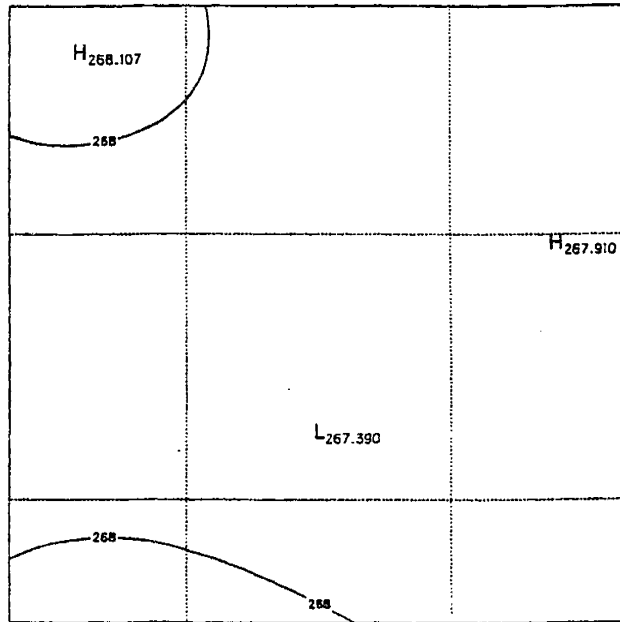


Figure 6.4 (a) Temperature in ° K at 850 mb, for January, "obs" refers to ECMWF data and "model" refers to differences between the simulated fields and the observed fields.

T AT P= 500.000. MEAN FROM 85010100 TO 85013100. Obs



T AT P= 500.000. MEAN FROM 85010100 TO 85013100. Model

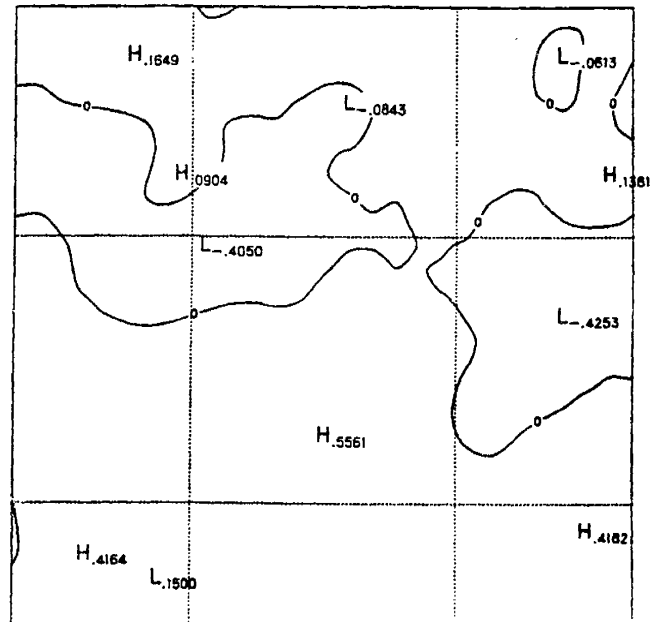
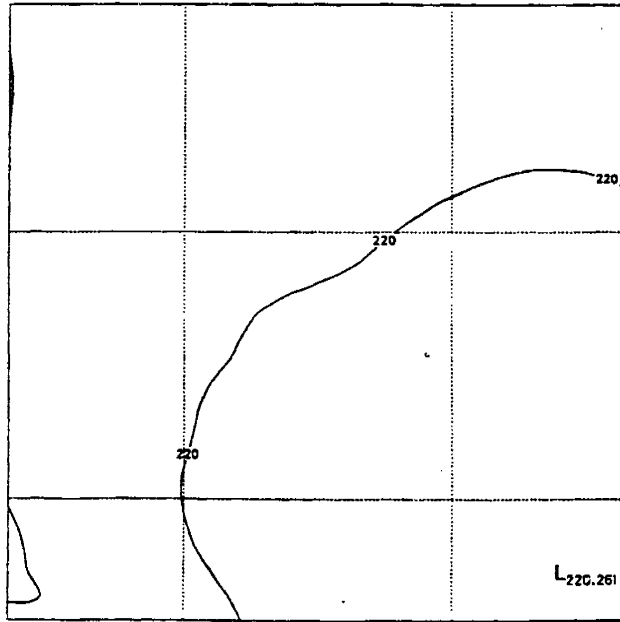


Figure 6.4 (b) same as 6.4(a) except at 500 mb.

T AT P= 200.000. MEAN FROM 85010100 TO 85013100. Obs



T AT P= 200.000. MEAN FROM 85010100 TO 85013100. Model

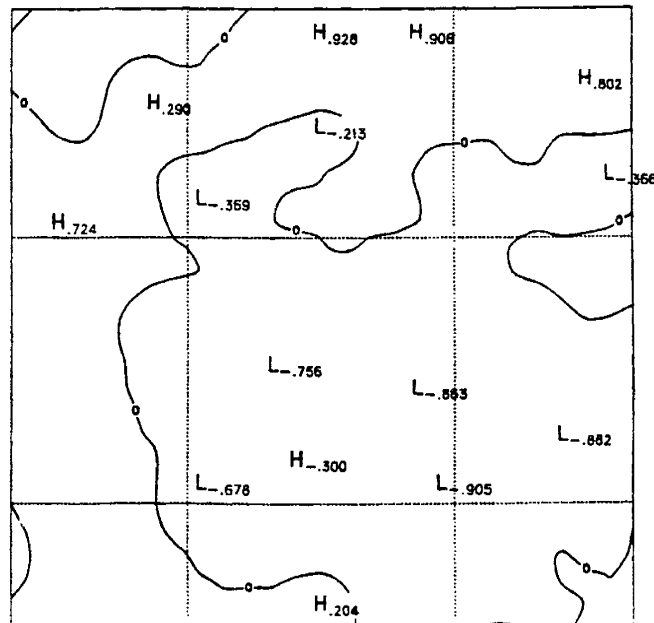
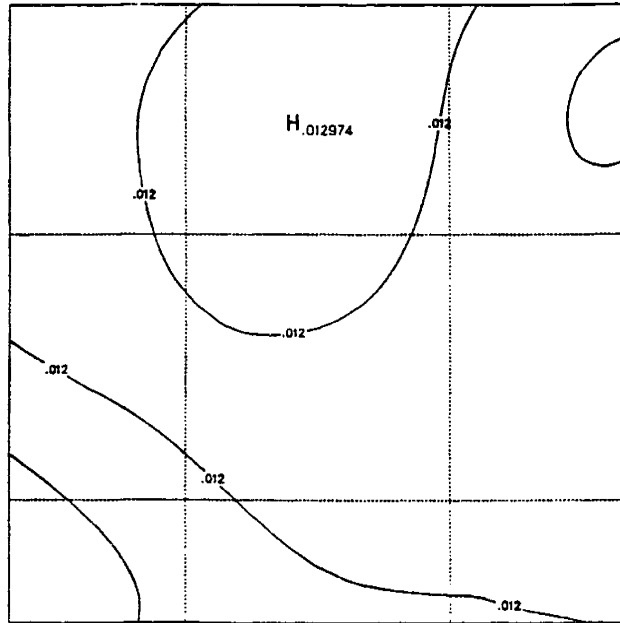


Figure 6.4 (c) same as 6.4(a) except at 200 mb.

Q AT P= 850.000. MEAN FROM 85010100 TO 85013100. Obs



Q AT P= 850.000. MEAN FROM 85010100 TO 85013100. Model

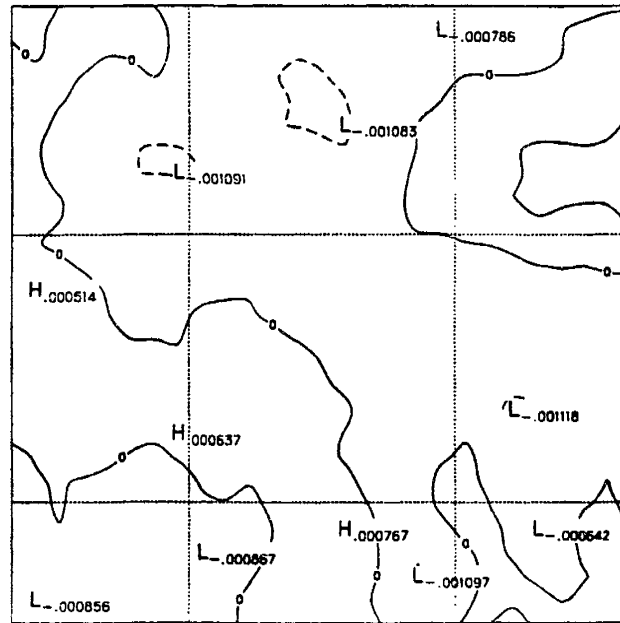
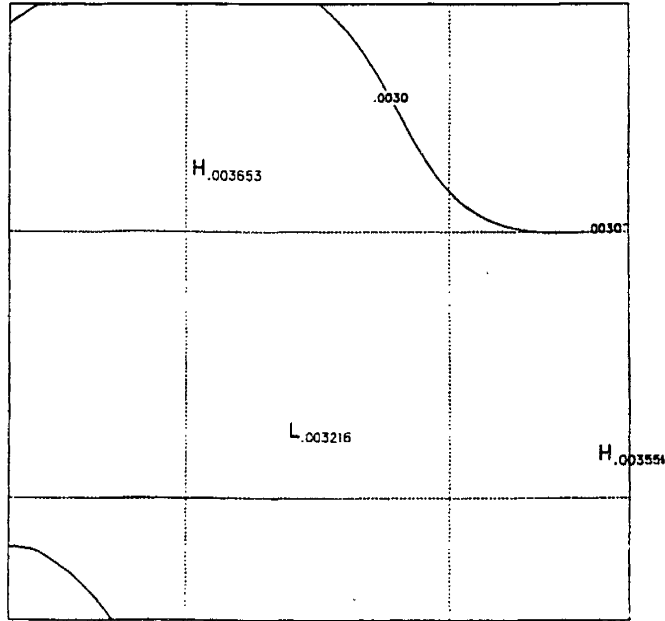


Figure 6.5 (a) Mixing ratio at 850 mb, for January, "obs" refers to ECMWF data and "model" refers to differences between the simulated fields and the observed fields.

Q AT P= 500.000. MEAN FROM 85010100 TO 85013100. Obs



Q AT P= 500.000. MEAN FROM 85010100 TO 85013100. Model

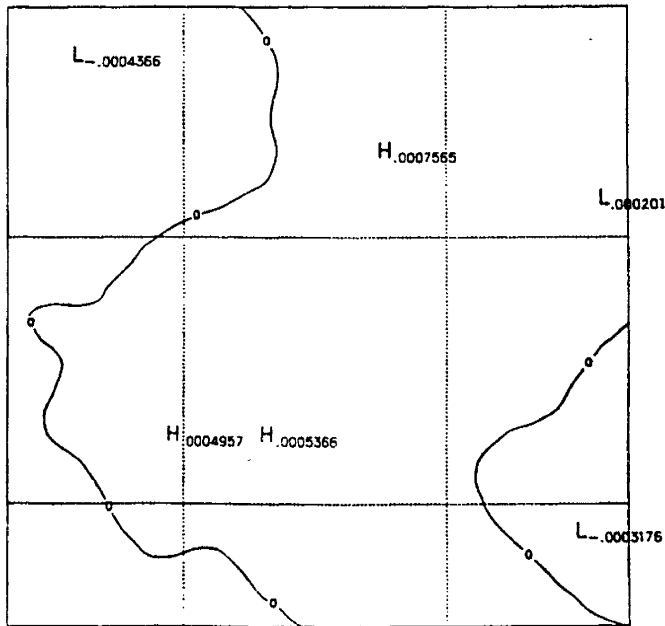


Figure 6.5 (b) same as 6.5(a) except at 500 mb.

Variable	Model	Observations	References
surface temperature	28.3° C	26.0 ° C*	(1)
net surface radiation	178	120	(2)
evaporation	140	107	(2)
sensible heat flux	37		
precipitation	184	270	(2)
runoff	86		
interception loss	22		
runoff ratio	47%	44%*	(3)
interception ratio	12%	10%	(2)

Table 6.2 : Pre-Deforestation climate in January, units are in mm/month. * indicates that the observation is an annual value. References are indexed as follows (1) Molion(1975), (2) Shuttleworth (1988b), and (3) Oltman (1967)

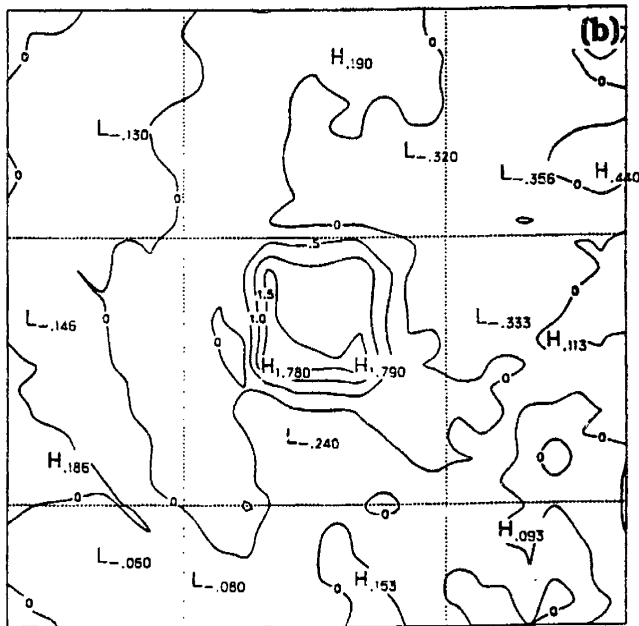
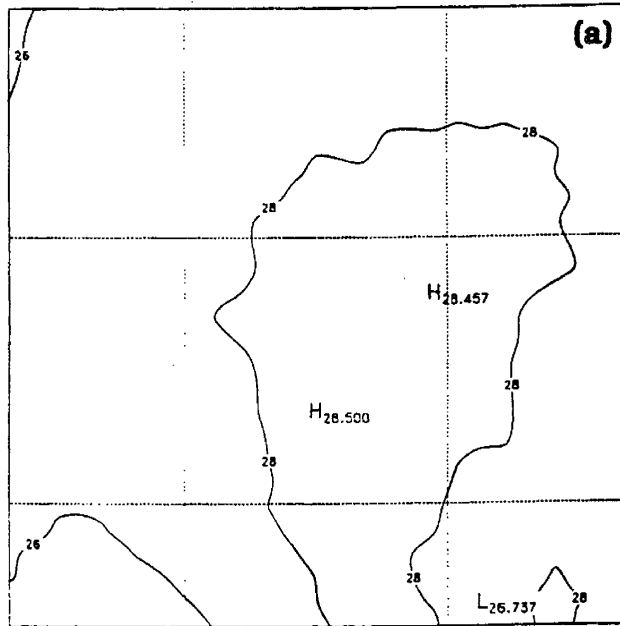


Figure 6.6 Ground temperature in ° C, for January. (a) pre-deforestation field (b) (post-deforestation field- pre-deforestation field).

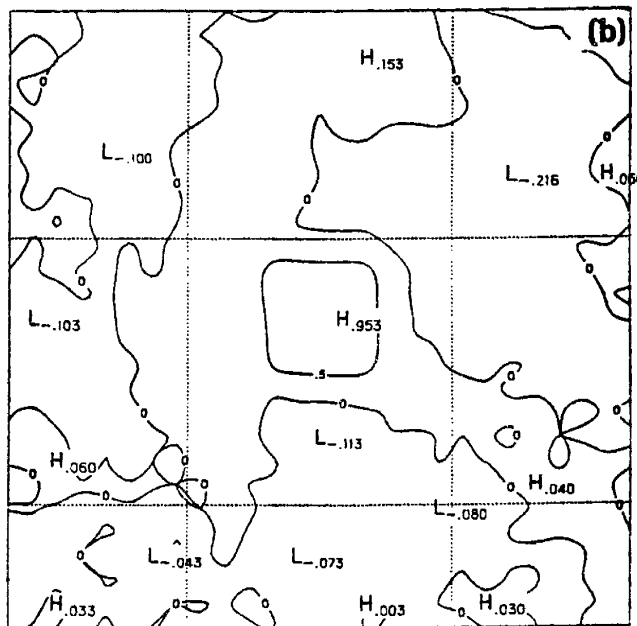
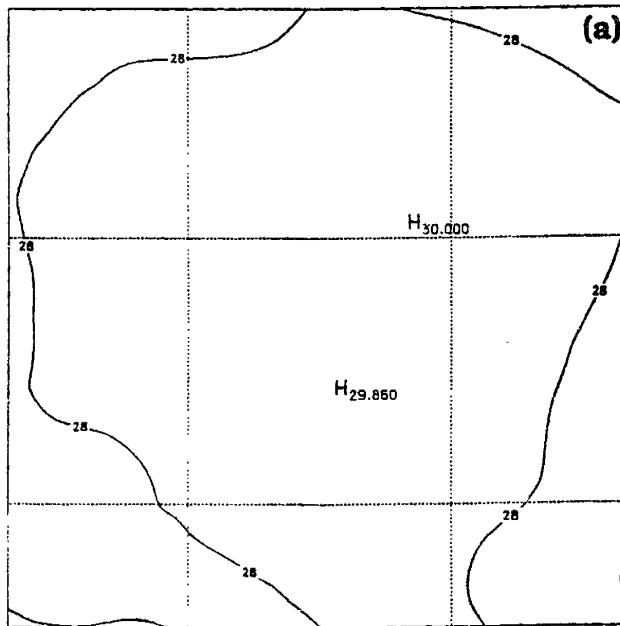


Figure 6.7 Air temperature in ° C, for January. (a) pre-deforestation field (b) (post-deforestation field- pre-deforestation field).

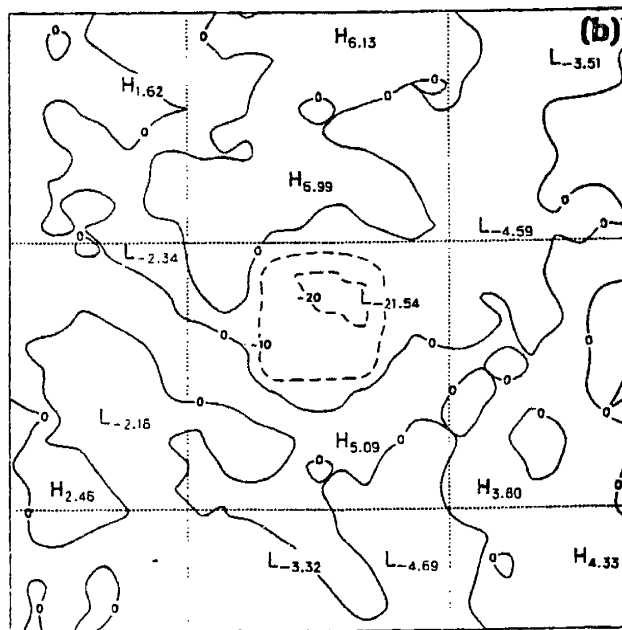
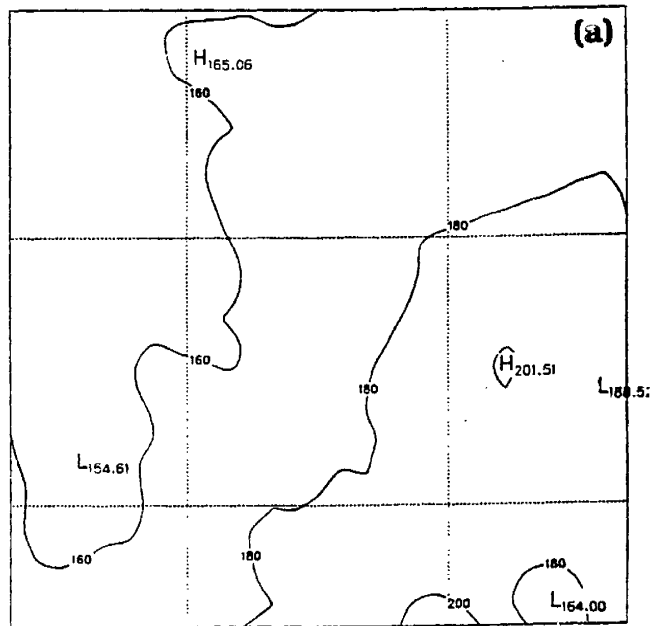


Figure 6.8 Net surface energy in W/m^2 , for January, (a) pre-deforestation field (b) (post-deforestation field- pre-deforestation field).

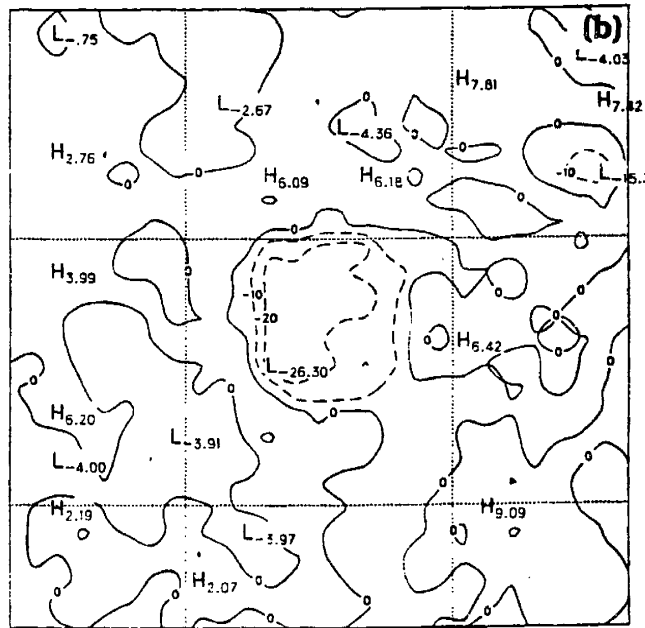
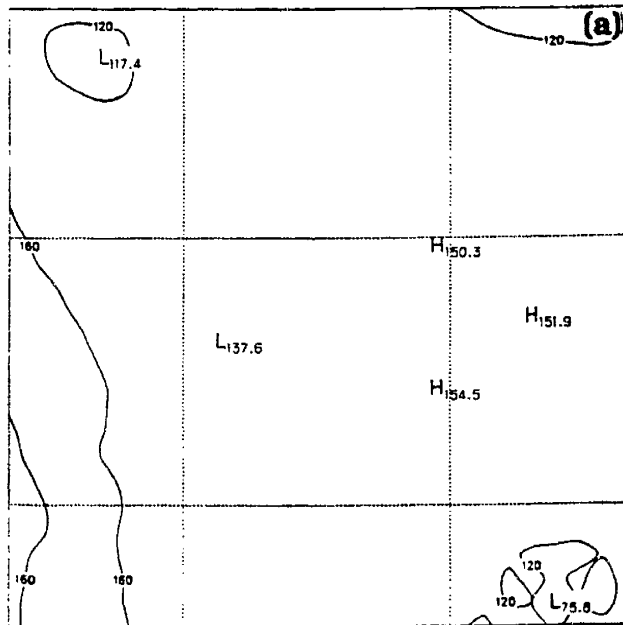


Figure 6.9 Evaporation in mm, for January. (a) pre-deforestation field (b) (post-deforestation field- pre-deforestation field).

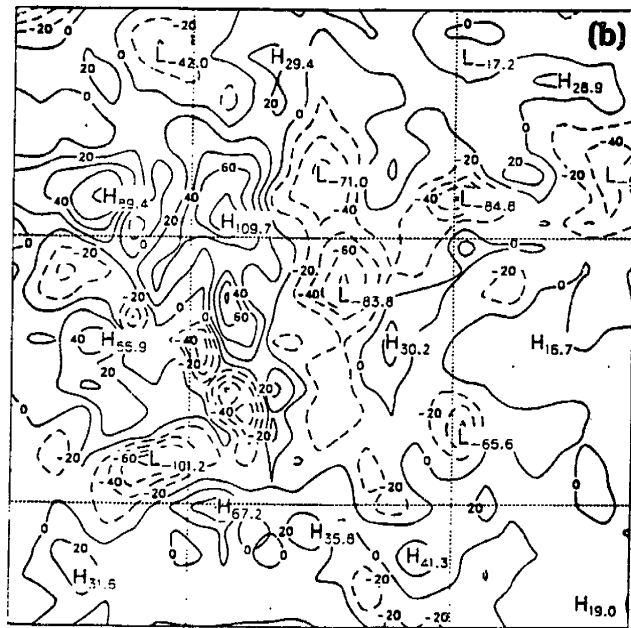
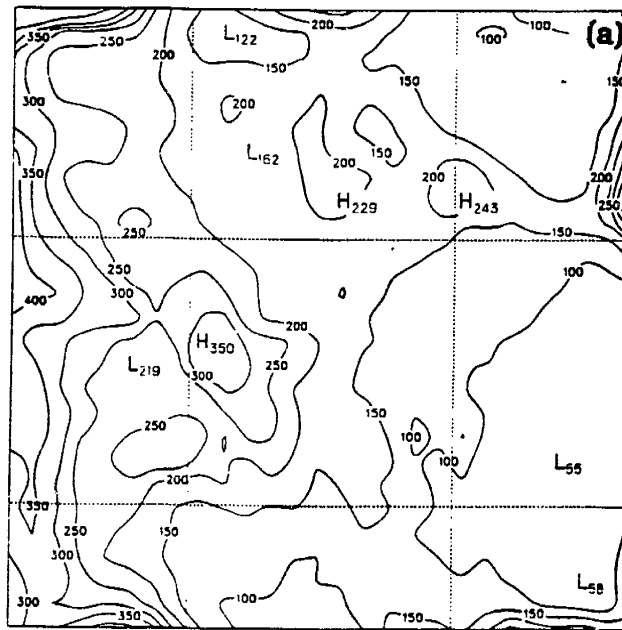


Figure 6.10 precipitation in mm, for January. (a) pre-deforestation field (b) (post-deforestation field- pre-deforestation field).

Variable	Predicted Change	
	January	July
Surface Temperature	+ 0.6° C	+0.7° C
Ground Temperature	+ 1.2° C	+1.2° C
Net Surface Radiation	- 8%	- 8 %
Evaporation	-14%	- 12 %
Precipitation	-10%	- 8%

Table 6.3 : Sensitivity of regional climate to small-scale deforestation in the Amazon Basin.

Table 6.2 compares the spatial averages of some of these fields with observations. Precipitation is underestimated by about 30%. This difference is large, but the accuracy of the model is reasonable when compared to the typical accuracy of climate models in predicting the distribution of precipitation. This large difference is due to underestimation of atmospheric moisture convergence into this sub-region by the ECMWF data. Underestimation of precipitation results in underestimation of cloudiness and for this reason overestimation of net radiation at the surface resulting in overestimation of evaporation. The model shows remarkable accuracy in predicting the runoff coefficient and the interception ratio in a rainforest environment. Figures 6.6, 6.7, 6.8, 6.9 and 6.10 show the fields of surface temperature, ground temperature, net surface energy, evaporation, and precipitation, which are simulated by the climate model.

6.4.2 January Climate: Post-Deforestation

The same Figures : 6.6, 6.7, 6.8, 6.9 and 6.10 show the difference between the post-deforestation and the pre-deforestation fields for the variables: surface temperature, ground temperature, net surface energy, evaporation, and precipitation. These difference fields measure the sensitivity of regional climate in January to deforestation of a small area in the center of the region. Table 6.3 presents the difference between the post-deforestation and the pre-deforestation fields for the variables mentioned above, averaged over the deforested area.

The sensitivity results are interpreted as follows: deforestation results in less absorption of solar radiation at the surface and as a

result the net radiation at the surface is reduced over the deforested region. Another important effect is the shorter roughness length of the deforested area; this effect reduces the eddy transport of heat and water vapor near the surface. The reduction of net radiation combined with the reduction in the efficiency of the eddy transport mechanism result in less evaporation from the deforested area. The reduction in evaporation means less evaporative cooling at the surface and that explains the warming of surface and ground temperatures. Less evaporation results in dryer boundary layer; it limits the supply of water vapor and reduces the energy available for convection and rainfall.

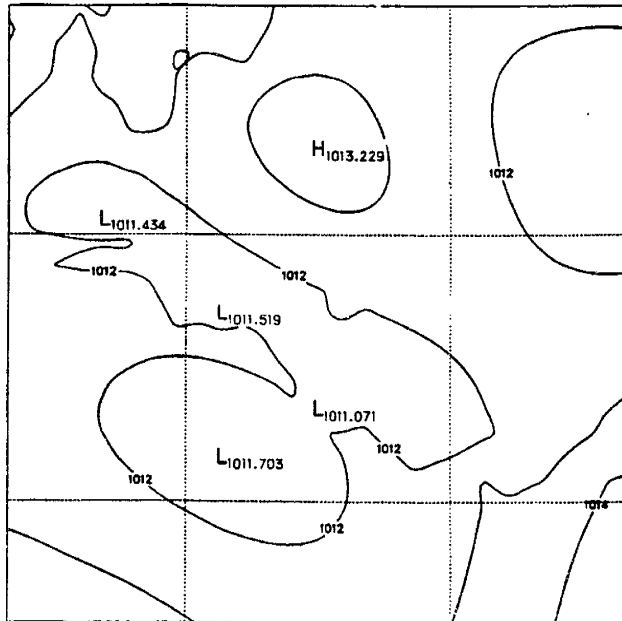
The warming of surface temperature increases the emission of long wave radiation by the surface; this secondary effect results in further reduction of the net radiation and evaporation at the surface. hence the reduction of surface net radiation due to deforestation is caused by two factors: the larger surface albedo and the increase in surface temperature.

6.5 Results for July

The results of the sensitivity experiments for July are presented in this section. The results of the control runs and the perturbed runs are presented separately. They describe the pre-deforestation and post-deforestation states of the land-atmosphere system as simulated by the climate model.

6.5.1 July Climate: Pre-Deforestation

SLP AT P=1000.000. MEAN FROM 85070100 TO 85073100. Obs



SLP AT P=1000.000. MEAN FROM 85070100 TO 85073100. Model

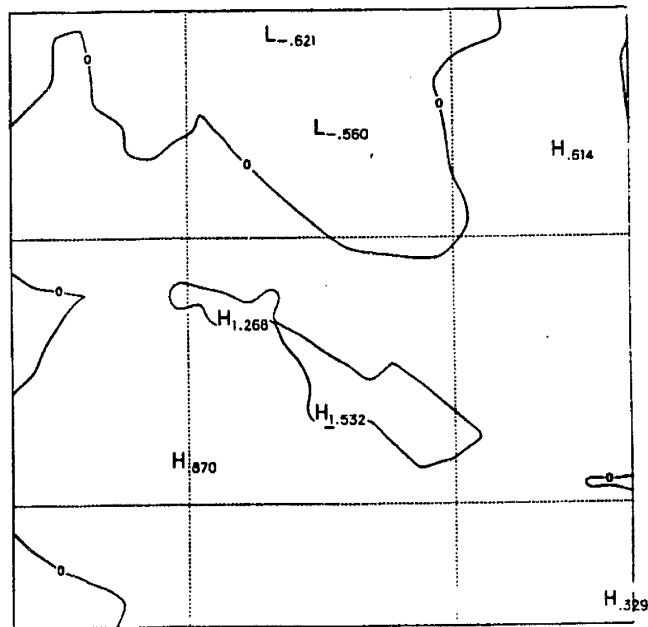
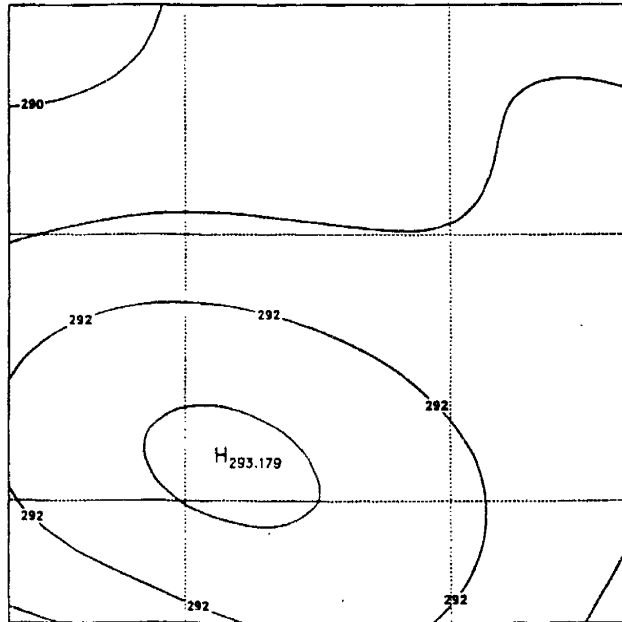


Figure 6.11 Sea level pressure in mb for July , "obs" refers to ECMWF data and "model" refers to differences between the simulated fields and the observed fields.

T AT P= 850.000. MEAN FROM 85070100 TO 85073100. Obs



T AT P= 850.000. MEAN FROM 85070100 TO 85073100. Model

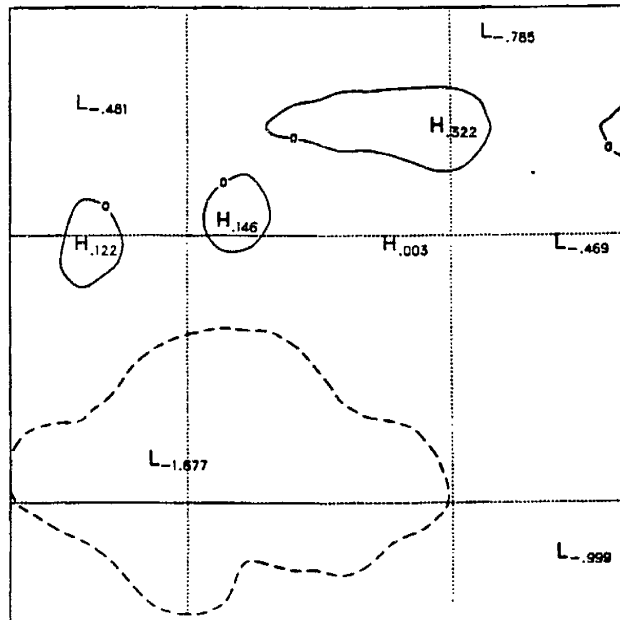
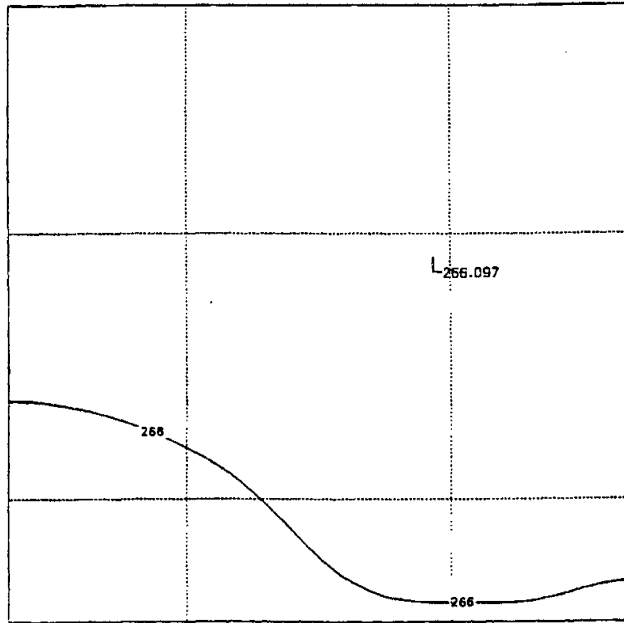


Figure 6.12 (a) Temperature in ° K at 850 mb for July, "obs" refers to ECMWF data and "model" refers to differences between the simulated fields and the observed fields.

T AT P= 500.000. MEAN FROM 85070100 TO 85073100. Obs



T AT P= 500.000. MEAN FROM 85070100 TO 85073100. Model

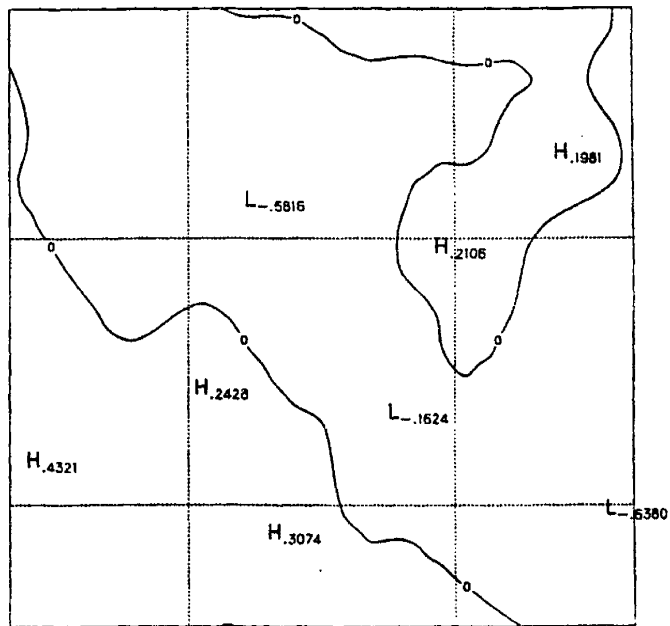
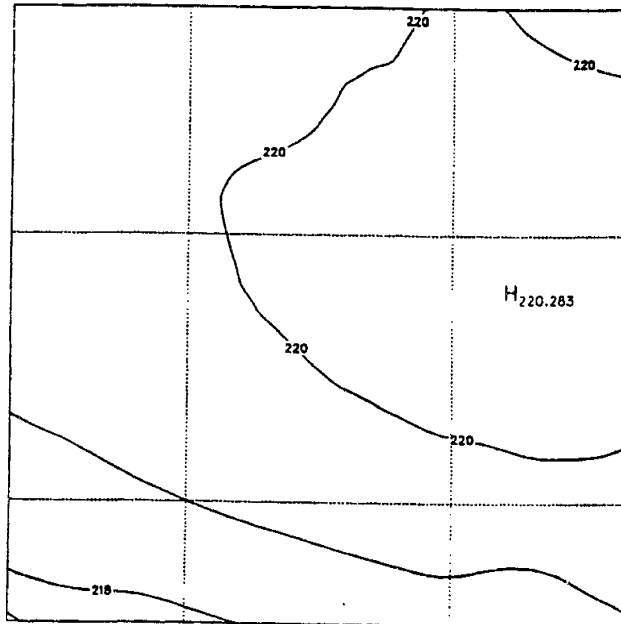


Figure 6.12 (b) same as 6.12(a) except at 500 mb.

T AT P= 200.000. MEAN FROM 85070100 TO 85073100. Obs



T AT P= 200.000. MEAN FROM 85070100 TO 85073100. Model

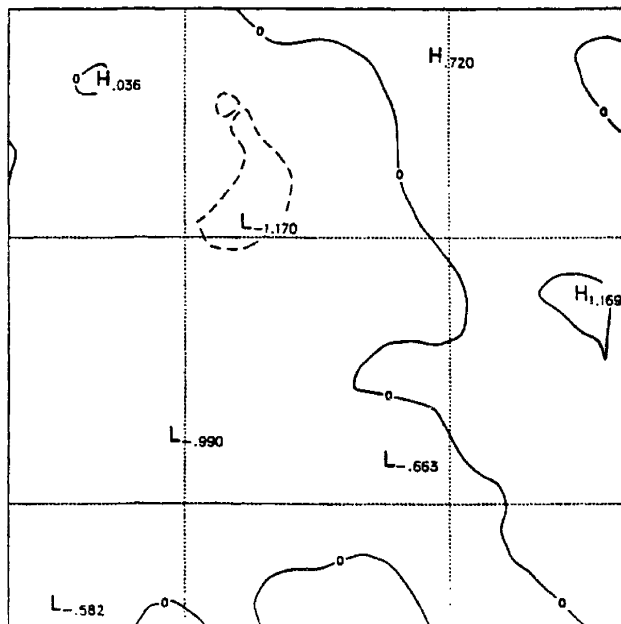
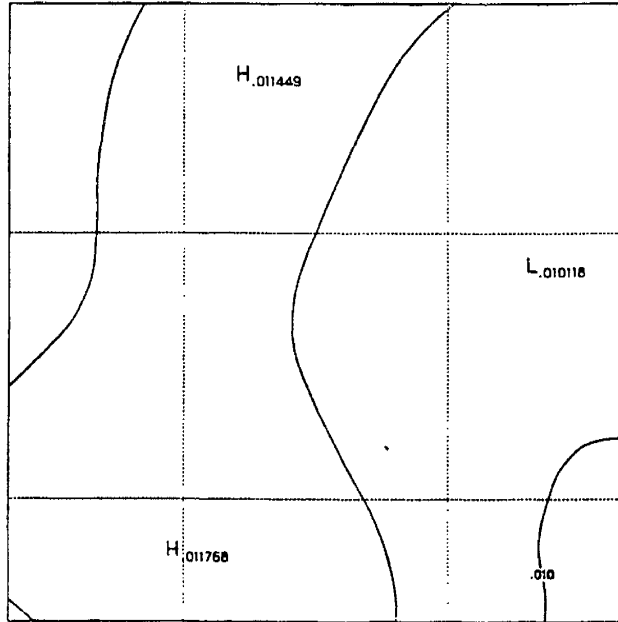


Figure 6.12 (c) same as 6.12(a) except at 200 mb.

Q AT P= 850.000. MEAN FROM 85070100 TO 85073100. Obs



Q AT P= 850.000. MEAN FROM 85070100 TO 85073100. Model

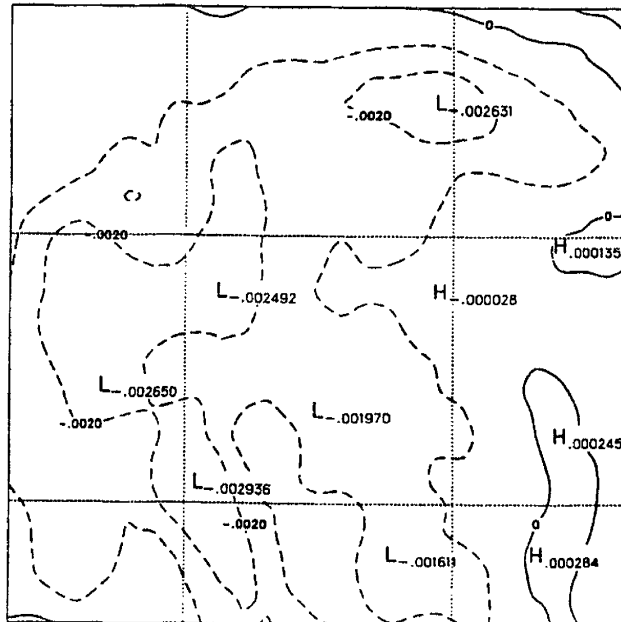
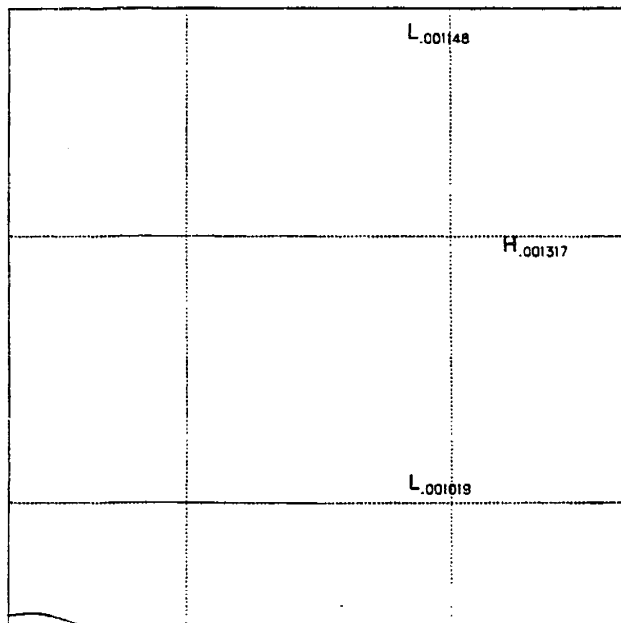


Figure 6.13 (a) Mixing ratio at 850 mb for July, "obs" refers to ECMWF data and "model" refers to differences between the simulated fields and the observed fields.

Q AT P= 500.000. MEAN FROM 85070100 TO 85073100. Obs



Q AT P= 500.000. MEAN FROM 85070100 TO 85073100. Model

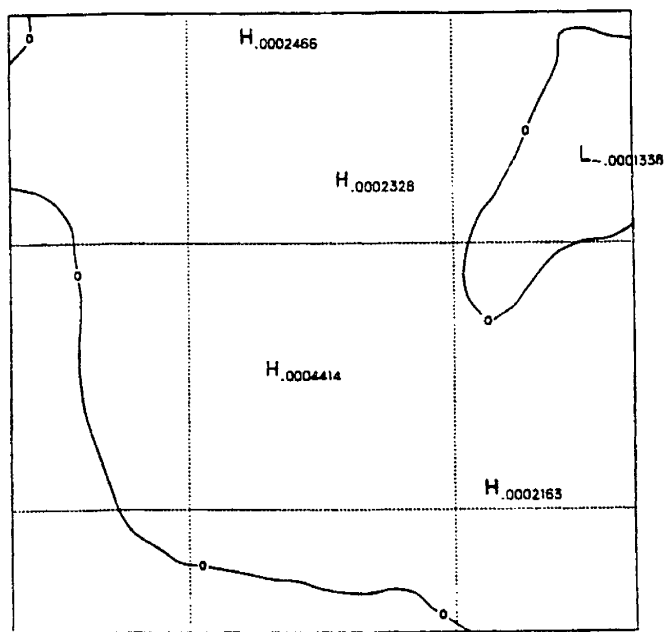
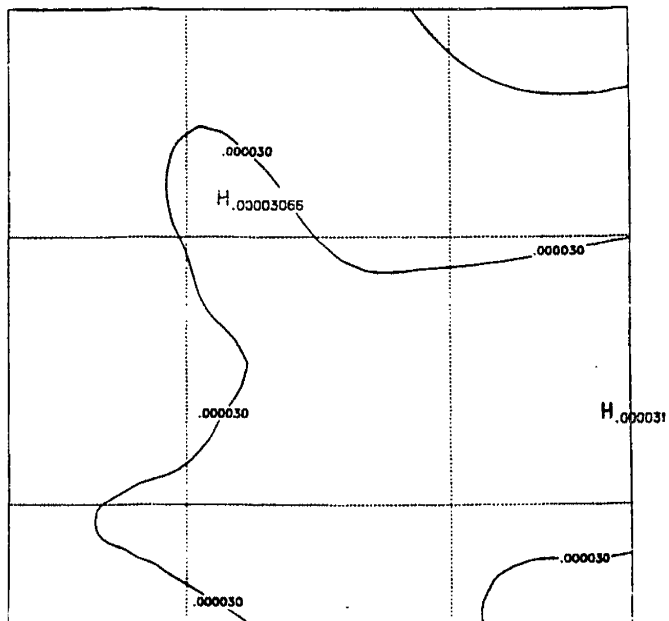


Figure 6.13 (b) same as 6.13(a) except at 500 mb.

Q AT P= 200.000. MEAN FROM 85010100 TO 85013100. Obs



Q AT P= 200.000. MEAN FROM 85010100 TO 85013100. Model

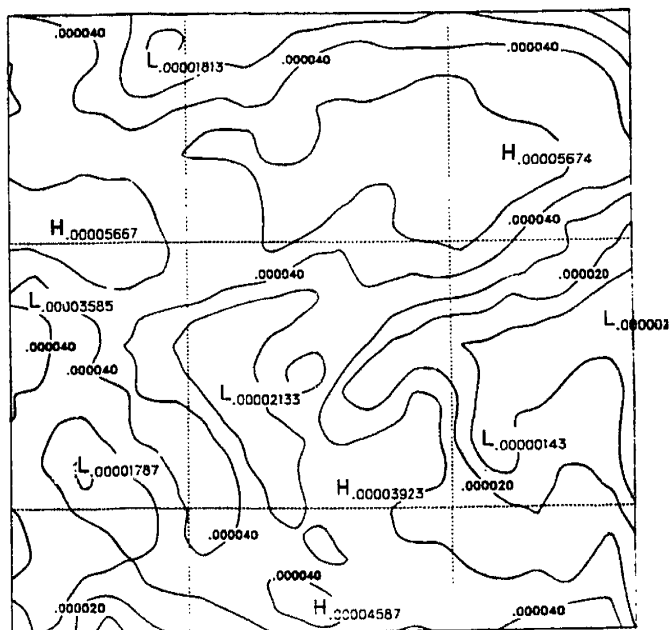


Figure 6.13 (c) same as 6.13(a) except at 200 mb.

The skill of the model in simulating the climate of the Amazon region is tested by comparing the fields of key atmospheric variables as simulated by the model and the corresponding climate from ECMWF data. Figures 6.11, 6.12, and 6.13 show fields of the following variables : sea level pressure, temperature and humidity(at 850 mb, 500 mb and 200 mb). The figures compare the fields simulated by the model with those from ECMWF data set. The comparison indicates that the model is capable of reproducing the average climate of the troposphere. The error in simulating water vapor amounts is similar to the case of January.

Table 6.4 compares the spatial averages of some of those fields with observations. It shows similar features as those in Table 6.2, namely underestimation of precipitation and cloudiness and overestimation of net surface radiation. Evaporation, runoff coefficient and interception ratio are accurately predicted by the model. Figures 6.14, 6.15, 6.16, 6.17 and 6.18 show the fields of surface temperature, ground temperature, net surface energy, evaporation, and precipitation, which are simulated by the climate model.

6.5.2 July Climate: Post-Deforestation

The same Figures: 6.14, 6.15, 6.16, 6.17 and 6.18 show the difference between the post-deforestation and the pre-deforestation fields for the variables: surface temperature, ground temperature, net surface energy, evaporation, and precipitation. These difference fields measure the sensitivity of regional climate in July to deforestation of the small area located in the center of the region. Table 6.3 presents the difference between the post-deforestation and the pre-

Variable	Model	Observations	References
surface temperature	26.2° C	26.0° C*	(1)
net surface radiation	165	131	(2)
evaporation	115	119	(2)
sensible heat flux	40		
precipitation	64	110	(2)
runoff	27		
interception loss	9		
runoff ratio	42%	44%*	(3)
interception ratio	14%	20%	(2)

Table 6.4 : Pre-Deforestation climate in July, units are in mm/month. * indicates that the observation is an annual value. References are indexed as follows (1) Molion(1975), (2) Shuttleworth (1988b), and (3) Oltman (1967)

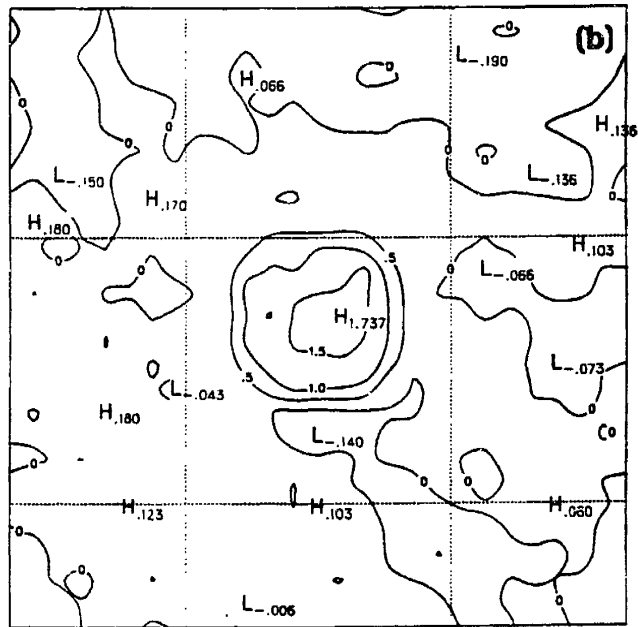
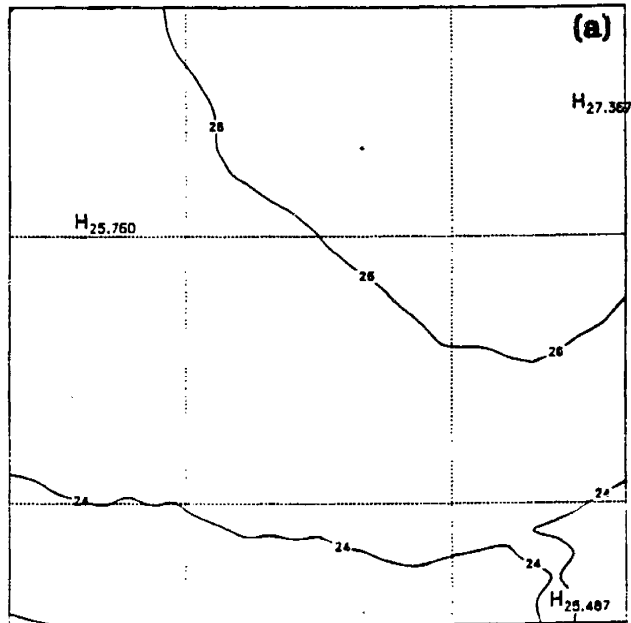


Figure 6.14 Ground temperature in ° C for July . (a) pre-deforestation field (b) (post-deforestation field- pre-deforestation field).

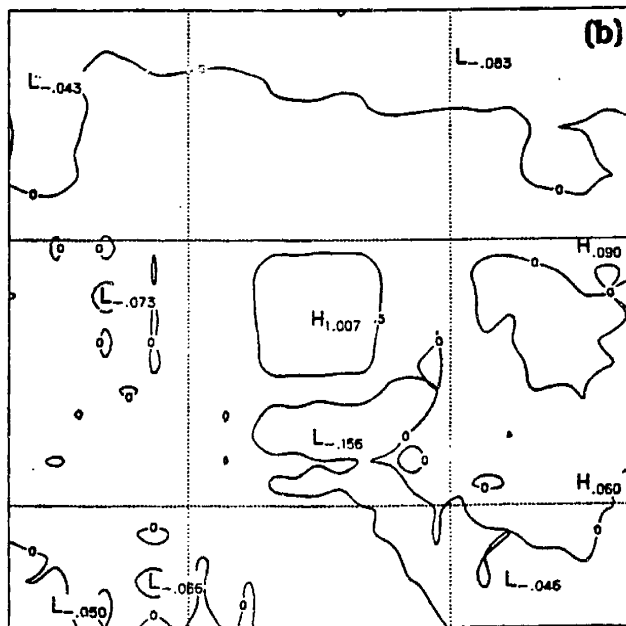
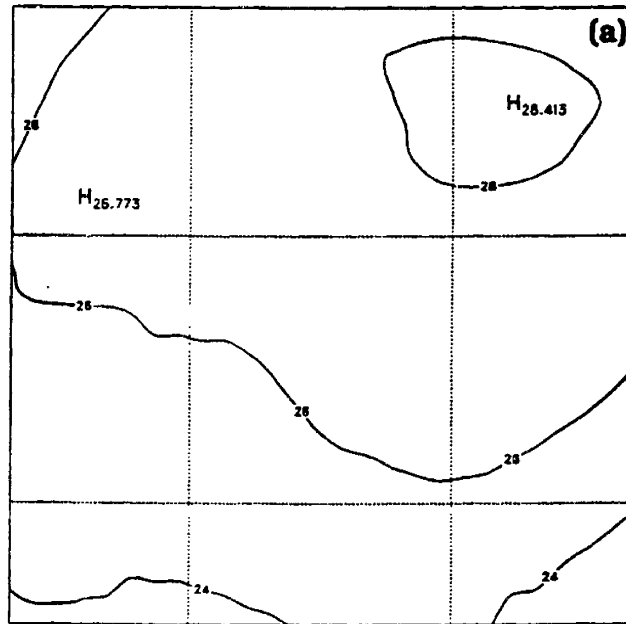


Figure 6.15 Air temperature in ° C, for July. (a) pre-deforestation field (b) (post-deforestation field- pre-deforestation field).

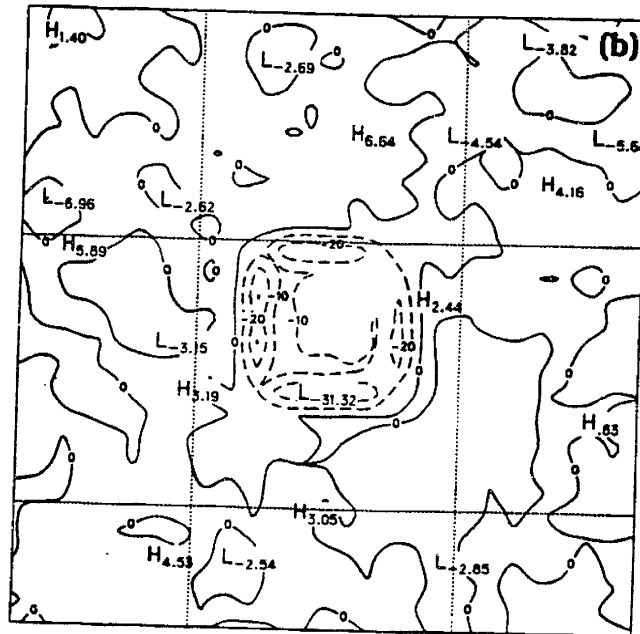
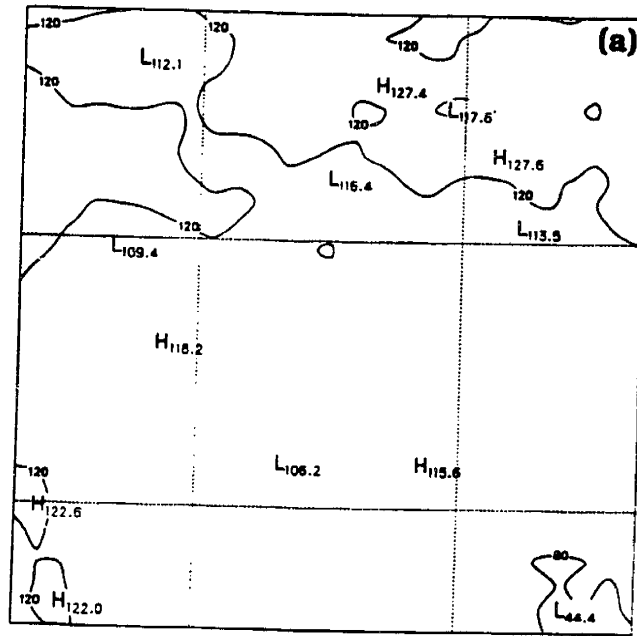


Figure 6.16 Net surface energy in W/m^2 , for July (a) pre-deforestation field (b) (post-deforestation field- pre-deforestation field).

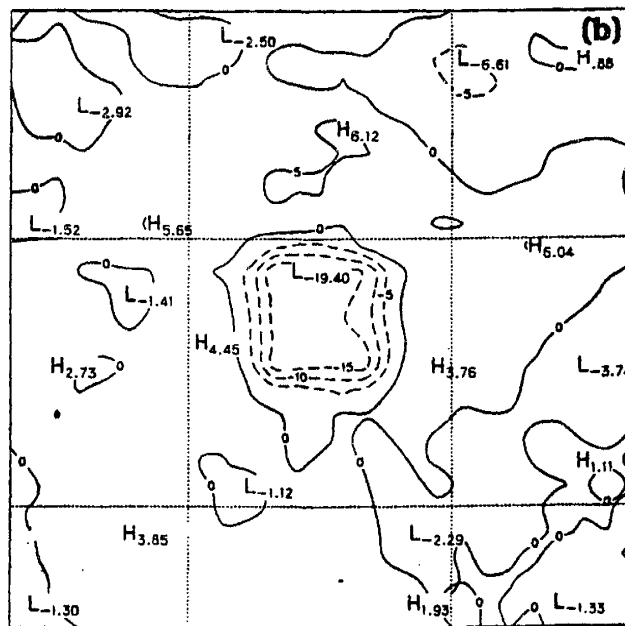
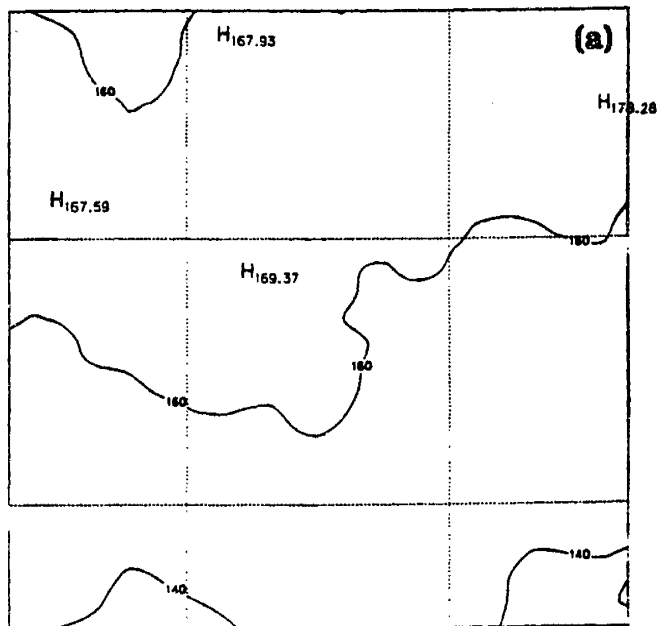


Figure 6.17 Evaporation in mm, for July. (a) pre-deforestation field (b) (post-deforestation field- pre-deforestation field).

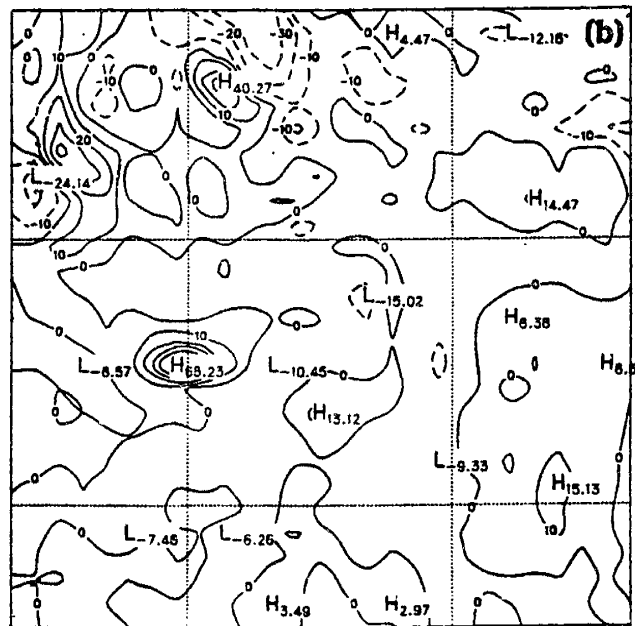
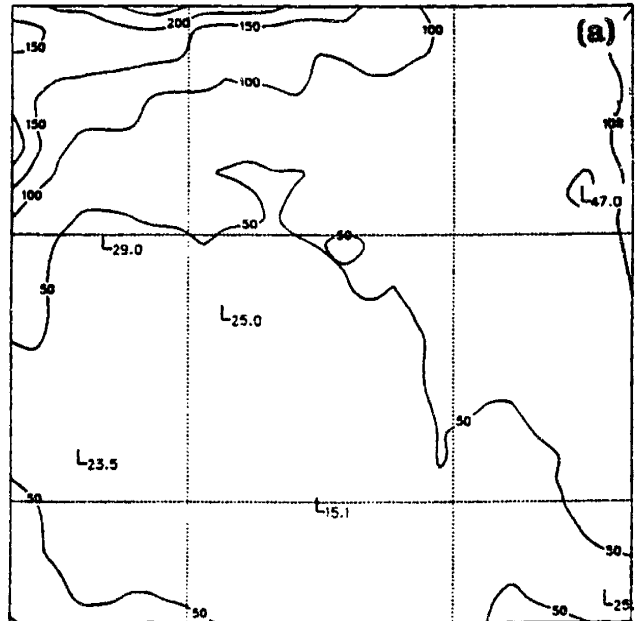


Figure 6.18 Precipitation in mm, for July. (a) pre-deforestation field (b) (post-deforestation field- pre-deforestation field).

deforestation fields for the variables mentioned above, averaged over the deforested area.

The physical interpretations of these sensitivity results are similar to those provided for the results of January in section 6.4.2. Although the relative changes in evaporation and precipitation are similar to those in the simulations for January, but the absolute values of these changes are different and that is due to the difference between summer and winter conditions in that region.

6.6 Discussion and Conclusions

The results presented in this chapter suggest that deforestation of small areas (~ 250 kilometers) is likely to result in the following changes over the deforested area : less evaporation, less precipitation and warmer surface temperature.

The predicted changes vary in absolute magnitude between summer and winter but the relative changes are of similar magnitude. The magnitudes of the precipitation changes are about - 9% ($\pm 5\%$) and the magnitudes of the evaporation changes are -13% ($\pm 5\%$). The change in surface temperature is about +0.6° C ($\pm 0.5^\circ$ C). These changes are smaller than those due to large-scale deforestation (see Table 7.1) by about a factor of 2. Possible reasons for this difference include the effects of the boundaries since boundary to area ratio is larger for the smaller regions. The boundary effects can be noticed in the figures which show the changes due to deforestation increasing from the boundary to the interior of the deforested region. Another important factor is the lower recycling ratio for smaller scales, the dependence of the recycling ratio on the scale considered is quantified

in Chapter 3. As the scale of the region considered decreases the potential for interactions between hydrology and climate decreases.

Except for the precipitation changes the predictions about the effects of deforestation are limited to the deforested area. Positive and negative precipitation changes of comparable magnitude occur over a larger area, possibly due to the following mechanism :

(1) A negative change in precipitation over the deforested area is equivalent to a negative change in the mass convergence field in the boundary layer.

(2) A localized decrease in the boundary layer mass convergence is equivalent to introducing a localized mass source in the boundary layer.

(3) The introduction of this mass source would create a pattern of divergence-convergence anomalies throughout the region resulting in these precipitation changes.

Since the climates for January and July are estimated from only three months of simulations, it would be difficult to conclude if the changes in the precipitation field are due to the above mechanism or if these changes are due to the sampling error.

The surface hydrology is simulated with reasonable accuracy. The surface runoff coefficient and the interception ratio predicted by the model are close to the observed values. This accuracy indicates that the modifications of BATS which are described in Chapters 4 and 5 represent significant improvements. These modifications include the physical-statistical representation of rainfall interception and surface runoff and the new formula for computing the fractional coverage of rainfall.

In the deforestation experiments which are described in this chapter, the size of the deforested area (~250 kilometers) is small compared to the equatorial Rossby radius of deformation (~1000 kilometers) which defines the physical scale for dynamics in the tropical atmosphere. Hence the changes in the regional climate due to small scale deforestation are not likely to excite any response which may alter the large-scale circulation in the tropics.

CHAPTER 7

Sensitivity of Regional Climate to Large-Scale Deforestation

7.1 Introduction

Deforestation of tropical rain-forests is occurring at alarming rates. A recent study estimates that the area of the world's largest rain-forest of the Amazon is shrinking at a rate of 20,000 square kilometers per year, Nobre et al. (1991). Large-scale removal of the rain-forest will have significant effects on the natural environment. The impact of deforestation goes beyond elimination of species and erosion of soil to the possible adverse effects on the regional and global climate. This Chapter deals with the effects of large-scale deforestation (~ 2500 kilometers) on the regional climate of the Amazon basin.

The recent studies by Dickinson and Henderson-Sellers (1988), Lean and Warrilow(1989) and Nobre et. al (1991), focus on the possible impacts on the regional climate due to large-scale deforestation in the Amazon. The common approach of these studies is to use General Circulation Models (G.C.M.s) in studying the possible effects of deforestation on climate. Due to the nature of the deforestation problem it is crucial to include realistic descriptions of the physical processes at the land-surface, the studies mentioned above include state of the art descriptions of land-surface processes. The three studies agree in predicting that large-scale deforestation of the total area of the Amazon forest will probably result in the following regional climatic changes : less evaporation, warmer surface temperature and less precipitation.

The three studies disagree in the magnitudes of these changes, nevertheless they agree in the sign of the change. The predictions of the three studies are described in Table 7.1, these predictions are averaged over large deforested areas which, roughly, correspond to the Amazon basin. The predictions in Table 7.1 refer to annual values. Figure 7.1 shows the spatial distribution of the changes predicted by the recent study of Nobre et al. (1991).

The results of the same deforestation studies predict significant changes in runoff, which is defined as the difference between precipitation and evaporation. Although the studies of Nobre et al. (1991) and Lean and Warrilow (1989) agree in predicting a reduction in runoff, Dickinson and Henderson-Sellers (1988) predict significant increase in runoff. Part of the increase in surface runoff, predicted by Dickinson and Henderson-Sellers (1988), is due to change in soil moisture and part of it is due to the increase in atmospheric moisture convergence. Nobre et al. (1991) argue that additional experiments are needed for explaining their predictions about moisture convergence and runoff. Lean and Warrilow (1989) deduce that the reduction in moisture flux convergence is due mainly to the increased surface albedo as opposed to the change in roughness. In the following we present a different perspective on the basic processes contributing to the change in tropical circulation and hence dictating the possible changes in moisture flux convergence. We emphasize the effects of the predicted changes in precipitation and surface temperature on the dynamics of the tropical atmosphere.

A decrease in precipitation is equivalent to a negative

	Dickinson and Henderson-Sellers (1988)	Lean and Warrilow (1989)	Nobre et al. (1991)
temperature (°C)	1.5	2.4	2.5
precipitation (mm/d)	- 0.27	- 1.34	-1.76
precipitation	-3%	-20%	-25%
evaporation	-8%	-27%	-30%
runoff (precipitation - evaporation)	+6%	-12%	-18%

Table 7.1 : Predictions of the spatially averaged regional changes in key atmospheric variables due to deforestation of the Amazon rain-forest.

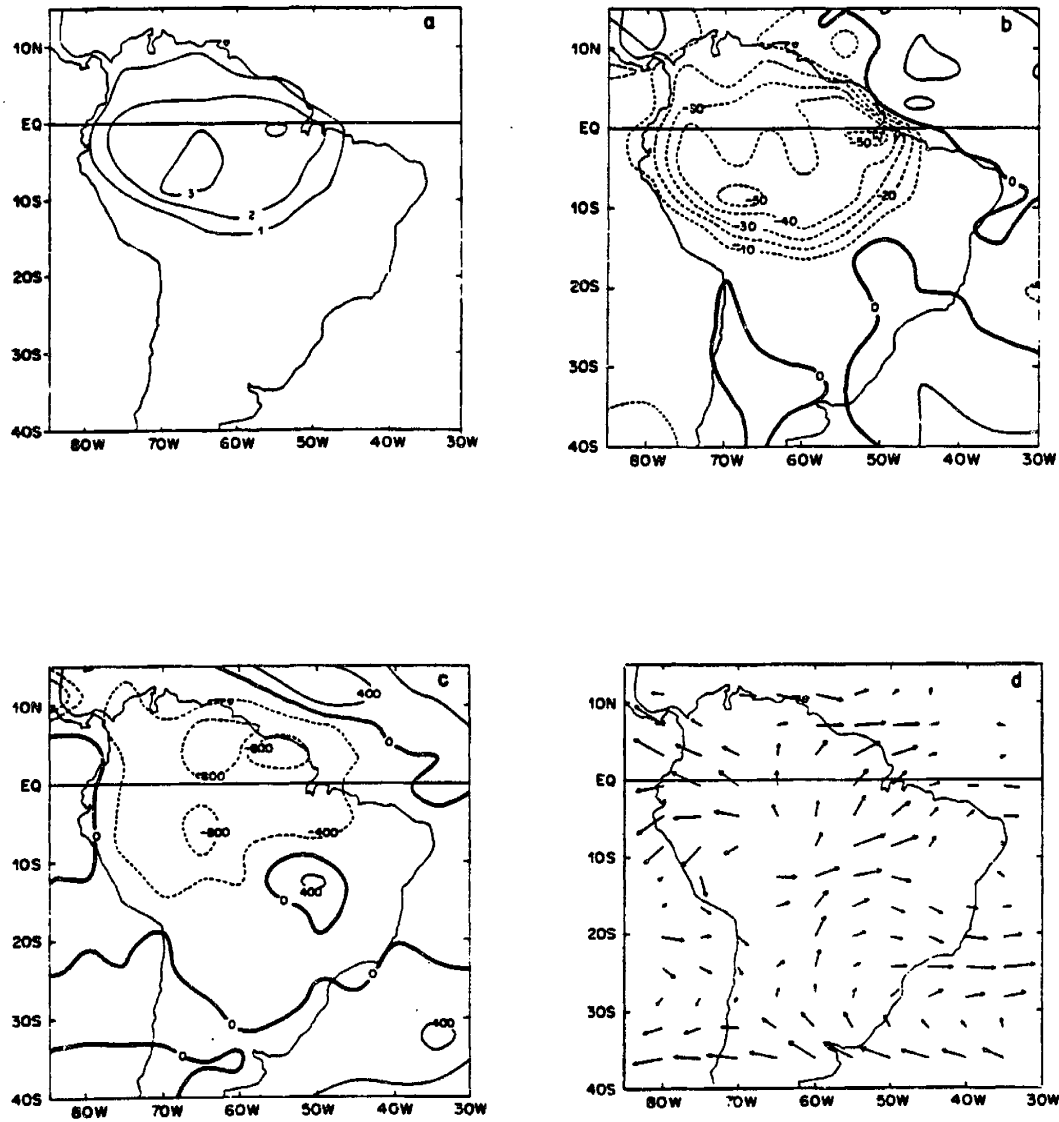


Figure 7.1 Predictions of the regional climatic change due to deforestation of the Amazon rainforest, Nobre et al. (1991). (a) temperature change in degrees C, (b) evaporation change in $W m^{-2}$, (c) precipitation change in mm, and (d) change in the wind vector at 700 mb.

anomaly in heating of the upper troposphere, the dynamics of the tropical atmosphere are sensitive to localized heating. The magnitude of the change in precipitation of about 20% and its large spatial extent suggest that the heating anomaly due to deforestation is likely to excite a significant response in the tropical atmosphere. Another important prediction is the change in surface temperature, in absence of other factors a positive surface temperature anomaly reduces surface pressure and results in a circulation converging towards the Amazon. It is suggested that the response of the tropical atmosphere to large-scale deforestation is forced, mainly, by the anomalies in heating and surface temperature. The objective in this chapter is to determine the relative contributions of the two processes, at least their orders of magnitude. The resulting change in the tropical circulation will determine if moisture convergence into Amazon basin will increase or decrease as a result of deforestation. The significance of this question stems from the fact that atmospheric moisture convergence into the Amazon basin is equivalent to runoff from the world's largest river.

A simplified linear model of the tropical atmosphere will be used in studying the response of the atmosphere to deforestation. The model is similar to that of Gill (1980) which was developed for describing the Walker circulation as a response of the tropical atmosphere to localized heating. The same model was later used by Zebiak (1982) in studying El Niño, particularly in simulating the response of the tropical atmosphere to the heating anomalies associated with this phenomenon. The success of the model in reproducing some of the circulation anomalies observed during El

Niño events suggests that the model includes the necessary processes for describing the response of the tropical atmosphere to the prescribed forcing. Further, the simple structure of the model may provide useful insight into the basic mechanisms contributing to the response of the tropical atmosphere to deforestation.

In the following, some of the effects of deforestation on climate will be reviewed. The links between deforestation and the predictions of Table 7.1 are discussed. A simple linear model of the tropical atmosphere is described, the model is then applied to the deforestation problem in the Amazon basin using the forcing predicted by the G.C.M.s experiments. The sensitivity of Amazonian runoff to large-scale deforestation is studied. The final section presents some concluding discussion.

7.2 Effects of Deforestation on Climate

Deforestation results in some important direct effects on climate. Removal of the rain-forest eliminates some of the bio-mass which absorbs most of the solar radiation incident on the surface. Less bio-mass results in less absorption and more reflection of solar radiation, hence a larger surface albedo. A larger surface albedo, everything else being equal, results in less energy available for evaporation from the surface. Replacement of the forest with a shorter vegetational cover reduces the roughness of the surface layer and causes reduction of the eddy transport of water vapor, heat and momentum near the surface. A shorter roughness length results in less evaporation and warmer surface temperature. Another factor which may affect evaporation is the reduction in the

leaf area, a smaller leaf area implies a reduction of the area active in transpiration and a similar reduction in the canopy storage available for interception. The direct effects of deforestation extend to the top soil layer which becomes more exposed to erosion and contains a shallower rooting zone. The top soil layer controls surface runoff and stores the moisture necessary for transpiration, hence changes to the top soil layer affects these two processes.

The most important feedbacks which may result from tropical deforestation are the possible effects on the rainfall producing mechanisms. Deforestation of small areas (~ 25 kilometers) changes the spatial distribution of sensible and latent heat fluxes. The resulting heterogeneity in the surface temperature and humidity fields play a significant role in initiation of convection and may favor meso-scale circulations which produce more rainfall. On the other hand deforestation of large areas (~ 2500 kilometers) reduces evaporation and results in a dryer boundary layer. The lack of moisture in the boundary layer affects precipitation significantly, not only less water is available to form clouds but even more important is the reduction of the energy available for convection. Reduction of rainfall over the deforested area is necessarily accompanied by reduced cloudiness and for this reason a smaller planetary albedo. The reduction in albedo due to the change in cloudiness may be large enough to offset the direct effect of increased surface albedo.

The results in Table 7.1 may be interpreted as follows, the three studies indicate that deforestation of the Amazon basin will probably result in less evaporation and precipitation. The reduction

in evaporation is largely due to the shorter roughness length while the reduction of precipitation is mainly due to the smaller amount of energy available for convection following deforestation. Since evaporation cools the surface, the reduction in evaporation results in the increase in surface temperature. The predicted changes in precipitation and surface temperature can be used as input to a linear model of the tropical atmosphere to study its response to deforestation, particularly changes of runoff.

7.3 A Simple Model of the Tropical Atmosphere

The original version of the model used here was introduced by Matsuno(1969), it has been developed further by Gill (1980) and used to describe the tropical circulations induced by latent heat release. We follow the suggestion of Neelin (1988) that the Gill model is basically a model of the boundary layer flow. The horizontal momentum equations are approximated by

$$f v' - \partial_x \Phi' - \epsilon u' = 0 \quad (7.1)$$

$$- f u' - \partial_y \Phi' - \epsilon v' = 0 \quad (7.2)$$

The variables and parameters in the above equations are defined as follows : u' and v' are perturbations in the horizontal components of mass flux in the boundary layer, Φ' is the mass-weighted integral of the perturbation in geo-potential height in the boundary layer, ϵ is the coefficient of Rayleigh friction and f is the Coriolis parameter. The three terms in the above equations represent the equilibrium

between Coriolis force, pressure gradient force and momentum dissipation. Since we are interested in equilibrium solutions, the time derivative terms are taken to be zero. The two equations are linearized about a basic state of no motion, hence the advective terms are assumed zero; the implications of this assumption are discussed later.

Continuity of the flow in the boundary layer can be described, in pressure coordinates, by

$$\partial_x u' + \partial_y v' + \frac{w'}{g} = 0 \quad (7.3)$$

where w' is the perturbation to the vertical velocity field above the boundary layer and g is gravitational acceleration.

In deriving the energy equation, it is assumed that energy balance in the tropics is mainly between diabatic processes, latent heat release and radiation, and adiabatic heating induced by vertical motion. This assumption is justified by the observation that temperature gradients are very small in the tropics and hence effects of heat advection are small. In representing radiation effect, it is assumed that temperature perturbations are equivalent to pressure perturbations and that the coefficient of Newtonian cooling is equivalent to the coefficient of Rayleigh friction. This assumption has no physical justification and is regarded the weakest in the model; it is usually adopted for simplifying the system of equations and in order to obtain an analytical solution. Neelin(1988) shows that the model results are not sensitive to this assumption unless it is used for describing the total climatological circulation. A simplified form of the energy equation is given by,

$$\frac{w'}{g} = \frac{(\epsilon \Phi' + a P')}{c^2} \quad (7.4)$$

The variables and parameters in the above equation are defined as follows : P' is perturbation to the precipitation field, a is a constant defined by $a = [L R \Delta p / (2 p c_p)]$, where L is the latent heat of condensation, R is the gas constant for dry air, c_p is the specific heat capacity of dry air at constant pressure, Δp is half the depth of the troposphere corresponding to the region heated by condensation of water vapor and p is a mid-level tropospheric pressure, about 500 mb, c is the wave speed defined by $c^2 = S R ((\Delta p)^2 / 2p)$, where S is static stability (taken in this Chapter as $S=4.2 \times 10^{-5} \text{ m K s}^2/\text{Kg}$). The two terms in the right-hand side of Equation 7.4 represent contributions of radiation and latent heat release. For details of the derivation of Equation 7.4 we refer to Neelin (1988).

Equations 7.3 and 7.4 are combined into

$$\epsilon \Phi' + c^2 (\partial_x u' + \partial_y v') = - a P' \quad (7.5)$$

Equations 7.1, 7.2 and 7.5 provide a close set of equations on the three variables u' , v' and Φ' ; the forcing is given by the latent heat release which is proportional to P' . Gill (1980) used a similar set of equations to study the response of the tropical atmosphere to localized heating.

Lindzen and Nigam(1987) studied the role of sea surface temperature gradients in forcing low-level winds and convergence in the tropics, they developed a simple model of the trade cumulus

boundary layer. It is found that the flow resulting from forcing the model by observed surface temperature is comparable to observed low-level flows. Neelin (1989) transformed the Lindzen-Nigam model into a form similar to the Gill model; the forcing is given by the anomaly in surface temperature instead of precipitation. According to this transformation the Lindzen-Nigam model can be described by the following set of equations,

$$f v' - \partial_x \Phi'' - \epsilon u' = 0 \quad (7.6)a$$

$$-f u' - \partial_y \Phi'' - \epsilon v' = 0 \quad (7.6)b$$

$$\epsilon \Phi'' + c^2 (\partial_x u' + \partial_y v') = -b T_s' \quad (7.6)c$$

which are similar to Equations 7.1,7.2 and 7.5, the precipitation forcing is replaced by the surface temperature forcing. The variables and parameters in the above equations are defined as follows, T_s' is perturbation in surface temperature , $b = \epsilon \delta p (H_0/(2T_0))$, where δp is the depth of the boundary layer in units of pressure, H_0 is the depth of the boundary layer in units of length and T_0 is a constant reference temperature ($T_0 = 288$ K , Lindzen and Nigam(1987)), $\Phi'' = g [h' - (H_0/(2T_0))] T_s'$, where h' is perturbation to the height of the boundary layer.

In the deforestation problem we are interested in the response of the atmosphere to anomalies in *both* precipitation and surface temperature. Since the set of Equations 7.1,7.2, and 7.5 and the set of Equations 7.6 are linear, we add the corresponding equations to get the following set of equations

$$f v' - \partial_x \Phi''' - \epsilon u' = 0 \quad (7.7)a$$

$$-f u' - \partial_y \Phi''' - \epsilon v' = 0 \quad (7.7)b$$

$$\epsilon \Phi''' + c^2 (\partial_x u' + \partial_y v') = -a/2 P' - b/2 T_s' \quad (7.7)c$$

The variable Φ''' is defined by $\Phi'''=(\Phi'+\Phi'')/2$. The two terms in the right-hand side of Equation 7.7c correspond to the precipitation and temperature forcings. Equations 7.7 are the set of equations which will be used for studying the response of the tropical atmosphere to deforestation.

7.4 Response of Tropical Atmosphere to Deforestation of Amazon Rain-forest

The response of the tropical atmosphere to deforestation will be studied using the simple model developed in the previous section. It is assumed that deforestation is equivalent to introducing anomalies in the precipitation and surface temperature fields. Hence the model is used for simulating the linear response of the tropical atmosphere to the forcing induced by changes in precipitation and surface temperature fields. The magnitudes of these anomalies are estimated from the G.C.M.s experiments.

Table 7.2 shows the magnitudes of the forcing terms corresponding to the predicted changes in surface temperature and precipitation. It also shows the total forcing due to deforestation. It is important to emphasize that the total forcing is the resultant of two *competing* processes, the positive surface temperature anomaly which favors a converging flow and the negative precipitation anomaly which favors a diverging flow. The

	Dickinson and Henderson-Sellers (1988)	Lean and Warrilow (1989)	Nobre et al. (1991)
temperature forcing (W / m ²)	+0.7	+ 1.1	+ 1.2
precipitation forcing (W / m ²)	-0.6	- 2.8	- 3.7
precipitation+temperature (deforestation) forcing (W / m ²)	+0.1	- 1.7	- 2.5

Table 7.2 : Estimates of the forcings due to predicted changes in surface temperature, precipitation and deforestation in the Amazon. In estimating these forcings the following typical values are used, $p = \Delta p = 500$ mb, $\delta p = 300$ mb, $H_0 = 3$ kilometers, $\epsilon = (2 \text{ day})^{-1}$.

convergence of atmospheric moisture towards the deforested area is measured by the difference between precipitation and evaporation. The anomalies in convergence of atmospheric moisture (runoff) predicted by the G.C.M.s experiments are given in Table 7.1. Comparison of the signs and magnitudes of these anomalies and the signs and magnitudes of the deforestation forcing, from Table 7.2, indicates consistency of the models results with our simple analysis. The consistency of our analysis using a simple model with the results of the more complicated G.C.M.s experiments suggests that the processes included in the simple model are the dominant processes relevant to the deforestation problem. The relative magnitude of the forcing due to surface temperature and that due to precipitation provide some idea about the relative importance of the two mechanisms in determining the total response. It seems that the two forcings are of the same order of magnitude, see Table 7.2.

The set of Equations 7.7 can be solved analytically for simple forms of the forcing function. We assume that the forcing due to surface temperature and precipitation anomalies have the form described by

$$\begin{aligned}
 FG &= FG_0 \cos(kx) (1-y) \exp\left[-\frac{y^2}{4}\right], & |x| < L \\
 FG &= & , & |x| > L
 \end{aligned}
 \tag{7.8}$$

where x and y are distances in the zonal and meridional directions respectively, both normalized by the equatorial Rossby radius $(c/2\beta)^{1/2}$, ($\beta = (\partial f / \partial y)|_{y=0}$, $\beta = 2.3 \times 10^{-11} \text{ m}^{-1} \text{ s}^{-1}$). For the set of parameters used in this study the Rossby radius is about 6 degrees

latitude. FG_0 is the magnitude of the forcing at the center point which is taken at the intersection of the equator and 60W longitude. It is assumed that $FG_0 = [a/2 P' + b/2 T_s']$. L is taken as 10 degrees latitude and ($k = \pi/2L$). The forcing function is shown in Figure 7.2.

The analytical solutions of Equations 7.7 corresponding to the forcing of Equation 7.8 are described in the Appendix 7.1. These solutions are the same as those of Gill(1980). For each of the three G.C.M. experiments, FG_0 is estimated from Table 7.2. Figures 7.3 and 7.4 show the boundary layer circulations corresponding to the forcings estimated from the results of Nobre et al. (1991) and Dickinson and Henderson-Sellers(1988), respectively. (The results of Lean and Warrilow(1989) are very similar to those of Nobre et al. (1991), hence the circulations corresponding to their results are not shown). The anomalies in the circulation due to deforestation are obtained by superposition of the anomalies due to the temperature and precipitation forcing. (Each of the two Figures, 7.3 and 7.4, uses a different scale in representing the mass flux vector, hence circulations from the two figures are not comparable).

The objective in studying the analytical solutions of this simple model is to provide *qualitative* comparison between the circulation anomalies induced by the two different forcings. The simulated responses of the linear model illustrate the competition between the circulation anomalies induced by the temperature and precipitation changes. In Figure 7.3, the converging circulation due to temperature has about half the strength of the diverging circulation due to precipitation, as a result the total circulation

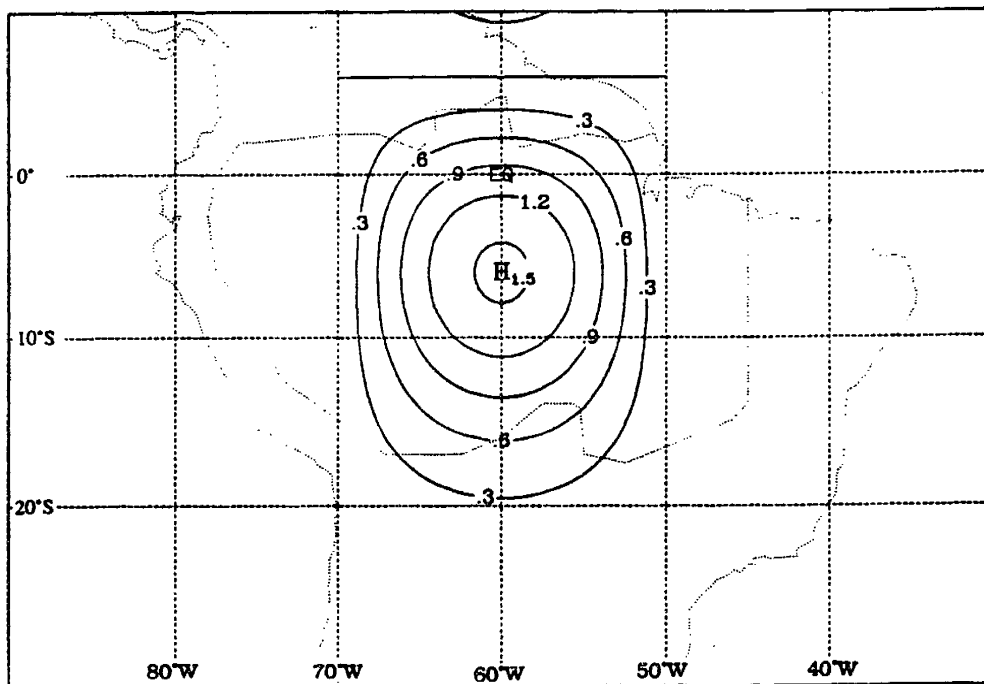


Figure 7.2 The forcing function of Equation 7.8 with $FG_0=1$ and $L= 10$ degrees latitude.

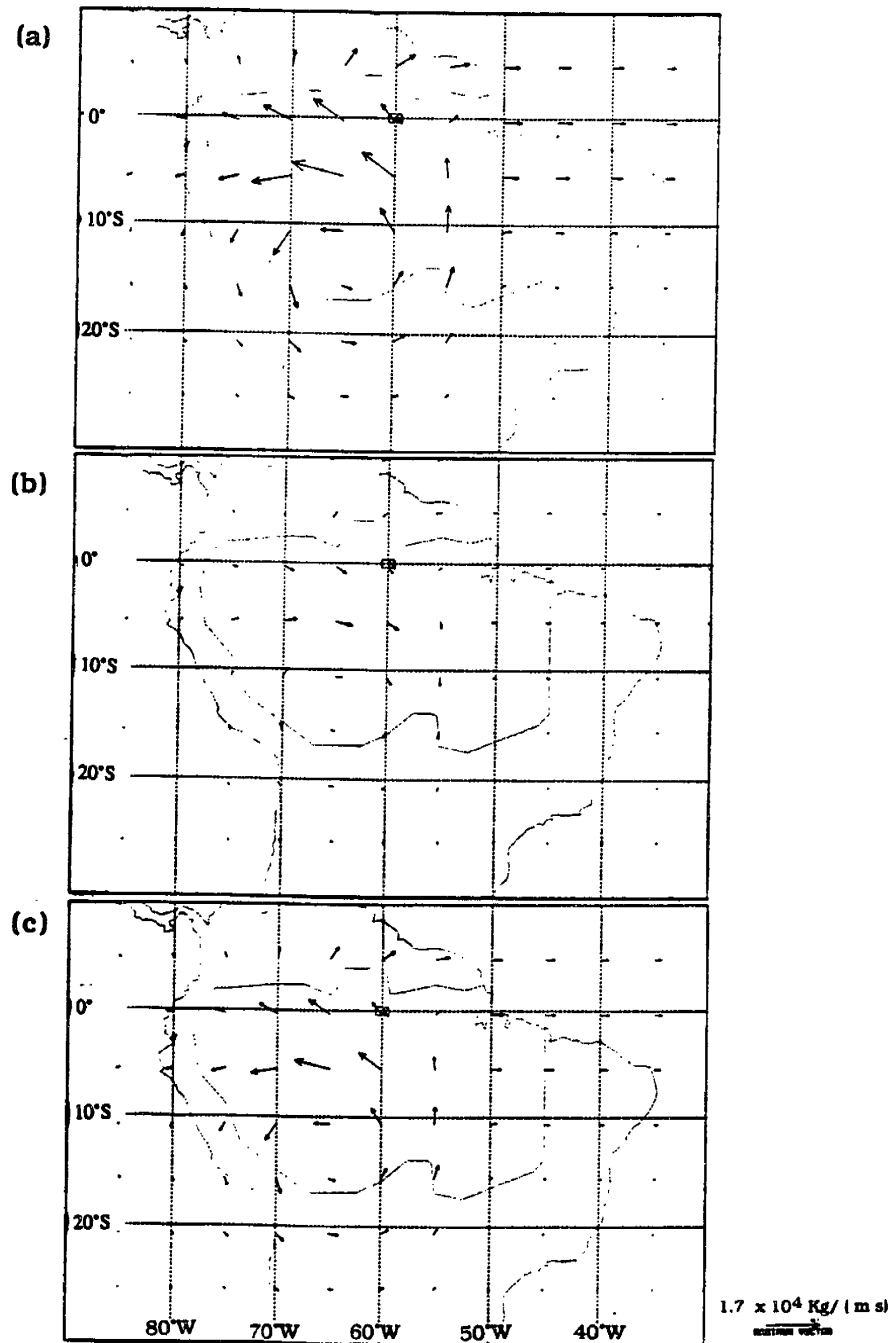


Figure 7.3 The boundary layer circulation resulting from forcing the model with (a) precipitation forcing, (b) temperature forcing and (c) both precipitation and temperature. Vector represents mass flux in $\text{Kg}/(\text{m s})$. The forcings are estimated from the results of Nobre et al. (1991).

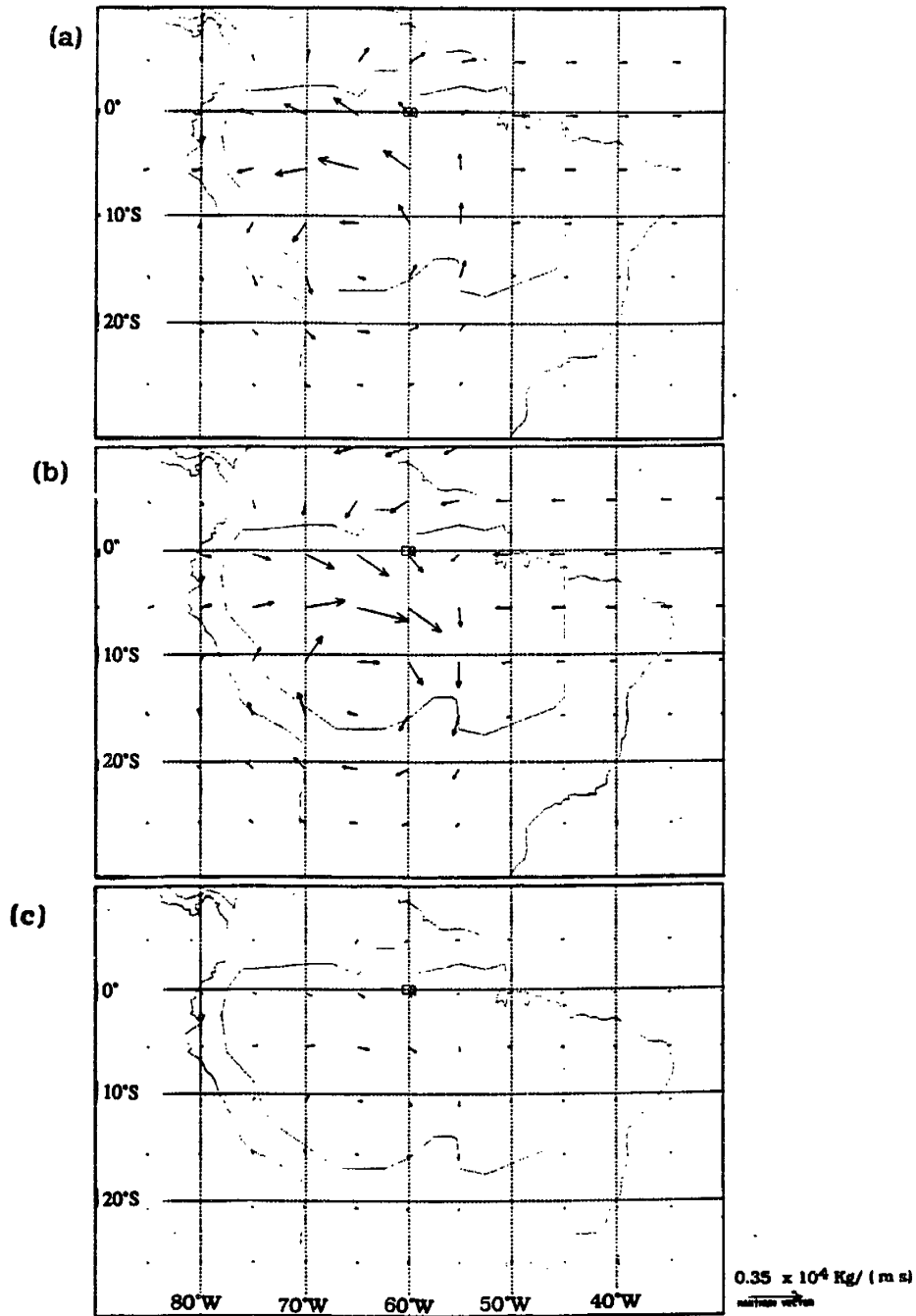


Figure 7.4 The boundary layer circulation resulting from forcing the model with (a) precipitation forcing, (b) temperature forcing and (c) both precipitation and temperature. Vector represents mass flux in $\text{Kg}/(\text{m s})$. The forcings are estimated from the results of Dickinson and Henderson-Sellers (1988).

anomaly due to deforestation is significantly milder than that due to precipitation alone. In Figure 7.4, which corresponds to the results of Dickinson and Henderson-Sellers(1988), the circulation anomalies due to the surface temperature and precipitation have equal magnitudes but opposite directions resulting in a negligible total circulation anomaly.

Lean and Warrilow (1989) performed two additional experiments, first they simulated the response of the atmosphere to increased surface albedo, then in a different experiment they simulated the response of the atmosphere to the reduction in surface roughness. They also performed a deforestation experiment which includes both effects. The average regional climatic changes from the three experiments are shown in Table 7.3. Based on these results they argue that the reduction in moisture flux convergence is, mainly, due to the increased surface albedo as opposed to the change in roughness. These results can be interpreted in terms of the linear model; the forcing due to precipitation and that due to surface temperature are estimated for each of the three experiments, see Table 7.3. Increased surface albedo leads to a larger decrease in runoff because the corresponding surface temperature forcing is negative, although very small. Hence in this case both the temperature and precipitation forcing result in diverging flow which explains the large reduction in runoff. The relatively large and positive temperature forcing in the roughness experiment leads to a converging flow resulting in a smaller reduction in runoff. These experiments illustrate our point that the competition between the precipitation and surface temperature

	increased albedo	decreased roughness	increased albedo & decreased roughness
temperature (°C)	-0.10	2.24	1.98
precipitation (mm/day)	- 0.75	- 0.69	-1.34
evaporation (mm/day)	-0.20	-0.43	-0.61
precipitation - evaporation (mm/day)	-0.55	-0.26	-0.73
.....			
temperature forcing(W / m ²)	- 0.05	+1.1	+ 0.9
precipitation forcing(W / m ²)	- 1.6	- 1.4	- 2.8
precipitation + temperature forcing (W / m ²)	- 1.65	- 0.3	- 1.9

Table 7.3 : Predictions of the spatially averaged regional changes in key atmospheric variables and the corresponding forcings, from the experiments of Lean and Warrilow (1989).

forcing is important in determining the changes of moisture flux convergence.

The linear model of the tropical atmosphere involves many assumptions and simplifications. In addition to the assumptions mentioned in the previous section, advection by the flow of the basic state is neglected and the effects of topography are not included. Although these effects may be important, the model includes the processes necessary to illustrate and compare the basic components of the response of the tropical atmosphere to deforestation. A qualitative comparison of Figure 7.1 (d) and Figure 7.3 (c) indicates some similarity between the response predicted by the G.C.M and that of the linear model, particularly the directions of the flux at the regions north-west, south-west and at the center of the Amazon. The differences between the two figures can be attributed to the non-linear effects which are not considered in our analysis and the different forms of the forcing function in the G.C.M. and in the linear model. We also note that Figure 7.1 (d) shows the flow at 700 mb while Figure 7.3 (c) shows the mass flux averaged over the boundary layer.

7.5 Sensitivity of Amazonian Runoff to Large-Scale Deforestation

The simple linear model presented in this Chapter can be used for studying the sensitivity of Amazonian runoff to large-scale deforestation. It is assumed that the change in runoff from the region can be estimated by the difference between the anomaly in atmospheric moisture convergence in the boundary layer and the corresponding anomaly in atmospheric moisture divergence in the

atmosphere above the boundary layer.

The change in convergence of boundary layer air mass, ΔCV , into a rectangular region covering the Amazon basin is estimated. The region is located between latitudes $5^\circ N$ and $20^\circ S$ and longitudes $45^\circ W$ and $75^\circ W$. In estimating ΔCV , we used the solutions for u' and v' which are given in Appendix 7.1, ΔCV is estimated as a linear function of FG_0 . The principle of conservation of mass requires that the change in divergence of air mass in the atmosphere above the boundary layer, ΔDV , should be equivalent to ΔCV . Hence the change in runoff, ΔR , is given by the following [$\Delta R = r_b \Delta CV - r_a \Delta DV = \Delta CV(r_b - r_a)$], where r_b and r_a are average mixing ratios in the boundary layer and in the atmosphere above the boundary layer, respectively. It is estimated that [$\Delta R = 0.19 (r_b - r_a) FG_0$], where FG_0 is given by the following relation $FG_0 = [a/2 P' + b/2 T_s']$ and ΔR is in mm/day. Figure 7.5 shows the sensitivity of runoff as function of the changes in precipitation and surface temperature. It is assumed that $r_b = 10$ g/Kg, $r_a = 4$ g/Kg and that runoff in the Amazon basin is about 900 mm/year.

Figure 7.5 illustrates the competition between the two mechanisms which are driven by the changes in precipitation and the changes in surface temperature. Further, the estimates in Figure 7.5 define the range of possible changes in runoff due to large-scale deforestation. That range of changes in runoff agrees with the predictions using the climate models in Table 7.1. Due to the simple structure of the model, the estimates of runoff changes due to specific changes in precipitation and surface temperature may not represent accurate predictions of the change in runoff.

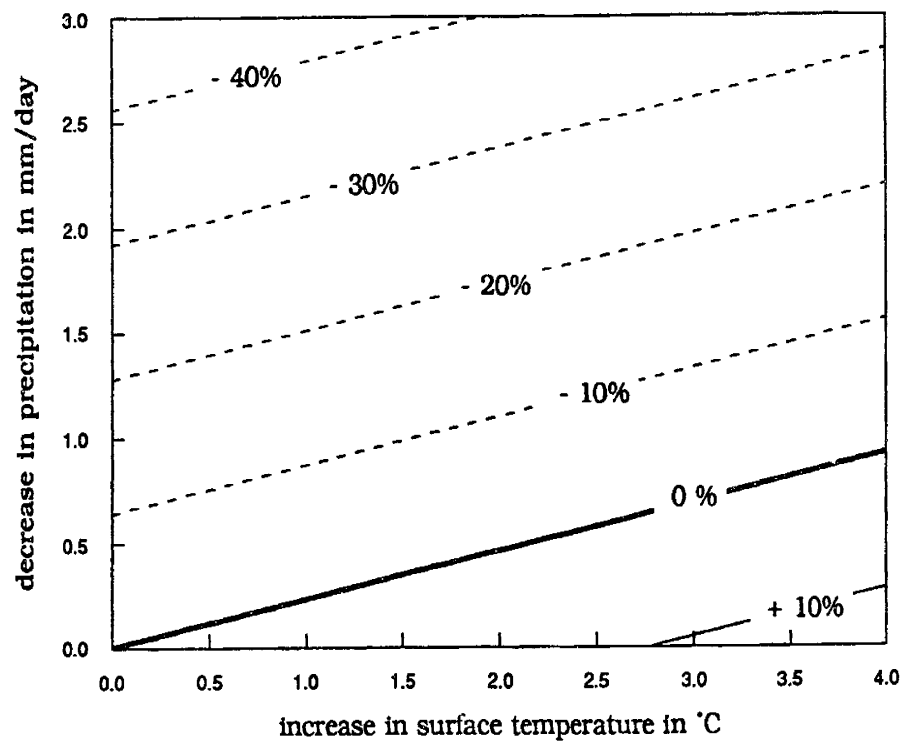


Figure 7.5 Sensitivity of Amazonian runoff to large-scale deforestation.

7.6 Concluding Discussion

The effect of deforestation of the Amazon rain-forest on the boundary layer circulation of the tropics is approximated by the linear response of a simplified model of the tropical atmosphere to anomalies in surface temperature and precipitation. The magnitudes of these anomalies are estimated from the results of G.C.M.s experiments. All three experiments considered in this study indicate that deforestation will result in a positive change in surface temperature and a negative change in heating of the upper troposphere due to reduction in precipitation. While the temperature anomaly induces a circulation converging towards the Amazon region, the precipitation anomaly induces a diverging flow of a similar strength. The two anomalies has opposite effects resulting in a circulation anomaly which is smaller than the larger of the two components. Due to the nature of the deforestation problem, a positive change in surface temperature combined with a negative change in precipitation, it is possible to have significant anomalies in surface temperature and precipitation but negligible effect on the circulation.

The dependence of the total response of the tropical atmosphere on the *difference* between the predicted strengths of the surface temperature forcing and the precipitation forcing suggests a high sensitivity of G.C.M.s' predictions of circulation changes. Given that climate models still need significant improvements to achieve reasonable accuracy in the description of important processes such as convection, radiation and land-surface processes, we should be cautious about the accuracy of their

predictions. This is particularly important when the prediction depends on the competition of two processes which are both modeled with poor accuracy. Convection parameterizations and the descriptions of land-surface processes are among the least accurate in current G.C.M.s and need significant validation efforts, see Emanuel and Raymond (1992) and Henderson-Sellers and Dickinson(1992).

It is interesting to compare the El Niño phenomenon and the deforestation problem. The former is the classical ocean-atmosphere interaction problem while the latter is the classical land-atmosphere interaction problem. The two problems are similar in the sense that in both cases the atmosphere responds to anomalies in the lower boundary conditions, specifically, it responds to anomalies in evaporation and surface temperature. In the El Niño case the sign of the precipitation (heating) anomaly coincides with the sign of the changes in surface temperature and evaporation. Observations indicate that during El Niño events all these anomalies occur, roughly, at the same locations, i.e. in phase with each other, which is likely to strengthen the overall effect on the tropical circulation. It is usually observed that the western Pacific region experiences negative anomalies in surface temperature, evaporation and precipitation while the eastern Pacific region experiences positive anomalies in the same three variables. In contrast, the predictions of G.C.M.s regarding the deforestation problem indicate that the regional changes in surface temperature and precipitation will have opposite signs. This difference in the sign of the predicted change will probably weaken

the overall effect on the tropical circulation.

The estimates of the forcing due to deforestation, which are given in Table 7.2, provide means for comparing the forcing on the dynamics of the atmosphere due to deforestation and that due to the greenhouse effect. Raval and Ramanathan (1989) estimate that the forcing due to the greenhouse effect of doubling CO₂ concentration is about 4 W/m²; from the results of this study it is estimated that the forcing due to deforestation is in the order of few W/m². From this comparison, it seems that the forcing due to deforestation is of the same order of magnitude as the forcing due to the greenhouse effect of doubling CO₂ concentration; one important difference is the localized nature of deforestation compared to the global distribution of the CO₂ forcing.

CHAPTER 8

Conclusions

8.1 Introduction

This chapter presents a summary of the results, general conclusions of the study, and suggestions for future research.

8.2 Summary of the Results

The results of this study are summarized in the following sections .

8.2.1 Precipitation Recycling in the Amazon Basin

1. A new model is developed for describing the precipitation recycling process. The model is based on the principle of conservation of mass; it assumes that atmospheric water vapor is well mixed and that the change of atmospheric moisture storage is small in comparison to atmospheric moisture fluxes.

2. The recycling model is applied in the Amazon basin using the ECMWF global data set to obtain new estimates of the spatial and temporal distributions of the precipitation recycling ratio. It is estimated that 25% of annual precipitation in the Amazon basin is contributed by evaporation within the basin.

3. The estimate of 25% is characteristic of the scale considered which is the total area of the Amazon basin. The recycling model is applied to a range of smaller areas within the Amazon basin and the dependence of the recycling ratio on spatial scale is investigated. It is

found that the recycling ratio is proportional to the square root of the linear scale.

4. The estimate of 25% for the precipitation recycling ratio in the Amazon basin is significantly smaller than the frequently quoted estimate of about 50%. It is shown in Chapter 3 that the estimate of 50% is inconsistent with the data on atmospheric moisture fluxes and with the data on isotopic composition of water in the Amazon basin.

8.2.2 Modeling of Rainfall Interception Over Large Areas

1. A new scheme is developed for describing rainfall interception over large areas; it combines the Rutter model of interception and statistical treatment of the spatial variability in rainfall and canopy storage. The scheme is designed for modeling rainfall interception over large areas comparable to the typical size of a grid-cell in a climate model.

2. The new scheme is compared to other schemes that do not include the effects of spatial variability; this comparison suggests that for accurate modeling of rainfall interception over large areas it is necessary to include the effects of spatial variability in *both* canopy storage and rainfall.

3. The new interception scheme is included into the Biosphere-Atmosphere Transfer Scheme (BATS) and used as part of a 3-D climate model in simulating the Amazon climate. The results of these simulations suggest that the scheme is capable of predicting the partition of precipitation into interception loss and throughfall in a rain-forest environment. Normalized interception loss predicted by the scheme is 0.12 and 0.14 for January and July respectively which are

close to the observations of 0.10 and 0.20 for the same two months, Shuttleworth (1988a).

8.2.3 Sensitivity of Regional Climate to Small-Scale Deforestation

1. Due to the nature of the deforestation problem, it is crucial to include into a climate model accurate descriptions of land-surface processes. New schemes for describing runoff production and rainfall interception are included into BATS; both of these schemes account for the effects of the sub-grid scale spatial variability. The new version of BATS which includes the improved hydrology schemes is implemented successfully into the NCAR/PSU climate model. These improvements are significant since they treat horizontal variability and hence balance some of the emphasis on vertical details of the biomass which is characteristic of BATS.

2. The NCAR/PSU climate model is used in simulating the regional climate of a limited area within the Amazon basin. The size of the region considered is 1600 kilometers x 1600 kilometers; it is located in the central and western sub-regions of the Amazon basin. The model is used in simulating the climates of January and July; it is driven by solar radiation and boundary conditions from the ECMWF data set for the years 1985, 1986 and 1989. In general, the climate simulated by the model agrees with observations to a certain degree which depends on the variable considered. The climate simulated by the model is assumed representative of the climate in the Amazon region.

3. Climate simulations are repeated assuming that a small sub-region located at the center and with a size of 250 kilometers x 250

kilometers is deforested. Deforestation is modeled by replacing the rain-forest with short grass. The differences between the climate simulated before deforestation and that simulated after deforestation provide estimates of the changes in climate due to small-scale deforestation. It is estimated that small-scale deforestation results in reducing evaporation by about 9% ($\pm 5\%$), and increases surface temperature by about 0.6°C ($\pm 0.5^{\circ}\text{C}$), the changes in evaporation and surface temperature are limited to the deforested area. Precipitation is reduced by about 13% ($\pm 5\%$) over the deforested area. The degree to which these predictions are valid in describing the possible climatic changes due to small-scale deforestation in the Amazon region depends on the accuracy of the climate model in describing the climate of the region.

8.2.4 Sensitivity of Regional Climate to Large-Scale Deforestation

1. A linear model of the tropical atmosphere is used in studying the possible effects of large-scale deforestation on the regional climate of the Amazon basin. The deforestation problem is posed in terms the response of the tropical atmosphere to changes in the lower boundary conditions. The simple structure of the linear model is utilized in interpreting the results of previous modeling studies on the Amazon deforestation problem.

2. It is suggested that the response of the tropical atmosphere to large-scale deforestation consists of two basic components : the response of the tropical atmosphere to the positive change in surface temperature and the response of the same circulation to the negative change in precipitation and latent heating.

3. The competition between these two basic components of the atmospheric response to deforestation may explain the sensitivity of climate models in predicting changes in atmospheric runoff (precipitation -evaporation).

8.3 General Conclusions

The new estimate of precipitation recycling in the Amazon basin of 25% is larger than the estimates for other regions of the world (e.g. 10% for the Mississippi, Benton et al. (1950) and 10% for Eurasia, Budyko (1956)). This high estimate of recycling indicates that evaporation within the Amazon basin is a significant source of atmospheric moisture in that region. It is concluded that there is significant potential for interactions between surface hydrology and the regional climate of the Amazon basin. A change in surface properties (e.g. land cover) will affect the surface evaporation regime and may *potentially* limit the supply of water vapor to the atmosphere. In the tropics, atmospheric moisture is not only the source of water for rainfall but also the source of energy for convection which is the main rainfall producing mechanism. As illustrated in Chapter 7, the large-scale dynamics of the tropical atmosphere are mainly driven by latent heat release which results from condensation of water vapor during precipitation events.

The sensitivity of regional climate to deforestation is studied at two different scales: a small-scale (~ 250 kilometers), and a large-scale (~2500 kilometers). The deforestation problem is studied at a small-scale comparable to the size of deforested areas which exist now in the Amazon basin. It is found that small-scale deforestation results

in the following changes in the regional climate: less evaporation, less precipitation and warmer surface temperature. The magnitudes of these changes are smaller than those due to large-scale deforestation which are predicted by previous modeling studies. The larger perimeter to area ratio for small areas results in more significant boundary effects in small deforested areas in comparison to large deforested areas; these boundary effects explain the smaller magnitudes of the changes resulting from small-scale deforestation.

The magnitudes of the changes due to deforestation of small areas are comparable to the accuracy in the measurements of the key variables involved. These predicted changes are also comparable in magnitude to the natural spatial variability of the same variables. Hence it would be difficult to detect the changes due to deforestation from field observations. The spatial distribution of the predicted changes due to deforestation indicates that the maximum changes are likely to occur near the center of the deforested region. This information can be utilized in designing field experiments for detection of the effects of deforestation using observations of surface temperature, evaporation, and precipitation. It is suggested that long records of simultaneous observations on these key variables at two sites are necessary for detecting the effects of deforestation; one site should be located in the forest and the other located in the deforested area. Both sites should be located away from the boundary between the two regions.

The results of the previous modeling studies which focus on large-scale deforestation in the Amazon predict that deforestation will result in less evaporation, less precipitation, and warmer surface

temperature. The same studies disagree in the sign of the predicted change in atmospheric runoff which is equivalent to atmospheric moisture convergence. The results of our linear analysis of the large-scale deforestation problem reveal some important mechanisms through which deforestation may result in changes of the tropical circulation. It is concluded that the two basic mechanisms by which the tropical atmosphere responds to large-scale deforestation are the response of the tropical atmosphere to the positive change in surface temperature and the response of the same circulation to the negative change in precipitation. While the former induces a converging anomaly in the tropical circulation, the latter induces a diverging anomaly.

The effects of large-scale deforestation on climate are summarized in Figure 8.1 . There are two major direct effects which result from removal of the forest : first, less biomass is available at the surface to absorb incoming solar radiation and hence more solar radiation gets reflected to the atmosphere. Second, replacement of the forest with a shorter vegetation reduces the roughness of the surface and as a result the eddy transport of heat, moisture and momentum are also reduced. The basic physics of evaporation suggests that both of these direct effects will work to reduce evaporation. But as concluded in this study, evaporation within the Amazon is a significant source of atmospheric moisture. Hence the reduction in evaporation reduces significantly the supply of atmospheric moisture to the boundary layer. A dry boundary layer has smaller Convective Available Potential Energy (CAPE) than a moist boundary layer. For this reason a dryer boundary layer would experience less convection

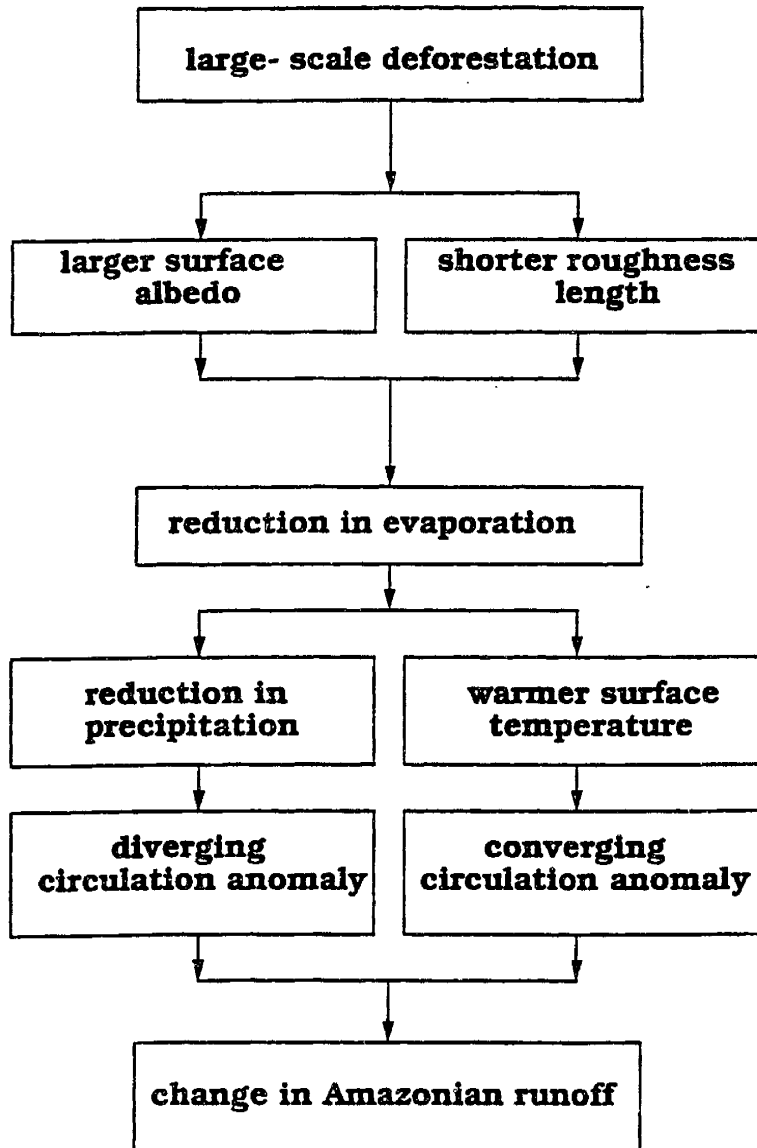


Figure 8.1 Effects of large-scale deforestation on climate.

and less precipitation. Since in general evaporation cools the surface, a reduction in evaporation results in a positive change in surface temperature. It is suggested in this study that the positive change in surface temperature and the negative change in precipitation are the agents which excite the basic components of the response in the tropical circulation to large-scale deforestation. The positive change in surface temperature lowers surface pressure and induces a converging circulation anomaly in the boundary layer. The precipitation mechanism is less obvious, it requires thinking of atmospheric convection as an air "pump" which intermittently supplies air from the boundary layer to the upper troposphere; when this "pump" functions it drives a converging circulation in the boundary layer. But when convection is reduced due to deforestation the convection "pump" functions less efficiently resulting in a diverging circulation anomaly. The effects summarized in Figure 8.1 are the primary effects on climate which result from large-scale deforestation. These effects lead to other secondary effects and feedbacks which are not emphasized in Figure 8.1, e.g. the increase in surface temperature would increase emissions of terrestrial radiation by the surface.

The new formulation of the deforestation problem in Chapter 7 quantifies the forcing on the tropical atmosphere due to deforestation. It is estimated that the order of magnitude of this forcing is about few watts per squared meter. This estimate is of the same order of magnitude as the estimates of the forcing due to the greenhouse effect of doubling CO₂ concentration, with the important difference that the former is a localized forcing while the latter is globally distributed.

Deforestation and the increase in emissions of carbon dioxide are global environmental problems caused by large-scale human activities. Given the observed rates of deforestation and carbon dioxide emissions, the predicted forcing of about few watts per squared meters seems to define the level of stress which will be exerted by these human activities on the global environment sometime in the next century.

8.4 Future Research

The new recycling model described in Chapter 3 can be used for studying the recycling process at other regions of the world. The assumptions of the model are valid at other regions and hence the model is applicable elsewhere. The results of such studies can be compared with the estimates obtained in the Amazon region.

The empirical finding that the recycling ratio scales with the square root of the linear scale is valid for the Amazon region and over the range of scales considered in this study. The factors which control the scaling relation of the recycling ratio are the scaling relations of evaporation and atmospheric moisture flux. The validity of this scaling relation at other regions of the world can be investigated by estimating the scaling of the recycling ratio at those regions and comparing with the estimate for the Amazon region.

The new interception scheme introduced in Chapter 4 involves assumptions about the spatial distribution of canopy storage and about the dependence between the statistical distributions of canopy storage and rainfall. The accuracy of these assumptions and the

sensitivity of the interception loss simulated by the scheme to such assumptions are open questions for future research.

The sensitivity of regional climate to small-scale deforestation is explored in this study by performing few experiments in the Amazon basin. More experiments can be designed to study the problem further, e.g. the size of the deforested area can be varied and the corresponding response of the regional climate can be measured. Another set of experiments should investigate the effect, if any, of the location of the deforested area.

The development and testing of climate models which are the tools used in deforestation studies should be a subject of active research for years to come. This research should focus in improving the land-surface scheme, the convection scheme, the radiation scheme, and the modeling of clouds. Until each of these schemes is reasonably accurate in mimicking nature, the error bar around any prediction by a climate model will be greater in magnitude than the prediction.

REFERENCES

- Anthes , R.A., 1977. A cumulus parameterization scheme utilizing a one dimensional cloud model, *Mon. Wea. Rev.* , **106**, 1045-1078.
- Anthes, R.A.,1990. Recent applications of the Penn. state/NCAR mesoscale model to synoptic, mesoscale and regional climate studies, *Bull. Amer. Meteor. Soc.* , **71**, 1610-1629.
- Anthes, R.A., E. Y. Hsie and Y.H. Kuo, 1987. Description of the Penn. state/NCAR mesoscale model version 4 (MM4), *NCAR tech. note, NCAR/TN-282+STR*, 66 pages.
- Anthes, R. A., Y.-H Kuo, E. -Y Hsie, S. Low-Nam and T. W. Bettge,1989. Estimation of skill and uncertainty in regional numerical models, *Quart. J. Roy. Meteor. Soc.*, **115**, 763-806.
- Benton, G.S., Blackburn, R.T. and Snead V.W., 1950. The role of the atmosphere in the hydrologic cycle, *Trans. Amer. Geophys. Union*, **31**, 61-73.
- Brubaker, K.L., D. Entekhabi and P.S. Eagleson, 1991. Atmospheric water vapor transport : estimation of continental precipitation recycling and parameterization of a simple climate model, *Parsons Laboratory technical report # 333*, Massachusetts Institute of Technology, Cambridge, Mass., 166 pages.
- Budyko, M.I., 1974. *Climate and Life*, International Geophysical Series, volume 18, Academic Press, 508 pages.
- Crum, T.D. and R.B. Stull, 1987. Field measurements of the amount of surface layer air versus height in the entrainment zone, *J. Atmos. Sci.* , **44**, 2743-2753.
- Chan, S. and P.S. Eagleson, 1980. Water balance studies of the Bahr Elghazal swamps, *Parsons Laboratory technical report # 261*, Massachusetts Institute of Technology, Cambridge, Mass., 317 pages.
- Charney, J.,1973. Dynamics of deserts and droughts in the Sahel, *Quart. J. Roy. Meteor. Soc.*, **101**, 193-202.
- Deardorff, J. W., 1972. Parameterization of the planetary boundary layer for use in general circulation models, *Mon. Wea. Rev.* , **100**, 93-106.
- Dickinson, R.E., 1981. Blowing in the wind : deforestation and long-range implications, *Studies in third world societies, publication # 14*, Department of Anthropology, College of William and Mary, Williamsburg, Va., 411-515.

Dickinson, R.E., 1984. Modeling evapotranspiration for three-dimensional global climate models. *Climate Processes and Climate Sensitivity*, J. E. Hansen and T. Takahashi (Eds.), American Geophysical Union, Washington D.C., 58-72.

Dickinson, R.E., 1989. Implications of tropical deforestation for climate : a comparison of model and observational descriptions of surface energy and hydrological balance, *Phil. Trans. R. Soc. Lond.*, **B324**, 423-430.

Dickinson R.E., A. Henderson-Sellers, P.J. Kennedy and M.F. Wilson, 1986. Biosphere-Atmosphere Transfer Scheme (BATS) for the NCAR community climate model, *NCAR tech. note, NCAR/TN-275+STR*, 69 pages.

Dickinson, R.E. and A. Henderson-Sellers, 1988. Modelling tropical deforestation : A study of GCM land surface parameterizations, *Quart. J. Roy. Meteor. Soc.*, **144**, 439-462.

Dolman, A.J. and D. Gregory, 1992. The parameterization of rainfall interception in GCMs, *Quart. J. Roy. Meteor. Soc.*, **188**, 445-467.

Eagleson, P.S., N.M. Fennessey, Q.Wang and I. Rodriguez-Iturbe, 1987. Application of spatial Poisson models to air mass thunderstorm rainfall, *J. Geophys. Res.* , **92(D8)** , 9661-9678.

Eltahir, E.A.B., 1989. A feedback mechanism in annual rainfall, Central Sudan, *J. Hydrol.* , **110**, 323-334.

Eltahir, E.A.B., and R. L. Bras, 1992. A description of rainfall interception over large areas, and On the estimation of the fractional coverage of rainfall in climate models, *MIT Center for Global Change Science report # 15*, Massachusetts Institute of Technology, Cambridge, Mass., 54 pages.

Emanuel, K.A. and D.J. Raymond, 1992. Report from a workshop on cumulus parameterization, *Bull. Amer. Meteor. Soc.* , **73**, 318-326.

Entekhabi, D. and P.S. Eagleson, 1989. Landsurface hydrology parameterization for atmospheric general circulation models including subgrid scale spatial variability, *J. Climate*, **2**, 816-831.

Figuroa, S. N. and C. A. Nobre, 1990. precipitation distribution over central and western tropical south America, *Climanálise*, **5**, 36-40.

Fowler, W.B. and Helvey J.D., 1974. Effect of large-scale irrigation on climate in the Columbia basin, *Science*, **184**, page 121.

- Fowler, W.B. and Helvey J.D., 1975. Irrigation increases rainfall ?, *Science*, **188**, page 281.
- Gill, A.E., 1980. Some simple solutions for heat-induced tropical circulation, *Quart. J. Roy. Meteor. Soc.*, **106**, 447-462.
- Giorgi F., 1990. Simulation of regional climate using a limited area model nested in a general circulation model, *J. Climate*, **3**, 941-963.
- Giorgi, F. and G.T. Bates, 1989. The climatological skill of a regional model over complex terrain, *Mon. Wea. Rev.*, **117**, 2325-2347.
- Harriss, R. C., S.C. Wofsy, M. Garstang, E.V. Browell, L.C. B. Molion, R.J. McNeal, J. M. Hoell, Jr., R.J. Bendura, S. M. Beck, R. L. Navaro, J.T. Riley and R.L. Snell. 1988. The Amazon Boundary Layer Experiment (ABLE 2A) dry season 1985, *J. Geophys. Res.*, **93(D2)**, 1351-1360.
- Henderson-Sellers, A. and R.E. Dickinson, 1992. Inter-comparison of land-surface parameterizations launched, *Trans. Amer. Geophys. Union*, **73**, 195-196.
- Holzman, B., 1937. Sources of moisture for precipitation in the United States, *U.S. Department of Agriculture Tech. Bull # 589*, 41 pages.
- Horton, R.E., 1943. Hydrologic interrelations between lands and oceans, *Trans. Amer. Geophys. Union*, **24**, 753-764.
- Illari, L., 1989. The quality of satellite PWC data and their impact on analyzed moisture fields, *Tellus*, **41A**, 319-337.
- Ives, R.L., 1936. Desert floods in the Sonoyta valley, *American Journal of Science*, **32**, 349-360.
- Jensen, J.C., 1935, The relation between surface evaporation from lakes and ponds to precipitation from local thunderstorms in the drought area, *Bull. Amer. Meteor. Soc.*, **16**, 142-145.
- Koster, R., J. Jouzel, R. Suozzo, G. Russell, W. Broecker, D. Rind and P. S. Eagleson, 1986. Global sources of local precipitation as determined by the NASA/GISS GCM, *Geophysical Research Letters*, **13**, 121-124.
- Lacis, A.A and J.E. Hansen, 1974. A parameterization for the absorption of solar radiation in the Earth's atmosphere, *J. Atmos. Sci.*, **31**, 118-133.

Lamb, R.G. 1982. Diffusion in the Convective Boundary Layer, *Atmospheric Turbulence and Air Pollution Modelling*, F.T.M. Nieuwstadt and H. van Dop (Eds.), Reidel Publishing Company, 159-229.

Lean, J. and D.A. Warrilow, 1989. Simulation of the regional climatic impact of Amazon deforestation, *Nature*, **342**, 411-413.

Lettau, H., K. Lettau and L.C.B. Molion, 1979. Amazonia's hydrologic cycle and the role of atmospheric recycling in assessing deforestation effects, *Mon. Wea. Rev.*, **107**, 227-238.

Lindzen, R. S. and S. Nigam, 1987. On the role of sea surface temperature gradients in forcing low-level winds and convergence in the tropics, *J. Atmos. Sci.*, **44**, 2418-2436

Lloyd, C.R., 1990. The temporal distribution of Amazonian rainfall and its implications for forest interception, *Quart. J. Roy. Meteor. Soc.*, **116**, 1487-1494.

Marques, J., M. Santos, N.A. Villa Nova, and E. Salati, 1977. Precipitable water and water vapor flux between Belem and Manaus, *Acta Amazonica*, **7**, 355-362.

Matsuno, T., 1969. Quasi-geostrophic motions in the equatorial area, *J. Met. Soc. Japan*, **44**, 25-43.

McDonald, J.E., 1962. The evaporation precipitation fallacy, *Weather*, **17**, 168-177.

McNish, A.G., 1936. Statistical aspects of long-range weather forecasting, *Trans. Amer. Geophys. Union*, **1**, 124-129.

Molion, L.C.B., 1975. A climatonic study of the energy and moisture fluxes of the Amazon basin with considerations of deforestation effects, Ph.D thesis, University of Wisconsin, Madison, 132 pages.

Newell, R.E., 1971. The Amazon forest and atmospheric general circulation, *Man's impact on the climate*, W.H. Mathews, W.W. Kellogg and G.D. Robinson (Eds.), MIT press, Cambridge, Mass., 457-459.

Neelin, J.D., 1988. A simple model for surface stress and low-level flow in the tropical atmosphere driven by prescribed heating, *Quart. J. Roy. Meteor. Soc.*, **114**, 747-770.

Neelin, J.D., 1989. On the interpretation of the Gill model, *J. Atmos. Sci.*, **46**, 2466-2468.

Newell, R.E., J.W. Kidson, D.G. Vincent and G.J. Boer, 1972. *The general circulation of the tropical atmosphere and interactions with extra-tropical latitudes, volume 1*, MIT press, Cambridge, Mass., 258 pages.

Nobre, C.A., P.J. Sellers and J. Shukla, 1991. Amazonian deforestation and regional climatic change, *J. Climate*, **4**, 957-988.

Oltman, R.E., 1967. Reconnaissance investigation of the discharge and water quality of the Amazon, *Biota Amazonica*, **3**, 163-185.

Paluch, I.R., 1979. The entrainment mechanism in Colorado cumuli, *J. Atmos. Sci.*, **36**, 2467-2478.

Raval, A. and V. Ramanathan, 1989. Observational determination of the greenhouse effect, *Nature*, **342**, 758-761.

Rodriguez-Iturbe, I. and P. S. Eagleson, 1987. Mathematical models for rainstorm events in space and time, *Water Resour. Res.*, **23**, 181-190.

Rodriguez-Iturbe I., D. Entekhabi and R. L. Bras, 1990 a. Non-linear dynamics of soil moisture at climate scales : stochastic analysis, *M.I.T. Center for Global Change Science report # 5*, Cambridge, Mass., 27 pages.

Rodriguez-Iturbe I., D. Entekhabi, J. Lee and R. L. Bras, 1990 b. Non-linear dynamics of soil moisture at climate scales : chaotic analysis, *M.I.T. Center for Global Change Science report # 6*, Cambridge, Mass., 42 pages.

Rutter A. J., K. A. Kershaw, P. C. Robins and A.J. Morton, 1971. A predictive model of rainfall interception in forests, I. derivation of the model from observations in a plantation of Corsican pine, *Agric. Meteorol.* , **9**, 367-384.

Rutter A. J., A.J. Morton and P. C. Robins , 1975. A predictive model of rainfall interception in forests, II. Generalization of the model and comparison with observations in some Coniferous and hardwood stands, *J. Appl. Ecol.*, **12**, 367-380.

Salati, E and Vose, P.B., 1984. Amazon basin: a system in equilibrium, *Science*, **225**, 129-138.

Salati E., A. Dall'Olio, E. Matsui and J.R. Gat, 1979. Recycling of water in the Amazon basin: an isotopic study, *Water Resour. Res.*, **15**, 1250-1258.

Shukla, J., C. Norbe and P. Sellers, 1990. Amazon deforestation and climate change, *Science* , **247**, 1322-1325.

Shuttleworth, W.J., 1988 a. Evaporation from Amazonian rainforest, *Phil. Trans. R. Soc. Lond.*, **B233**, 321-346.

Shuttleworth, W.J., 1988 b. Macrohydrology-the new challenge for process hydrology, *J. Hydrol.* , **100**, 31-56.

Shuttleworth, W.J. and R.E. Dickinson, 1989. Comments on 'modelling tropical deforestation : a study of G.C.M. land-surface parameterizations' , *Quart. J. Roy. Meteor. Soc.*, **115**, 1177-1179.

Stidd, C. K., 1975. Irrigation increases rainfall ?, *Science*, **188**, 279-280.

Trenberth K.E. and Olson J.G., 1988. ECMWF global analyses 1979-1986: circulation statistics and data evaluation, *NCAR Technical Note NCAR/TN -300+STR*, 94 pages.

Zebiak, S. Z., 1982. A simple atmospheric model of relevance to El Niño, *J. Atmos. Sci.* , **39**, 2017-2027.

APPENDIX 3.1

Relative Magnitude of the Change in Water Vapor Storage

The monthly outflow of water vapor, O , and the change in storage of water vapor during a month, δN , are compared in Figure 3.2. (notice that inflow, I , and outflow, O , are of the same order of magnitude)The data shows that

$$\delta N \ll O \quad (A3.1.1)$$

But in deriving the model equations we are assuming that

$$\delta N_w \ll O_w, \delta N_o \ll O_o \quad (A3.1.2)$$

In the following we show that the inequality A3.1.1 combined with the well-mixed atmosphere assumption of Equation 3.2 result in the inequality A3.1.2.

Since ($N = N_w + N_o$) and ($O = O_w + O_o$), Equation 3.2 can be rewritten as

$$\rho = N_w / N = O_w / O \quad (A3.1.3)$$

, and since ρ is assumed constant during any month, Equation A3.1.3 results in

$$\delta N_w = \rho \delta N, \quad (A3.1.4a)$$

$$O_w = \rho O \quad (A3.1.4b)$$

By dividing Equation A3.1.14a by Equation A3.1.4b we get

$$\delta N_w / O_w = \delta N / O \quad (A3.1.5)$$

Hence the observation that $\delta N \ll O$ combined with the well-mixed atmosphere assumption implies that $\delta N_w \ll O_w$. Similarly it can be shown that the observation $\delta N \ll O$ combined with the well-mixed atmosphere assumption implies that $\delta N_o \ll O_o$.

APPENDIX 4.1

Interception in BATS

The BATS uses a simple description of canopy drainage. Whenever canopy storage, C , exceeds the maximum allowed storage, C_{\max} , canopy drainage occurs to restore storage back to C_{\max} .

$$D_r = \frac{(C - C_{\max})}{\Delta t} \quad (\text{A4.1.1})$$

Evaporation is given by

$$e = e_c \cdot \left(\frac{C}{C_{\max}} \right)^{\frac{2}{3}} + e_t \cdot \left(1 - \left(\frac{C}{C_{\max}} \right)^{\frac{2}{3}} \right) \quad (\text{A4.1.2})$$

where e_t is transpiration by the plant and e_c is evaporation from wet canopy. The effects of spatial variability in rainfall or canopy storage are not included in this scheme.

APPENDIX 4.2

Shuttleworth Interception Scheme

Shuttleworth (1988b) suggested that the effects of spatial variability on interception and runoff can be modelled by assuming rainfall, P , is exponentially distributed in space. The canopy storage, C , is assumed constant in space. This assumption is the main difference between Shuttleworth scheme and the new scheme introduced in Chapter 4. The Shuttleworth scheme treats the spatial variability of rainfall but neglects spatial variability of canopy storage.

By making an analogy between the top soil layer and canopy layer Shuttleworth suggested that the maximum canopy "infiltration" rate is given by

$$IF = \frac{(S - C)}{\Delta t} \quad (A4.2.1)$$

where S is the amount of water retained by the canopy after being completely wet and then drained for a "sufficiently" long period.

Throughfall is then modelled by

$$\begin{aligned} T &= P - IF, & P > IF \\ T &= 0, & P < IF \end{aligned} \quad (A4.2.2)$$

where P is precipitation, and the expected value of throughfall is given by

$$E(T) = \int_{P=0}^{\infty} T(P) \cdot f_p \, dP = E(P) \cdot e^{-\left[\frac{q_p IF}{E(P)}\right]} \quad (A4.2.3)$$

where f_p is the statistical distribution of precipitation which is defined by Equation 4.5. q_p is the fraction of the area with $P > 0$.

The corresponding description of evaporation is not specified in Shuttleworth (1988b), for comparison purposes it is assumed that evaporation is described by Equation 4.2.

APPENDIX 4.3

Continuity Equation for the New Interception Scheme

The derivation of the continuity equation for the new scheme is complicated by the fact that canopy storage does not exceed the maximum storage specified as C_m . Three possible conditions are considered :

* $C \leq C_m$ and $0 \leq P < \infty$, the rate of change of storage is given by Equation 4.3.

* $C > C_m$ and $(1-p)P > D_m$, the rate of change of storage is zero.

* $C > C_m$ and $(1-p)P < D_m$, the rate of change of storage is given by Equation 4.3 with $D_r = D_m$. The rate of change of the spatially averaged canopy storage is given by,

$$\begin{aligned} \frac{\partial (E(C))}{\partial t} = & (1-p) \int_{P=0}^{\infty} P \cdot f_p \cdot dP \cdot \int_{C=0}^{C=C_m} f_C \cdot dC \\ & - \int_{P=0}^{\infty} f_p \cdot dP \cdot \frac{e_c}{S} \cdot \int_{C=0}^{C_m} C \cdot f_C \cdot dC \\ & - \int_{P=0}^{\infty} f_p \cdot dP \cdot \int_{C=0}^{C_m} K \cdot e^{\left(\frac{C}{b}\right)} \cdot f_C \cdot dC \\ & + (1-p) \int_{P=0}^{\frac{D_m}{(1-p)}} P \cdot f_p \cdot dP \cdot \int_{C=C_m}^{\infty} f_C \cdot dC \\ & - \int_{P=0}^{\frac{D_m}{(1-p)}} f_p \cdot dP \cdot \frac{e_c}{S} \cdot \int_{C=C_m}^{\infty} C \cdot f_C \cdot dC \\ & - D_m \cdot \int_{P=0}^{\frac{D_m}{(1-p)}} f_p \cdot dP \cdot \int_{C=C_m}^{\infty} f_C \cdot dC \end{aligned}$$

which is equivalent to,

$$\begin{aligned}
\frac{\partial (E(C))}{\partial t} &= (1-p) E(P) \cdot (1-q_c \cdot e^{-\left(\frac{q_c \cdot C_m}{E(C)}\right)}) \\
&\quad - \frac{e_c E(C)}{S} \cdot (1-e^{-\left(\frac{q_c \cdot S}{E(C)}\right)}) \\
&\quad + \frac{q_c^2 \cdot K \cdot b}{(b \cdot q_c - E(C))} \cdot (1-e^{-\left(\frac{(b \cdot q_c - E(C)) \cdot C_m}{b \cdot E(C)}\right)}) \\
&\quad + (1-p) \cdot \left(E(P) - \left(q_p \cdot \frac{D_m}{(1-p)} - E(P) \right. \right. \\
&\quad \left. \left. + \frac{q_p \cdot e_c}{(1-p)} \right) \cdot e^{-\left(\frac{q_p \cdot D_m}{E(P) \cdot (1-p)}\right)} \right) \\
&\quad \cdot q_c \cdot e^{-\left(\frac{q_c \cdot S}{E(C)}\right)} + q_p \cdot q_c \cdot (e_c + D_m) e^{-\left(\frac{q_p \cdot D_m}{E(P) \cdot (1-p)}\right)} \\
&\quad \cdot e^{-\left(\frac{q_c \cdot C_m}{E(C)}\right)} - D_m \cdot q_c \cdot e^{-\left(\frac{q_c \cdot C_m}{E(C)}\right)}
\end{aligned} \tag{A4.3.3}$$

APPENDIX 7.1
Analytical Solution of the Linear Model

Following are expressions for the perturbations in the boundary layer flux, they represent the solution of Equations 7.7 corresponding to the forcing of Equation 7.8 .

First, in the zonal direction

$$u' = FG_0 \left[\frac{-k(1 + \epsilon e^{-6\epsilon L}) e^{3\epsilon(x+L)}}{2(k^2 + 9\epsilon^2)} (y^2 - 3) + \frac{k(1 + e^{-10\epsilon L}) e^{5\epsilon(x+L)}}{2(k^2 + 25\epsilon^2)} (y^3 - 6y) \right] e^{-\frac{y^2}{4}}, \quad x < -L \quad (A7.1.1)$$

$$u' = FG_0 \left[\frac{-\epsilon \cos(kx) - k(\sin(kx) + e^{-\epsilon(x+L)})}{2(k^2 + \epsilon^2)} \right] e^{-\frac{y^2}{4}} - FG_0 \left[\frac{3\epsilon \cos(kx) + k(\sin(kx) - e^{3\epsilon(x-L)})}{2(k^2 + 9\epsilon^2)} (y^2 - 3) \right] e^{-\frac{y^2}{4}} + FG_0 \left[\frac{5\epsilon \cos(kx) + k(\sin(kx) - e^{5\epsilon(x-L)})}{2(k^2 + 25\epsilon^2)} (y^3 - 6y) \right] e^{-\frac{y^2}{4}}, \quad |x| < L \quad (A7.1.2)$$

$$u' = FG_0 \left[\frac{-k(1 + e^{-2\epsilon L}) e^{\epsilon(L-x)}}{2(k^2 + \epsilon^2)} \right] e^{-\frac{y^2}{4}}, \quad x > L \quad (A7.1.3)$$

and in the meridional direction,

$$v' = FG_0 \left[\frac{-4\epsilon k (1+e^{-6\epsilon L}) e^{3\epsilon(x+L)}}{(k^2+9\epsilon^2)} y + \frac{6\epsilon k(1+e^{-10\epsilon L}) e^{5\epsilon(x+L)}}{(k^2+25\epsilon^2)} (y^2-1) \right] e^{-\frac{y^2}{4}}, \quad x < -L. \quad (A7.1.4)$$

$$v' = FG_0 \left[\cos(kx) - \frac{12\epsilon^2 \cos(kx) + k(\sin(kx) - e^{3\epsilon(x-L)})}{(k^2+9\epsilon^2)} \right] y e^{-\frac{y^2}{4}} + FG_0 \left[\frac{30\epsilon^2 \cos(kx) + k(\sin(kx) - e^{5\epsilon(x-L)})}{(k^2+25\epsilon^2)} (y^2-1) + \cos(kx)y^2 \right] e^{-\frac{y^2}{4}}, \quad |x| < L \quad (A7.1.5)$$

$$v' = 0, \quad x > L \quad (A7.1.6)$$

For details of the derivation of these expressions we refer to Gill (1980). In deriving these expressions, it is assumed that $(2\epsilon k \ll 1)$ and the equations are solved using an equatorial β -plane approximation. FG_0 is normalized using the equatorial Rossby radius as a length scale and the time scale given by $(2\beta c)^{-1/2}$. The resulting u' and v' are dimensionless.

BIOGRAPHICAL NOTE

Elfatih Eltahir was born in Omdurman, Sudan, in October of 1961. He received a Bachelor of Science with First Class Honors in Civil Engineering from the University of Khartoum in November 1985. He then started his graduate studies in Galway, Republic of Ireland, in August 1986. He received a Master of Science with First Class Honors in Hydrology from the National University of Ireland in August 1988. The title of the Master thesis was "Drought Frequency Analysis of Annual Rainfall Series in Central and Western Sudan".

In August 1988 he started his studies at the Massachusetts Institute of Technology working towards a Master of Science in Meteorology from the Department of Earth, Atmospheric and Planetary Sciences and a Doctor of Science in Hydroclimatology from the Department of Civil and Environmental Engineering. The title of the Master thesis was " The Estimation of the Fractional Coverage of Rainfall in Climate Models ".

Elfatih Eltahir is the son of Ali Babiker Eltahir and Nafisa Hassan Musa. He has two brothers : Mohammed and Omer, and four sisters : Maha, Ilham, Lama, and Mai. He and his wife Shahinaz were married in December 1991.